GEOMATRIX

FINAL REPORT

PART 2

SEISMIC HAZARD ANALYSIS RESULTS AND SENSITIVITY SEISMIC HAZARD IN SOUTHERN ONTARIO

Prepared for:

Atomic Energy Control Board
280 Slater Street, 7th Floor
Ottawa, Ontario K1P 5S9, Canada

AECB Contract No. 87055-5-5072/001/SS

Prepared by:

Geomatrix Consultants, Inc.
100 Pine Street, 10th Floor
San Francisco, CA 94111

August 1997
Project No. 3678

Geomatrix Consultants

GEOMATRIX

TABLE OF CONTENTS

FIGURES

TABLE OF CONTENTS
(Continued)

TABLE OF CONTENTS
(Continued)

TABLE OF CONTENTS
(Continued)

TABLE OF CONTENTS
(Continued)

TABLE OF CONTENTS
(Continued)

APPENDICES

DRAFT REPORT
PART 2
SEISMIC HAZARD ANALYSIS RESULTS AND SENSITIVITY
SEISMIC HAZARD IN SOUTHERN ONTARIO

1.0 INTRODUCTION

This draft report is Part 2 of a three-part report on the Seismic Hazard of Southern Ontario study conducted for the Atomic Energy Control Board of Canada. Part 1 presented the characterization of the seismic sources that could affect the ground motion hazard at the Darlington and Pickering sites and the selection of ground motion attenuation relationships for use in the probabilistic seismic hazard analysis (PSHA). The Part 2 report presents the results of the PSHA, including sensitivity analyses. Part 3 presents recommendations regarding the most significant technical issues to the seismic hazard and data collection and other activities that could address these issues.

This PSHA was focused on assessing the uncertainties in identifying and characterizing seismic sources that may be significant to the seismic hazard at the Darlington and Pickering sites, rather than establishing absolute hazard levels. We have attempted to incorporate all credible models and have made assessments of their relative credibility based on our review of the literature and discussions with active researchers. To complete the uncertainty characterization we have also made an assessment of the current level of uncertainty in characterizing ground motions on hard rock sites in eastern North America. However, we have not made an evaluation of the effect of the local site conditions.

1.1 PSHA Calculation Procedure

PSHA provides an assessment of the likelihood (typically on an annual basis) that a specified level of ground motion will be exceeded. The basic components of the PSHA formulation are shown schematically on Figure 1-1 and are as follows:

(1) The sources of potentially damaging future earthquakes are identified. A *seismic source* in a PSHA is a region having relatively uniform seismicity characteristics. Seismic sources are typically identified based on geologic and observed seismicity data. The types of sources typically identified are specific geologic structures, such as faults, and areal source zones representing tectonic provinces or zones of seismicity.

(2) The frequency of earthquake occurrence—or earthquake recurrence—in each source is assessed and expressed as a frequency versus magnitude relationship. This includes an evaluation of the maximum event that a source can produce. The probability distribution of distance from individual earthquakes to the site is also defined.

(3) Appropriate ground motion models are selected for estimating site ground motions from each of the sources. The estimates include both the expected levels of ground motion and the variation about the expected value that any single recording may exhibit.

(4) Relationships between ground motion level and probability (frequency) of exceedance are developed. These define what are called *hazard curves*. Hazard curves for various spectral frequencies are obtained by repeating the PSHA calculation using attenuation relationships for each spectral frequency. Specific design ground motion levels for site evaluation can then be chosen by selecting an appropriate probability of exceedance. The corresponding ground motion levels at each spectral frequency form what is called an *equal-hazard* response spectrum.

The mathematical formulation used for PSHA was first proposed by Cornell (1969, 1971). Assuming that the occurrence of damaging earthquakes can be represented as a Poisson process, the probability that a ground motion parameter, Z, will exceed a specified value, z in time period t is given by:

$$P(Z>z|T) = 1.0 - e^{-\nu(z)\cdot t} \leq \nu(z)\cdot t \qquad \text{(1-1)}$$

where $\nu(z)$ is the average frequency during time period t at which the level of ground motion parameter Z exceeds value z at the site resulting from all earthquakes on all sources

in the region. The inequality at the right of Equation (1-1) is valid regardless of the appropriate probability model for earthquake occurrence, and $\nu(z) \cdot t$ gives an accurate and slightly conservative estimate of $P(Z>z)$ for probabilities of 0.1 or less, provided $\nu(z)$ is the appropriate average value for time period t. The relationship between z and $\nu(z)$ define a hazard curve, such as those shown in part (4) of Figure 1-1.

The frequency of exceedance, $\nu(z)$, is a function of the frequency of earthquake occurrence, the randomness of size and location of future earthquakes, and the randomness in the level of ground motion the earthquakes may produce at the site of interest. Is computed by the expression:

$$\nu(z) = \sum_{n} \alpha_n(m^0) \int_{m^0}^{m^u} f(m) \left[\int_0^{\infty} f(r|m) \cdot P(Z>z|m,r)\, dr \right] dm \qquad (1\text{-}2)$$

where $\alpha_n(m^0)$ is the frequency of earthquakes on source n above a minimum magnitude of engineering significance, m^0; $f(m)$ is the probability density of earthquake size between m^0 and a maximum earthquake the source can produce, m^u; $f(r|m)$ is the probability density function for distance to an earthquake of magnitude m occurring on source n, and $P(Z>z|m,r)$ is the probability that, given an earthquake of magnitude m at distance r from the site, the peak ground motion will exceed level z. The product of $\alpha_n(m^0)$ and $f(m)$ defines the earthquake recurrence curve and $f(r|m)$ specifies the distance distributions shown on part (2) of Figure 1-1. The attenuation relationships shown on part (3) of Figure 1-1 are used to obtain the conditional probability of exceeding z, $P(Z>z|m,r)$ for each magnitude m earthquake occurring at a distance r from the site.

The seismic hazard model for the southern Ontario region developed in the Part 1 report treats all of the parameters of Equation (1-2) as uncertain and specifies discrete probability functions for each one. The result is a large number of alternative parameter sets, each

parameter set with a finite probability that it represents the correct parameter set. The computation of $\nu(z)$ is made for a particular parameter set and the result is assigned the probability associated with that parameter set. The process is repeated over all parameter sets, producing a discrete probability density for the frequency of exceedance, $\nu(z)$. The probability density for $\nu(z)$ is then used to compute the mean or expected hazard and various percentiles of the distribution that define the uncertainty in the hazard given the uncertainty in the input parameters.

The computational scheme used to compute the hazard involves replacing the integrals of Equation **(1-2)** with summations over small magnitude and distance intervals. The distance density function, $f(r)$, was computed numerically over each source region (assuming either a uniform density or a spatially varying density computed using a Gaussian kernel density estimator) assuming that each earthquake has a finite rupture length dependent on magnitude and that the orientation of the rupture is random. The local sources were modeled as a set of parallel line sources with a width of 10 km to address the uncertainty in the location of the actual source. The probability function $P(Z>z|m,r)$ was computed assuming that peak ground motions are lognormally distributed about the specified attenuation relationships using the standard deviations specified for the selected attenuation relationships. The minimum magnitude of engineering significance, m^0, was set at m_b 5.0.

1.2 Summary of PSHA Inputs

The probabilistic formulation specified by Equation **(1-2)** addresses the randomness inherent in the natural phenomena of earthquake generation in time and space, and of seismic wave propagation. The randomness in the physical process has come to be called *aleatory* uncertainty (SSHAC, 1996). The Part 1 report presented the basis for the characterization of the required inputs to the PSHA, emphasizing characterization of the uncertainty associated with the selection of models and model parameters to represent the various aspects of the PSHA. This uncertainty, arising from incomplete data and/or

alternative interpretations of the data, has come to be called *epistemic* uncertainty. In the Part 1 report, the epistemic uncertainties were developed in the form of discrete probability distributions using a *logic tree* formulation to organize the assessments into a complete probability model for the seismic hazard analysis.. The combined logic tree for the PSHA contains 19 levels of uncertainty. The specific items addressed are:

1. Alternative ground motion attenuation relationships - three models were selected to represent the uncertainty in characterizing earthquake source spectra.

2. Attenuation relationship epistemic uncertainty - addresses uncertainty in average properties of the earthquake source, travel path, and shallow crustal response.

3. Regional source modeling approach - three alternative approaches considered, geologic-tectonic zonation, composite lineament-seismicity analysis, and seismicity based zonation.

4. Uncertainty in the basis for zonation - for the geologic zonation the issue addressed was the significance of the Iapetan rifted margin (IRM)/ southern Grenville region (SGR) boundary and for the seismicity approach the alternatives considered were the use of source zones versus regional smoothing of seismicity parameters in 1° latitude × 1° longitude cells without the constraint of source zone boundaries.

5. Uncertainty in the location of the Iapetan rifted margin/southern Grenville region boundary - three alternative locations were considered.

6. Extension of the St. Lawrence rift system into the Lake Ontario region.

7. Northern boundary of the hypothesized St. Lawrence extension - two alternative locations for the northern boundary of the postulated extension of the St. Lawrence rift system were considered.

8. Consideration of the aulacogens (the Ottawa graben (OG), the Saguenay graben (SG), and the postulated St. Lawrence rift system extension (SLE) as separate source zones or as part of the larger IRM regional zone.

9. Spatial distribution model for regional zones - alternatives considered were the assumption that the spatial density of future earthquakes is uniform within the source zone or assumption that the spatial distribution is nonuniform and conforms to the distribution of recorded seismicity.

10. Constraints placed on the *b*-value in fitting seismicity parameters for the local sources. An *a priori* value was selected based on the seismicity parameters for the regional sources and the local source *b*-value was either weakly or strongly constrained to match the selected prior value.

11. Rouge River faults association - three alternatives considered, (1) the Rouge River faults are an independent source, (2) they are associated with the Niagara-Pickering linear zone, or (3) they are associated with the Georgian Bay linear zone.

12. Smoothing parameter for spatial density estimation - three values of h, the smoothing constant in the Gaussian kernel density estimation function were considered, 25, 10 and 100 km, as well as four alternatives (see Appendix A) for the degree of smoothness imposed in the regional seismicity parameter estimation method developed by Veneziano and van Dyck (1985).

13. Uncertainty about the possible association of the Niagara-Pickering linear zone with the Akron magnetic boundary.

14. Probability that local sources [Rouge River(RR) faults, Niagara-Pickering linear zone (NPLZ), Georgian Bay linear zone (GBLZ), Toronto-Hamilton seismic zone (THSZ), Clarendon-Linden fault system (CLFS), Hamilton-Presqu'ile fault (HPF), and the Wilson-Port Hope lineament (WPHL)] are seismogenic.

15. Appropriate source model for local sources - two alternatives considered: (1) source zones with an exponential magnitude distribution and a maximum magnitude distribution similar to the regional zone in which they lie, or (2) faults with a characteristic magnitude distribution and a maximum magnitude distribution based on estimated rupture dimensions.

16. Alternative estimates of the earthquake occurrence rate for the Rouge River fault when they are treated as a fault-type local source, either using recorded seismicity or an estimate of fault slip rate.

17. Uncertainty in the maximum magnitude for the individual sources.

18. Uncertainty in the earthquake recurrence rates for the individual sources.

19. Uncertainty in the *b*-values for the individual sources.

The basis for the assessments at each level of the logic tree are discussed in the Part 1 report. The seismicity parameters (occurrence rates, *b*-values, and maximum magnitudes) developed for each of the sources using the approaches described in the Part 1 report are presented in Appendix A to this report. The selection of the ground motion attenuation relationships is also discussed in the Part 1 report. Appendix B to this report presents the method used to generate the attenuation function coefficients.

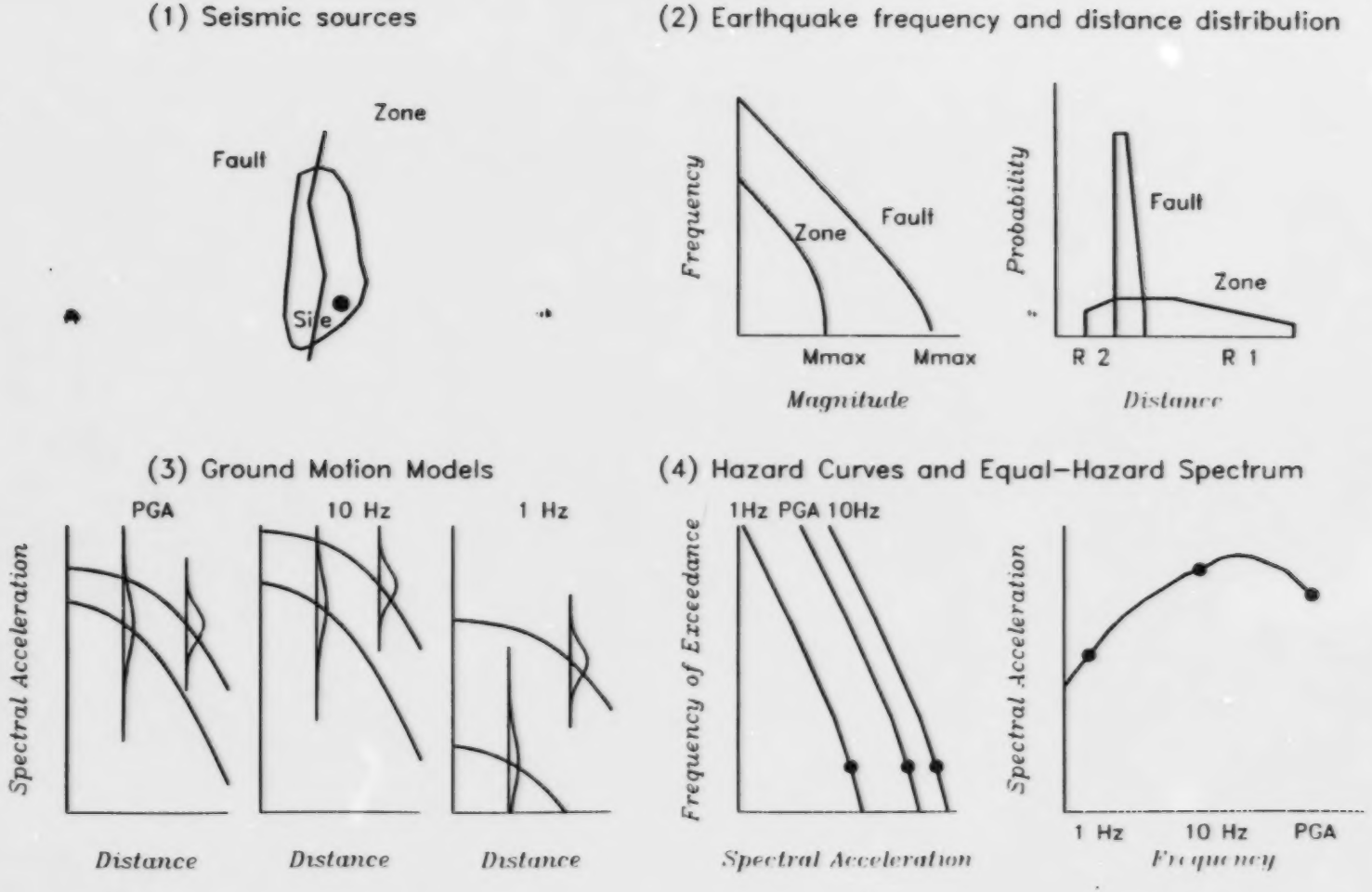

Figure 1-1 **Schematic diagram of the components of PSHA.**

2.0 SEISMIC HAZARD ANALYSIS RESULTS

The results of the PSHA for the Pickering and Darlington sites are presented on Figure 2-1 for peak ground acceleration and 1 Hz spectral acceleration (5 percent damping). The evaluation of the hazard analysis and sensitivity are presented in terms of these two ground motion measures. These two ground motion measures span the frequency range of primary interest for nuclear power plants. The results for spectral accelerations at high spectral frequencies ($>$ 5 Hz) show similar trends to those for peak acceleration and those at low spectral frequencies show similar trends to the results for 1 Hz spectral acceleration.

The plots on Figure 2-1 show the mean hazard curves defining the mean frequency of exceeding specified ground motion levels over all of the uncertainties in seismic source and ground motion characterization defined in the Part 1 report. The range in the results is shown by curves defining the 5^{th}-, 15^{th}-, 50^{th}- (median), 85^{th}-, and 95^{th}-percentiles of the distributions for frequency of exceedance computed from the logic tree. These percentile hazard curves define confidence intervals for the hazard resulting from uncertainties in specifying the inputs to the analysis. The results shown are typical of seismic hazard estimates in central and eastern North America in that there is a wide confidence band reflecting the large uncertainties in most of the input parameters. The results are also typical in that the distribution for frequency of exceedance is skewed such that the mean hazard lies above the central point (median) of the distribution and the amount of skewness increases with increasing peak ground motion level.

Below we analyze the results in terms of (1) the contributions to the mean hazard, (2) sensitivity analyses that illustrate the effect of various modeling assumptions on the mean hazard, and (3) the contributions to the uncertainty in the hazard. These analyses are made for both the regional sources and the local sources.

2.1 Contributions to Mean Hazard

Figure 2-2 shows the mean hazard curves from Figure 2-1 together with the mean hazard curves for the regional and local sources. These results indicate that the regional sources are the dominant contributors to the hazard at small ground motion levels and that the local sources become the dominant contributor to the hazard at large ground motion levels. The local sources become dominant at smaller ground motion levels when considering the hazard peak acceleration than when considering the hazard for 1 Hz spectral acceleration.

The regional source model involves three alternative approaches to zonation. Figures 2-3a, 2-3b, 2-3c, 2-4, and 2-5 illustrate the contributions of individual sources to the regional source hazard for each of the modeling approaches.

Figures 2-3a, 2-3b, and 2-3c show the contributions of various sources to the hazard from regional sources defined on the basis of geology and tectonics. Figure 2-3a shows the contributions to the regional source hazard for the assumption that the Iapetan rifted margin/southern Grenville region boundary is significant to the hazard and that there is no extension of the St. Lawrence rift system into the Lake Ontario region. These sources are shown on Plates 1a through 3b of the Part 1 report. Figure 2-3b shows the results for the assumption that there is an extension of the St. Lawrence rift system into the Lake Ontario region and that the aulacogens (Ottawa graben, Saguenay graben, St. Lawrence extension) represent separate source zones. These sources are shown on Plates 4a through 9a of the Part 1 report. Figure 2-3c shows the results for an extension of the St. Lawrence rift system and the aulacogens are not separate from the Iapetan rifted margin regional source zone. These sources are shown on Plates 4b through 9b of the Part 1 report. The hazard curves shown on Figures 2-3a, 2-3b, and 2-3c are averaged over the three alternative Iapetan rifted margin/southern Grenville region boundaries For high spectral frequency ground motions, the major contributors to the hazard are the southern Grenville region source zone and the southwestern extension of the St. Lawrence rift system (assuming that

it exists as a separate source). The sites lie within or very near the southern Grenville region source zone. If the St. Lawrence extension is assumed to be part of a larger Iapetan rifted margin source, then the Iapetan rifted margin source becomes the largest contributor to the high spectral frequency ground motion hazard. The relative contributions of the various sources change somewhat when low spectral frequency ground motions are considered. The Iapetan rifted margin source is a major contributor to the hazard regardless of the zonation assumptions and the distant Great Meteor Hotspot (GMH) source becomes more significant. This is because these sources are more likely to have larger maximum magnitudes, especially the Great Meteor Hotspot source zone and low spectral frequency ground motions are more sensitive to the magnitude of the earthquake.

Figure 2-4 shows the contributions of the various source zones defined in the composite lineament-seismicity regional model (Plate 11 of the Part 1 report). The sites lie within the Rochester source zone, an area of low seismicity compared to the surrounding sources. The major contributors to the hazard are the more active Niagara zone to the southwest and for low spectral frequency ground motions the active Maniwaki zone to the northeast and other regional sources outside of the area defined by the composite lineament-seismicity regional model. The Maniwaki zone encompasses essentially the same region as the Great Meteor Hotspot zone in the geologic regional model. The other regional sources were taken from the seismicity based model shown on Plate 13 of the Part 1 report.

Figure 2-5 shows the contributions of the various source zones to the hazard for the seismicity based regional model (Plate 13 of the Part 1 report). The controlling sources for high spectral frequency ground motion hazard are the Niagara-Attica trend (NAT) and the source zone that includes sites, the Ontario background source (OBGH). As was the case for the other two regional models, the distant sources with high activity and larger maximum magnitudes have a significant contribution to the hazard for low spectral frequency ground motions.

Figure 2-6 shows the contributions of the individual local sources to the total hazard from local sources. The hazard curve for each local source are weighted by the probability that the source is seismogenic. The largest contributors to the hazard are the Niagara-Pickering linear zone (NPLZ) and the Clarendon-Linden fault system (CLFS). Among the local sources, the Clarendon-Linden fault system has the highest probability of being seismogenic (0.4). The Niagara-Pickering linear zone has the second highest probability of being seismogenic and it lies very close to the Pickering site. The hazard from local sources is higher at the Pickering site because more of them lie near this site than near the Darlington site.

Another way of examining the contributions to the hazard is to disaggregate the results to show the relative contributions from earthquakes in individual magnitude and distance increments. These results are displayed on Figures 2-7 and 2-8. Figure 2-7 shows, ¼ unit magnitude intervals, histograms of the relative contributions of earthquakes to the hazard at ground motions with return periods of approximately 1,000, 10,000, and 100,000 years (annual frequencies of exceedance of 10^{-3}, 10^{-4}, and 10^{-5}, respectively). Results are further separated by source type. These results indicate that there is a shift to contributions from larger magnitude earthquakes as the frequency of exceedance decreases (return period increases) and that the hazard for low spectral frequency ground motions is controlled by larger magnitude earthquakes than those that control the hazard for high spectral frequency ground motions. Figure 2-8 presents the same disaggregation histograms now separated into the contributions from three distance ranges. These results indicate that at low annual frequencies of exceedance nearby earthquakes become increasingly important to the hazard. They also show that distant events have a larger contribution to the low spectral frequency ground motion hazard.

2.2 Sensitivity Analyses

The following section presents the results of sensitivity analyses that examine the impact of the alternative modeling and parameter assumptions represented in the 19 levels of the overall seismic hazard model logic tree. These analyses are accomplished by selecting a node of the logic tree and computing the mean hazard giving each branch in succession a weight of unity and all of the other branches at that node a weight of zero. For example, Figure 2-9 examines the impact of the three alternative regional modeling approaches on the hazard from regional sources. The plots display mean hazard curves for regional sources that assume in turn that the geologic approach is correct (weight of 1.0), the composite lineament-seismicity model is correct, or the seismicity- based model is correct. The plots also show the mean hazard curve for the regional sources (the weighted average of the three alternative regional modeling approaches) and the 5th- and 95th-percentile hazard curves computed considering all of the uncertainties in the regional source hazard. The variation in the hazard curves for the individual regional source modeling approaches compared to the spread between the 5th- and 95th-percentile hazard curves indicates the relative contribution of the uncertainty in this issue to the total uncertainty in the hazard.

2.2.1 Regional Sources

Figure 2-9 shows the effect of the three alternative approaches to defining regional sources on the hazard. The results indicate that the alternative regional modeling approaches do not result in large differences in the computed hazard. There is greater sensitivity displayed by the high spectral frequency ground motion hazard because the alternative regional modeling approaches have more impact on the configuration of the regional sources in the vicinity of the sites than on the configuration of the distant active sources. As indicated on Figure 2-8, nearby earthquakes play a larger role in the high spectral frequency ground motion hazard than in the low spectral frequency ground motion hazard.

The next level of the regional source model logic tree addresses the significance of the Iapetan rifted margin/southern Grenville region boundary. Figure 2-10 shows hazard results for the case when the Iapetan rifted margin is separated from the southern Grenville region, forming two large regional zones, and for the case when the entire Grenville domain (GD) is combined into a single regional zone (see Plate 10 of the Part 1 report). These two cases are compared with the mean, 5th- and 95th-percentile hazard curves computed for just the geologic regional model. Assuming the entire Grenville province is a single regional zone results in higher hazard because it averages the distant higher seismicity regions into the regional source zone that contains the site, resulting in a predicted higher rate of earthquake activity in the site vicinity. The mean hazard curve lies close to the hazard curve for the separate Iapetan rifted margin/southern Grenville region zonation model because this regional modeling assumption was given much higher weight (0.9) compared to that of a single Grenville regional source zone (0.1).

Figure 2-11 shows the impact of the alternative locations for the Iapetan rifted margin/southern Grenville region boundary on the hazard computed assuming that the Iapetan rifted margin/southern Grenville region boundary is significant. The highest hazard is produced by assuming that the boundary is at the CMBBZ, which places the sites in the more active Iapetan rifted margin regional zone (see Plates 2a and 2b of the Part 1 report). The lowest hazard results from assuming that the boundary is in the area of the Western Adirondack Uplift (WAU), resulting in a large distance from the sites to the Iapetan rifted margin regional zone. Again, the sensitivity is greater for high spectral frequency ground motion hazard than for low spectral frequency ground motion hazard because the alternative Iapetan rifted margin/southern Grenville region boundaries do not affect the source zone configuration in the active area north of the Ottawa graben.

Figure 2-12 shows the impact of assumptions about the existence of an extension of the St. Lawrence rift system into the Lake Ontario region and the location of the northern

boundary of such an extension. The results indicate that such an extension would have a significant impact if the northern boundary lies to the north of the sites, placing them in the Iapetan rifted margin regional zone.

Figure 2-13 shows the impact of considering the aulacogens in the regional geologic model (the Ottawa and Saguenay grabens and the postulated St. Lawrence rift system extension) as either separate source zones or as part of the Iapetan rifted margin regional zone. The results indicate a very slight increase in the hazard when the aulacogens are considered to be part of the Iapetan rifted margin regional zone because in results in a slight increase in the average rate of earthquakes in the site vicinity.

Figure 2-14 shows the impact of the alternative spatial density models considered for the geologic regional source model. Two alternatives were considered, uniform spatial density and a nonparametric spatial density derived by using kernel density estimation. Three alternative values were used for the standard deviation of the Gaussian kernel, h, 25, 50, and 100 km. Assuming a uniform density produces the highest hazard because it averages the areas of high seismicity rate along the St. Lawrence in the Iapetan rifted margin regional zone (and in the Ottawa Graben when it is considered part of the Iapetan rifted margin regional zone) together with the areas of low seismicity near the sites, resulting in a higher average seismicity rate near the site. The use of a small value for h results in a lower hazard at the sites because it restricts the higher seismicity to the south from extending into the site region.

The other modeling issue related to regional zonation is the alternative approaches used for the seismicity-based regional source model. Two approaches were used, one using source zones defined on the basis of spatial patterns of seismicity (see Plate 13 of the Part 1 report) and one using the regional smoothing algorithm developed by Veneziano and van Dyck (1985). The latter approach estimates the seismicity parameters in 1° latitude × 1°

longitude cells, imposing a specified degree of smoothness in the activity rate and/or the *b*-value. Four alternative degrees of smoothness were used, ranging from no constraint (high spatial variability) on the activity rate and a weak constraint (moderate spatial variability) on the *b*-value (option A) to a weak constraint (moderate spatial variability) on the activity rate and a moderate constraint (low spatial variability) on the *b*-value. (option D) (see Appendix A). The seismicity source zone approach produced similar levels of hazard to that of the spatial smoothing approach, except at low annual frequencies of exceedance, where the results are slightly lower for high spectral frequency motions because the seismicity zone approach restricted the seismicity in the vicinity of Niagara to larger distances from the site than does the smoothing approach.

The remaining uncertainties addressed in modeling the regional sources are in the maximum magnitude, seismicity rate, and *b*-value for the individual sources. The uncertainty in these parameters were represented by the distributions given in Appendix A. To display the sensitivity of the hazard results to the alternative seismicity parameter values, the distribution in the frequency of exceedance was disaggregated to show the effect of uncertainty in one parameter averaged over the uncertainties in all of the remaining parameters. These results are presented in Figures 2-16, 2-17 and 2-18 for maximum magnitude, seismicity rate, and *b*-value, respectively. Each figure presents the mean hazard for regional sources, the 5^{th}- and 95^{th}-percentile hazard curves considering all of the uncertainties in the regional source hazard model and the 5^{th}- and 95^{th}-percentile hazard curves considering the uncertainty in only the specified parameter. The maximum magnitudes that were incorporated into the analysis range from m_b 5.5 to 7.5+. This variability produces a significant effect on the computed hazard, with greater effect for low spectral frequency ground motion hazard because of the larger contribution from large magnitude earthquakes (Figures 2-7 and 2-8).

There was generally only a small degree of uncertainty in the seismicity rate for the regional zones because the number of recorded earthquakes was sufficient to constrain the estimate in the maximum likelihood approach used (see Appendix A). As a result, the range in seismicity rates has a small impact on the hazard. It should be noted that the range in seismicity rates reflected on Figure 2-17 is *given* a particular source zonation. Alternative source zonations do lead to significant differences in the average seismicity rate and these results are reflected in the sensitivity analyses presented previously.

The *b*-values for the individual source zones are less well constrained by the recorded seismicity and small variations in *b*-value may result in significant differences in the predicted frequency of larger earthquakes. Thus, as indicated by the results shown on Figure 2-18, the variability in *b*-values has a moderate effect on the computed hazard.

2.2.2 Local Sources

In the logic tree for local sources, the first source modeling issue addressed is the association of the Rouge River faults with other potential sources. Three alternatives were considered: the Rouge River faults are a potentially independent source, they are associated with the Niagara-Pickering linear zone source, or they are associated with the Georgian Bay linear zone source. Figure 2-19 shows the mean hazard from local sources computed under each of the three assumptions. (Note that the 5th-percentile hazard curve does not appear on the plots because there is a greater than 0.05 probability that none of the local sources are seismogenic, and thus the hazard from them is zero.) The alternative assumptions concerning the association of the Rouge River faults with other sources lead to very similar estimates of hazard because the association of the faults with either the Niagara-Pickering linear zone or the Georgian Bay linear zone has a very minor impact on the probability that they are seismogenic, and the Rough River faults have a very low probability of being seismogenic if they are a separate feature.

The next fourteen figures show the sensitivity to whether an individual local source is known to be seismogenic or known to be not seismogenic. The assessment of the probability that the individual local sources are seismogenic is presented in Table 3-3 of the Part 1 report. Figures 2-20a and 2-20b show the results of the sensitivity analysis for the Rouge River faults in terms of the effect on the hazard from local sources only and the effect on the total hazard, respectively. There is a significant increase in the hazard if the Rouge River faults are assumed to be seismogenic, particularly at Pickering, the closest site to the faults. However, if the Rouge River faults are assumed to be not seismogenic, there is only a very minor decrease in the hazard.

Figures 2-21a, b, 2-22a, b, 2-23a, b, 2-24a, b, 2-25a, b, and 2-26a, b show similar sensitivity studies for the Niagara-Pickering linear zone, Georgian Bay linear zone, Toronto-Hamilton seismic zone, Hamilton-Presqu'ile fault, Wilson-Port Hope lineament, and Clarendon-Linden fault system, respectively. Each analysis produced similar results, an increase in the hazard if the source is assumed to be seismogenic and a smaller decrease in the hazard if the source is assumed to be not seismogenic. The smaller decrease in hazard when an individual source is assumed to be not seismogenic occurs because the probability that each is seismogenic was assessed to be significantly less than 0.5 in most cases, and because there are multiple sources contributing to the hazard from local sources. The relative impact between the hazard at the two sites depends on which site is closer to the particular source in question.

The next level of the logic tree for the local sources addresses is the use of a *prior* in the estimation of the *b*-value for the local sources. Because of the limited seismicity associated with individual local sources, the *b*-values are poorly constrained and require stabilization to constrain the uncertainty estimates to reasonable values. As discussed in Appendix A, this accomplished by imposing a prior estimate of the *b*-value based on the results of fitting the seismicity parameters for the regional source zones. The alternatives considered were

the use of a weak constraint or a strong constraint on the *b*-value. A weak constraint allows for greater variability in the *b*-value and for greater departure from the regional *b*-value. Figure 2-27 shows the impact of a strong versus weak prior on the computed hazard. The use of a weak prior results in slightly higher hazard because it allows for the possibility of smaller *b*-values, which lead to higher predicted frequencies for large events.

Two alternatives were considered for modeling the characteristics of the local sources. One approach was to consider that the local sources act as concentrations of seismicity within the regional zones, and thus, have the attributes of the host regional zone. Under this assumption, the magnitude distribution was assumed to conform to the truncated exponential distribution appropriate for regions and the maximum magnitude distribution was assumed to be the same as that of the regional zone in which the source lies. The other approach was to assume that the local sources act truly as individual faults with the characteristics one would attribute to them. Under the fault-like assumption, the magnitude distribution was assumed to conform to the characteristic magnitude model and the maximum magnitude distribution was estimated from postulated maximum rupture dimensions. Consideration of fault-like behavior resulted in larger maximum magnitudes and for a much higher predicted frequency of large events. As a result, the alternative modeling assumptions for the local sources have a major impact on the hazard, as illustrated on Figure 2-28.

In addition, when utilizing the fault-like assumption for the behavior of the Rouge River faults source, two alternatives were used to estimate the seismicity rate, one based on recorded seismicity and one based on fault slip rate estimates. These two approaches yielded similar estimates of the hazard.

The remaining uncertainties addressed in modeling the local sources are in the maximum magnitude, seismicity rate, and *b*-value for the individual sources. The uncertainty in

these parameters were represented by the distributions given in Appendix A. These results are presented in Figures 2-29, 2-30 and 2-31 for maximum magnitude, seismicity rate, and *b*-value, respectively. The effect of the variability in maximum magnitudes is smaller for the local sources than for the regional sources because these sources are close to the site and earthquakes smaller than those near the maximum magnitude have a large contribution to the hazard. The seismicity parameters (seismicity rate and *b*-value) for the local sources were estimated from much smaller data sets than used to obtain the seismicity parameters for the regional sources. Thus, there is a larger statistical uncertainty in the local source seismicity parameters than in the regional source seismicity parameters. The larger uncertainty in seismicity rate leads to a larger range in possible values and a greater contribution to the uncertainty in the hazard. The effects of variability in *b*-value are slightly less for the local sources than for the regional sources, again because of the greater certainty in the *b*-values estimated from a small data set.

2.2.3 Ground Motion Attenuation

The uncertainty in characterizing ground motion attenuation was modeled in two ways. First, three alternative relationships were used to represent the uncertainty in modeling the earthquake source. These relationships were the model developed by EPRI (1993) (also published as Toro and others, 1997), the model developed by Atkinson and Boore (1995) (also published as Atkinson and Boore, 1997), and a model developed using the earthquake source spectra proposed by Haddon (1996). Figures 2-32a, 2-32b, and 2-32c compare the hazard computed assuming that each of the three attenuation models is the correct model for regional sources, local sources, and all sources, respectively. The Haddon (1996) source model predicts substantially larger high spectral frequency motions than the other two attenuation models and results in significantly higher hazard for peak acceleration. At spectral frequencies near 1 Hz, there are significant differences in the source spectra between all three attenuation models resulting in significant differences in the estimates of 1 Hz spectral acceleration. The two-corner earthquake source spectra model employed by

Atkinson and Boore (1995) predicts much lower 1 Hz motions, especially for larger magnitude earthquakes. The use of the Haddon (1996) source spectra predicts higher motions than that of the standard Brune source spectra model employed in the EPRI (1993) relationships, but the differences are less than those at higher spectral frequencies. As a result, there is a large spread in the predicted motions between the three alternative attenuation models.

The second level of uncertainty addressed in characterizing ground motion attenuation was in estimating the average parameters of the earthquake source spectra, crustal path characteristics and shallow crustal response. These uncertainties were modeled using the epistemic uncertainty relationships developed by EPRI (1993) which characterize the uncertainty in a ground motion attenuation relationship by a lognormal distribution about the median ground motion. Three alternative attenuation relationships were developed for each of the attenuation models, one using the specified median model parameters, one using the 5th-percentile of the lognormal distribution in the median ground motion (-1.645 standard deviations), and one using the 95th-percentile of the lognormal distribution in the median ground motion (+1.645 standard deviations). Figures 2-33a, 2-33b, and 2-33c shows the variability in the computed hazard resulting from the epistemic uncertainty model. Hazard results are shown for the median, 5th-, and 95th-percentile attenuation relationships. The effect is significant, indicating similar variability as that shown for the alternative source spectral models for high spectral frequency ground motions and slightly smaller variability that the effect of the source model for low spectral frequency ground motions.

2.3 Contributions to Uncertainty

The percentile hazard curves on the proceeding figures display the uncertainty in the frequency of exceeding various ground motion levels. The uncertainty can be measured by the variance in the frequency of exceedance computed from the discrete distribution

defined by the logic tree. This variance can then be disaggregated to obtain the portion due to each level of uncertainty in the logic tree. Figures 2-34, 2-35, and 2-36 present the results of such a disaggregation of the variance for the regional sources, the local sources, and the combined hazard from all sources, respectively. In each figure separate histogram plots show the percent of the total variance in the annual frequency of exceedance contributed by the uncertainty in each of the 19 levels of uncertainty in the seismic hazard model described in Section 1.1. These percentages provide a quantitative measure of the variability in the hazard shown in the sensitivity analyses for individual elements of the uncertainty model compared to the total variability in the hazard. Histograms are provided for ground motions with the same three return periods used in Figures 2-7 and 2-8.

The results shown on Figure 2-34 for the regional sources indicate that the largest contributors to the uncertainty in the hazard are the uncertainties in defining the appropriate ground motion attenuation relationships. The source characterization issues with the largest contributors to uncertainty in the hazard are the alternative regional zonation bases and *b*-value uncertainty for high spectral frequency ground motions and uncertainty in maximum magnitude and *b*-value for low spectral frequency ground motions. As indicated on Figures 2-2 through 2-8, the low spectral frequency ground motion hazard has a greater contribution from the distant active sources whose configuration is not changed significantly by the alternative zonation approaches. For these distant sources, the frequency of larger earthquakes and their maximum size are the primary factors affecting the hazard at the site. The high spectral frequency ground motion hazard is controlled to a greater extent by nearby earthquakes. Thus variations in zonation that affect the distance to the more active sources has more impact on the computed hazard.

Figure 2-35 indicates that the important issues are somewhat different for the local sources. For these sources, the largest contributor to the uncertainty in the hazard is typically the

uncertainty in whether or not the local sources are seismogenic, uncertainty in the *b*-value, and the alternative modeling of local sources (as zones or as faults). The latter two issues affect the frequency of large events on the source. Uncertainty in the seismicity rate for the local sources is more significant because the seismicity rates are less well constrained than those for the regional sources.

Figure 2-36 shows the contributions to the uncertainty in the total hazard. These results are a combination of the results presented on the previous two figures and reflect the relative importance of the regional and local sources to the hazard as a function of spectral frequency and ground motion level (or equivalently, frequency of exceedance). Because the local sources have a greater impact on the high spectral frequency ground motion hazard for a give frequency of exceedance, the seismic hazard characterization uncertainties important to these sources have greater impact on the uncertainty in the total hazard. Similarly, the seismic hazard characterization uncertainties important to the regional sources play a greater role in defining the uncertainty in the hazard for low spectral frequency ground motions.

2.4 Development of Equal-hazard Response Spectra

The PSHA computation was repeated for 8 spectral frequencies: 100 Hz (PGA), 35 Hz, 25 Hz, 10 Hz, 5 Hz, 2.5 Hz, 1 Hz, and 0.5 Hz. Figure 2-37 shows the mean hazard curves for the 8 spectral frequencies for the Pickering and Darlington sites. The mean hazard curves were then used to obtain spectral accelerations at the 8 spectral frequencies with return periods of 500, 1,000, 2,000, 5,000, 10,000, and 20,000 years. The 8 spectral accelerations for a specified return period define an equal-hazard spectrum. The resulting equal-hazard spectra are shown on Figures 2-38 and 2-39 for the Pickering and Darlington sites, respectively. This process was repeated for the 5th- to the 95th-percentile hazard curves and response spectra were drawn through these points. The resulting spectral

curves define the uncertainty in the equal-hazard spectra. The uncertainty bands typically span an order of magnitude in spectral acceleration.

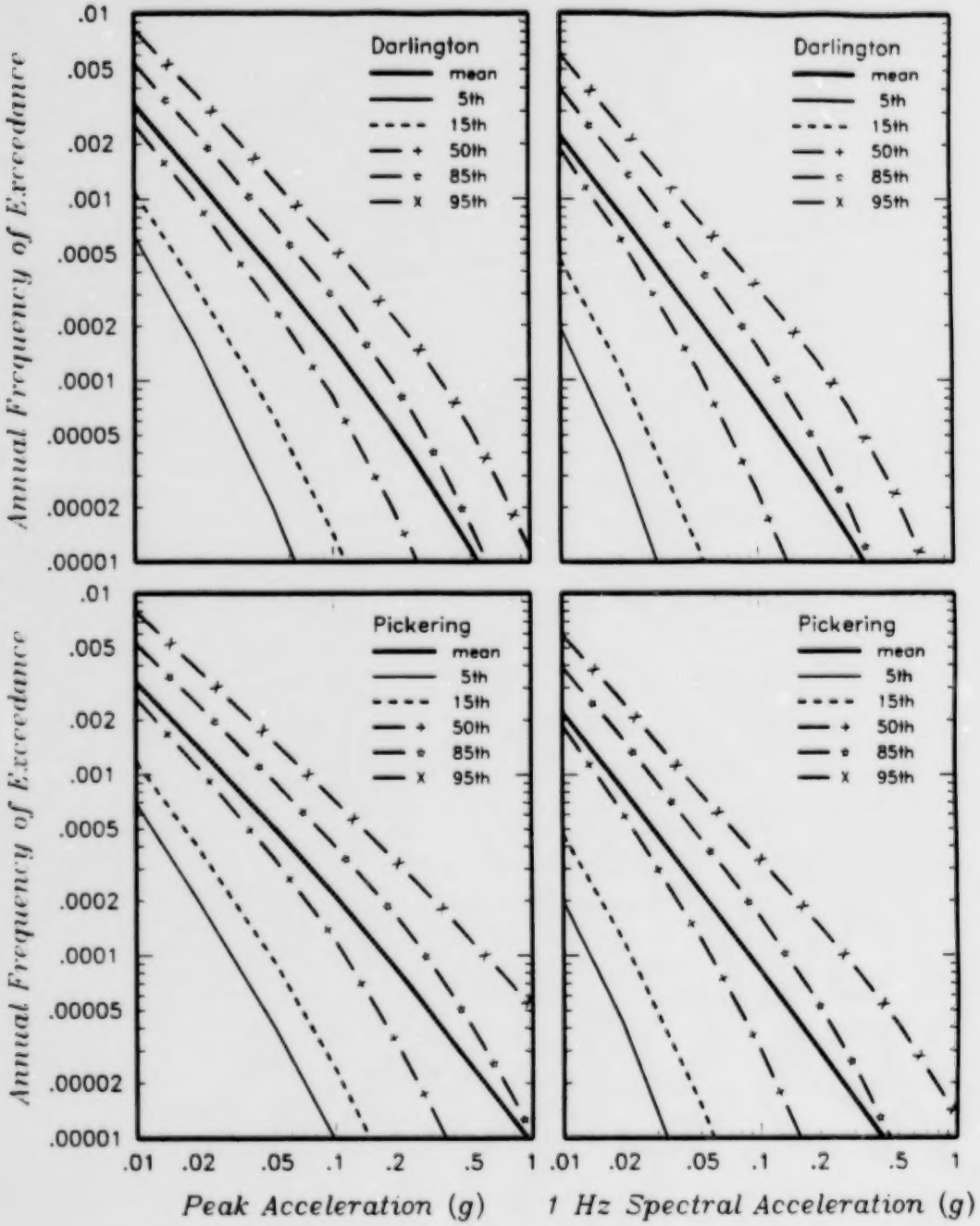

Figure 2-1 Computed hazard curves for Darlington and Pickering sites for peak acceleration and 1 Hz spectral acceleration. Shown are the mean hazard curves for all uncertainties defined in the Part 1 report and the 5th to 95th percentiles of the distributions for frequency of exceedance defined by the uncertainties.

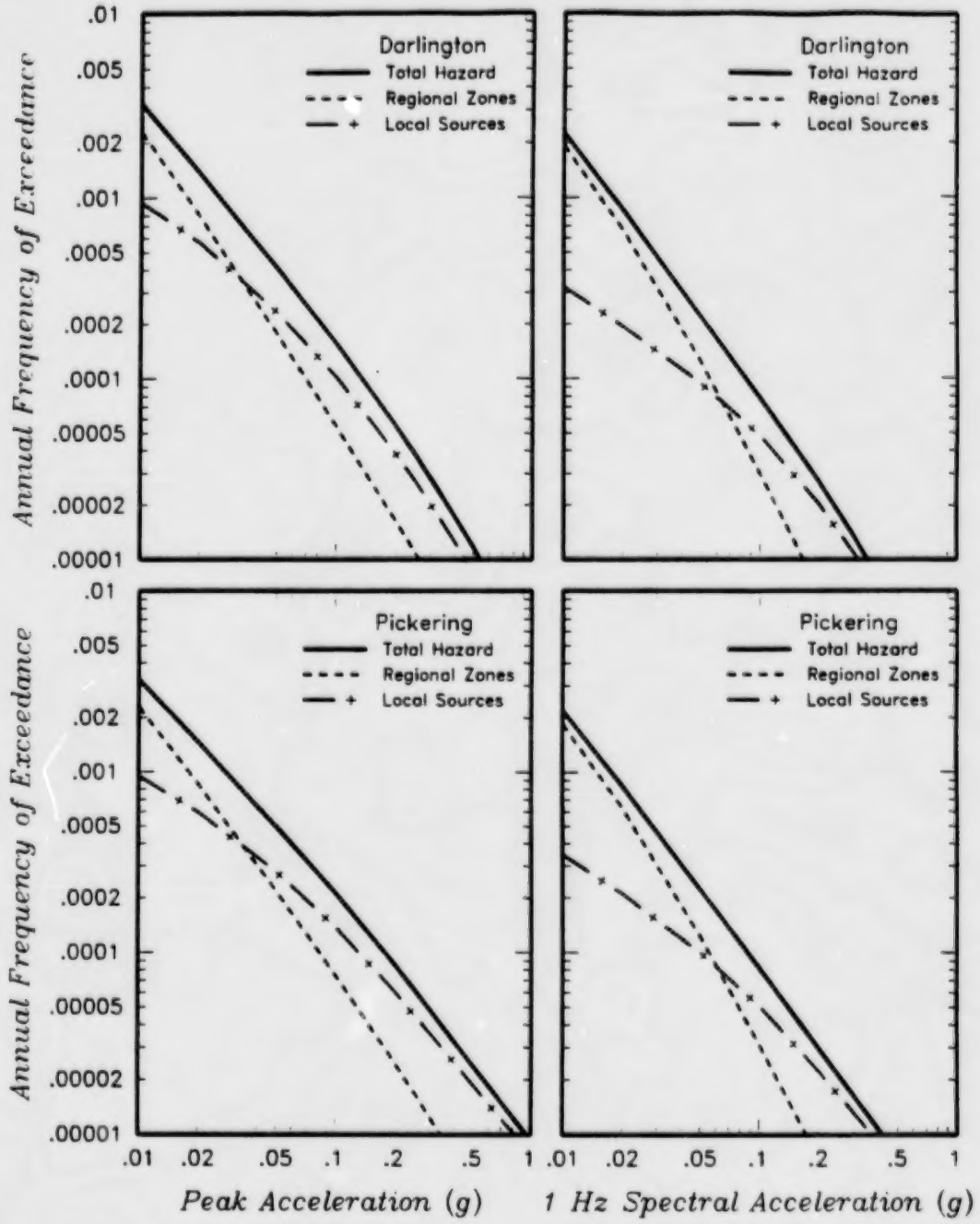

Figure 2-2 **Contribution of regional and local sources to the total mean hazard for the Darlington and Pickering sites.**

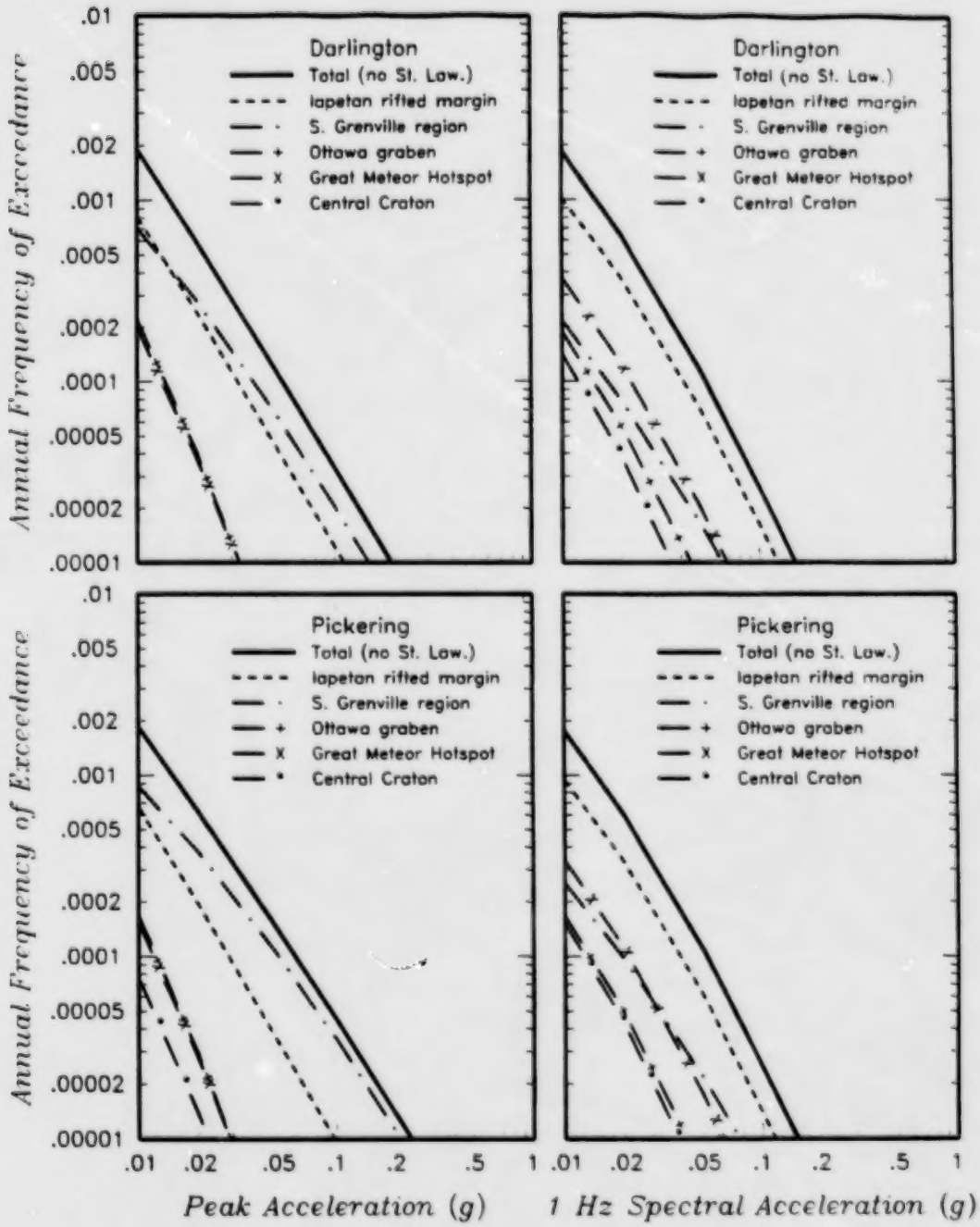

Figure 2-3a Contribution of the various major regional source zones to the total hazard from regional sources (assuming that the Iapetan rifted margin (IRM)/southern Grenville region (SGR) boundary is significant, there is an extension of the St. Lawrence rift system, and that there is no extension of the St. Lawrence rift system). (see Plates 1a through 3b of the Part 1 report).

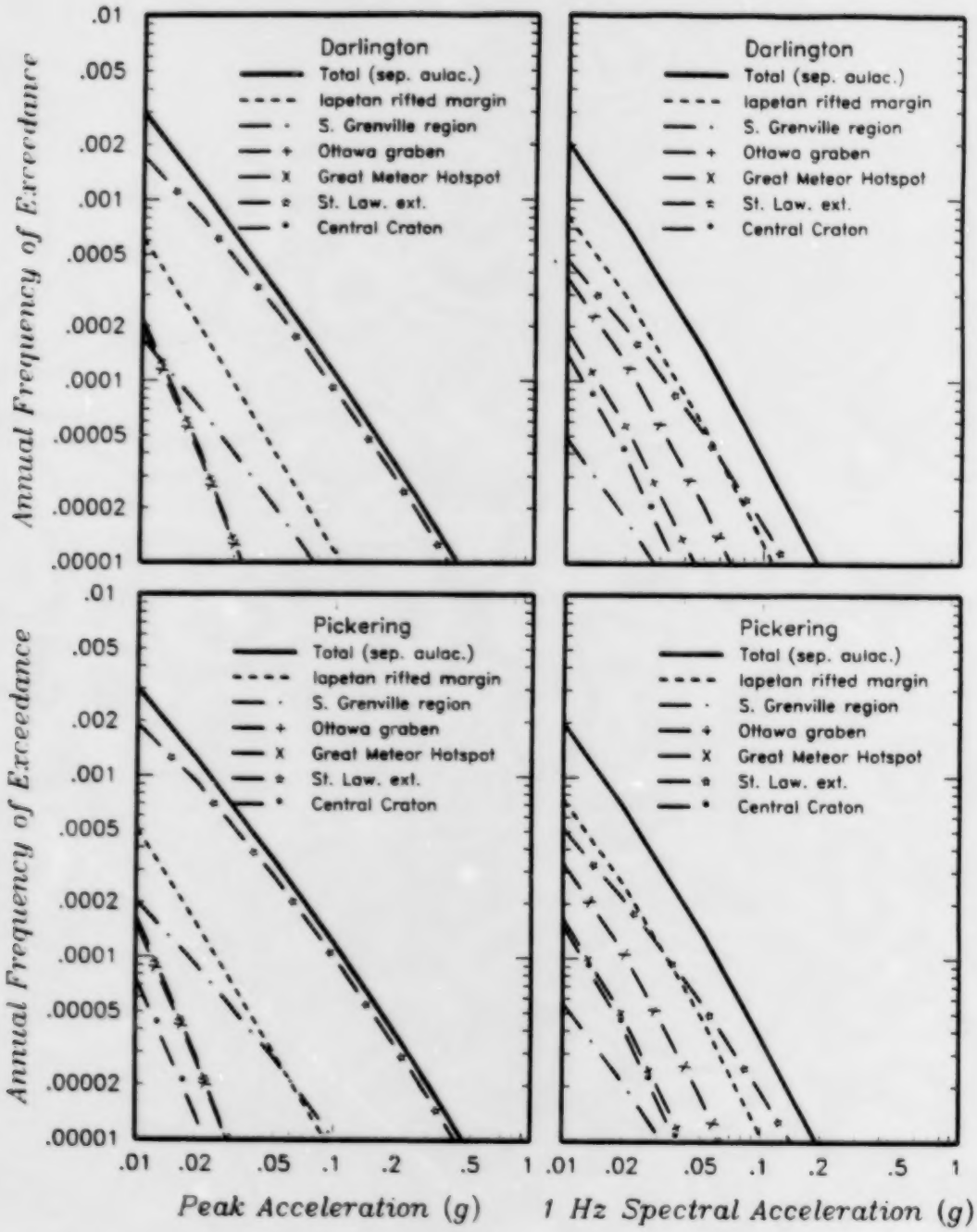

Figure 2-3b Contribution of the various major regional source zones to the total hazard from regional sources (assuming that the Iapetan rifted margin (IRM)/southern Grenville region (SGR) boundary is significant, there is an extension of the St. Lawrence rift system, and that the aulacogens are separate sources). (see Plates 4a through 9a of the Part 1 report).

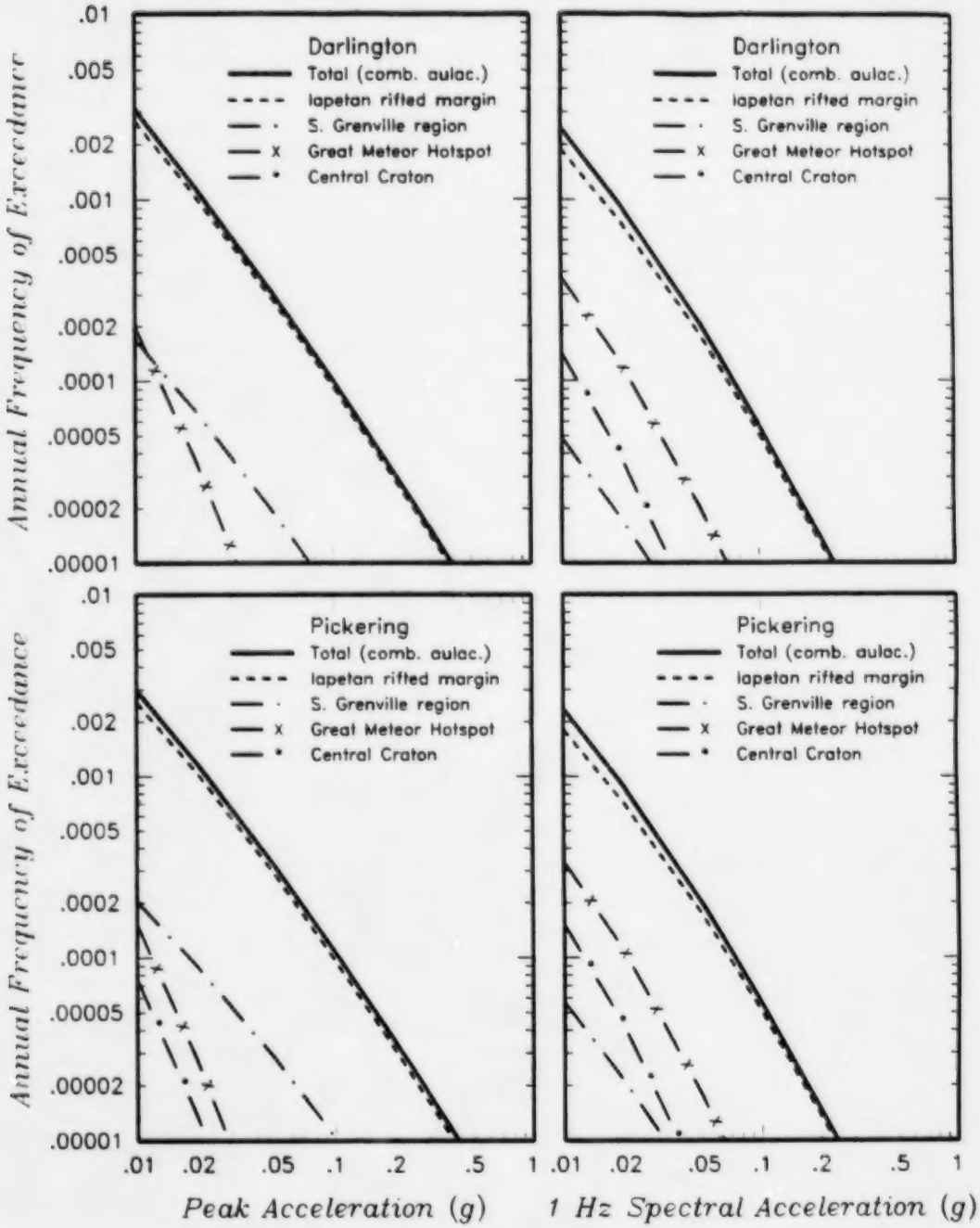

Figure 2-3c Contribution of the various major regional source zones to the total hazard from regional sources (assuming that the Iapetan rifted margin (IRM)/southern Grenville region (SGR) boundary is significant and the aulacogens are combined with the Iapetan rifted margin source zone). (see Plates 4b through 9b of the Part 1 report).

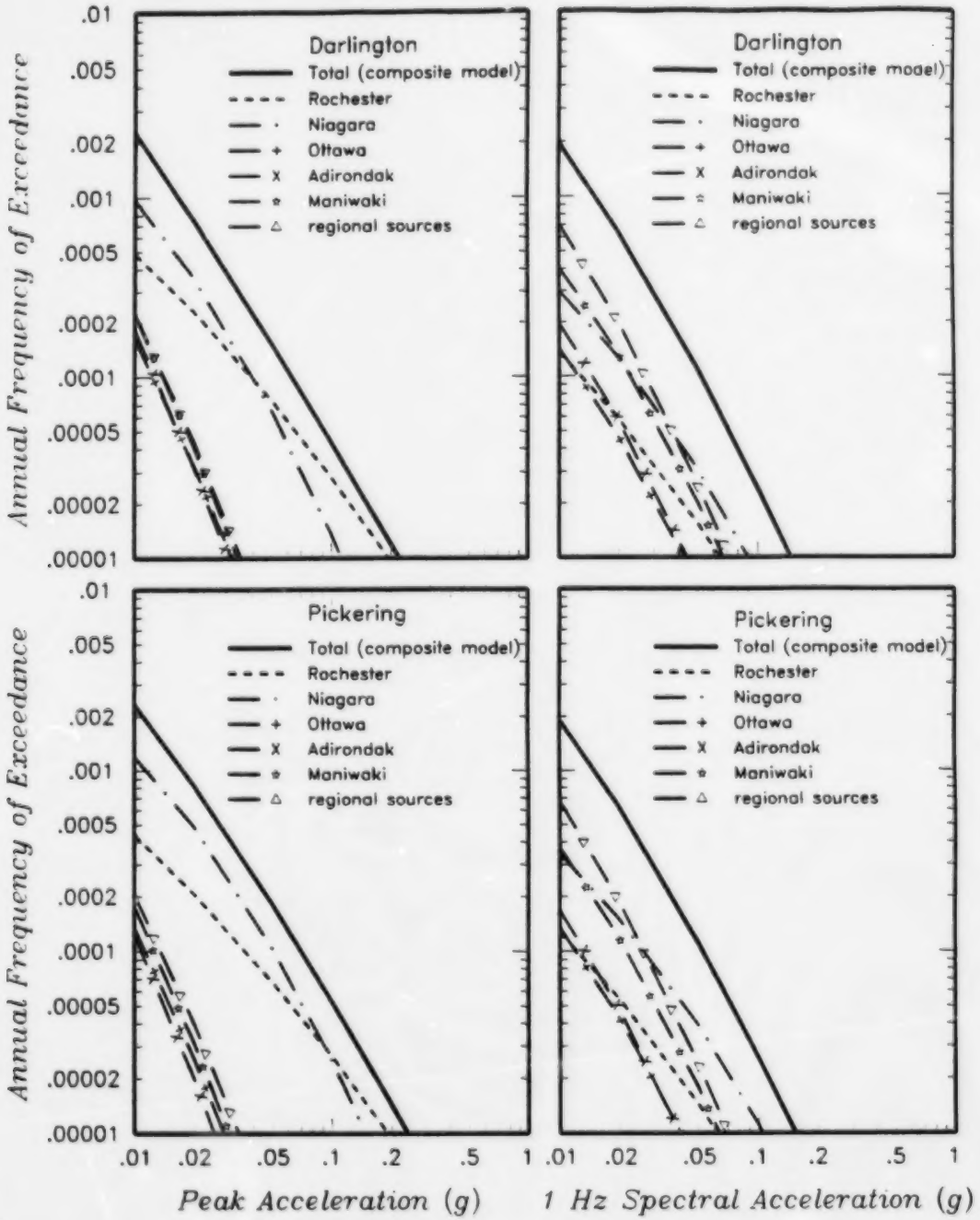

Figure 2-4 **Contribution of the various source zones to the regional lineament/seismicity composite model (see Plate 11 of the Part 1 report).**

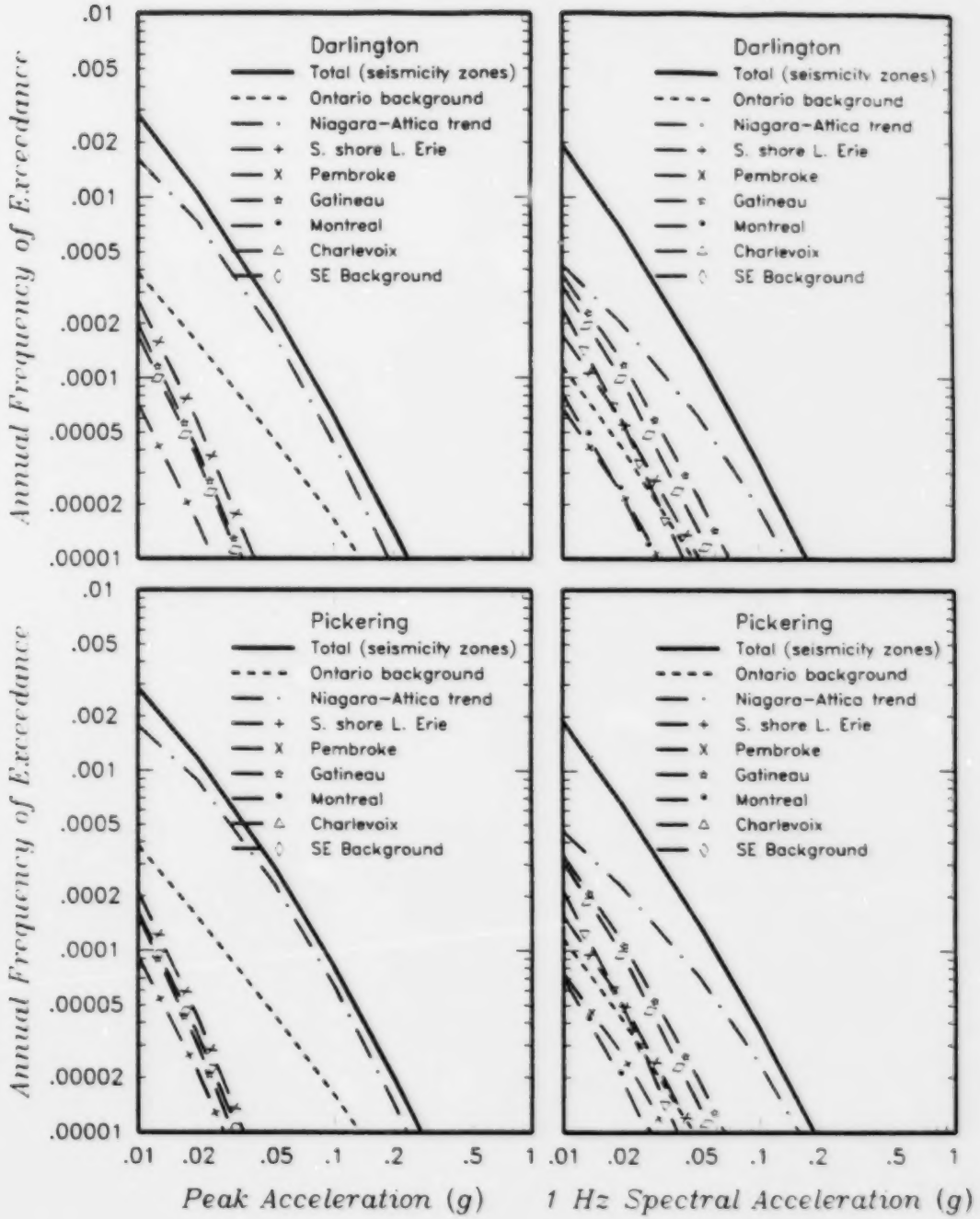

Figure 2-5 **Contribution of various source zones to the total hazard using the seismicity zones from Adams and others (1996) (see Plate 13 of the Part 1 report).**

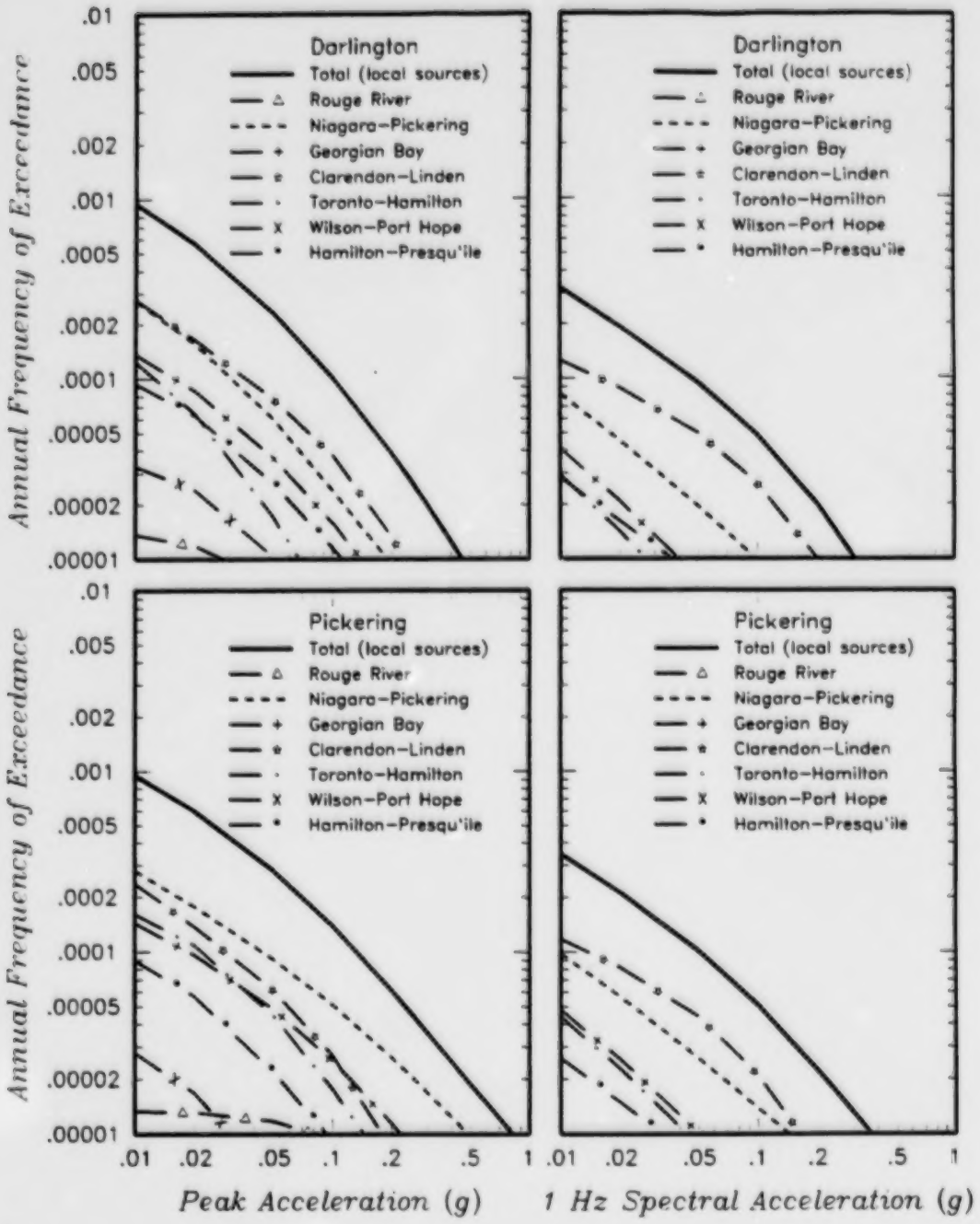

Figure 2-6 Contribution of the various local sources (weighted by their probability of being seismogenic) to the total hazard from local sources.

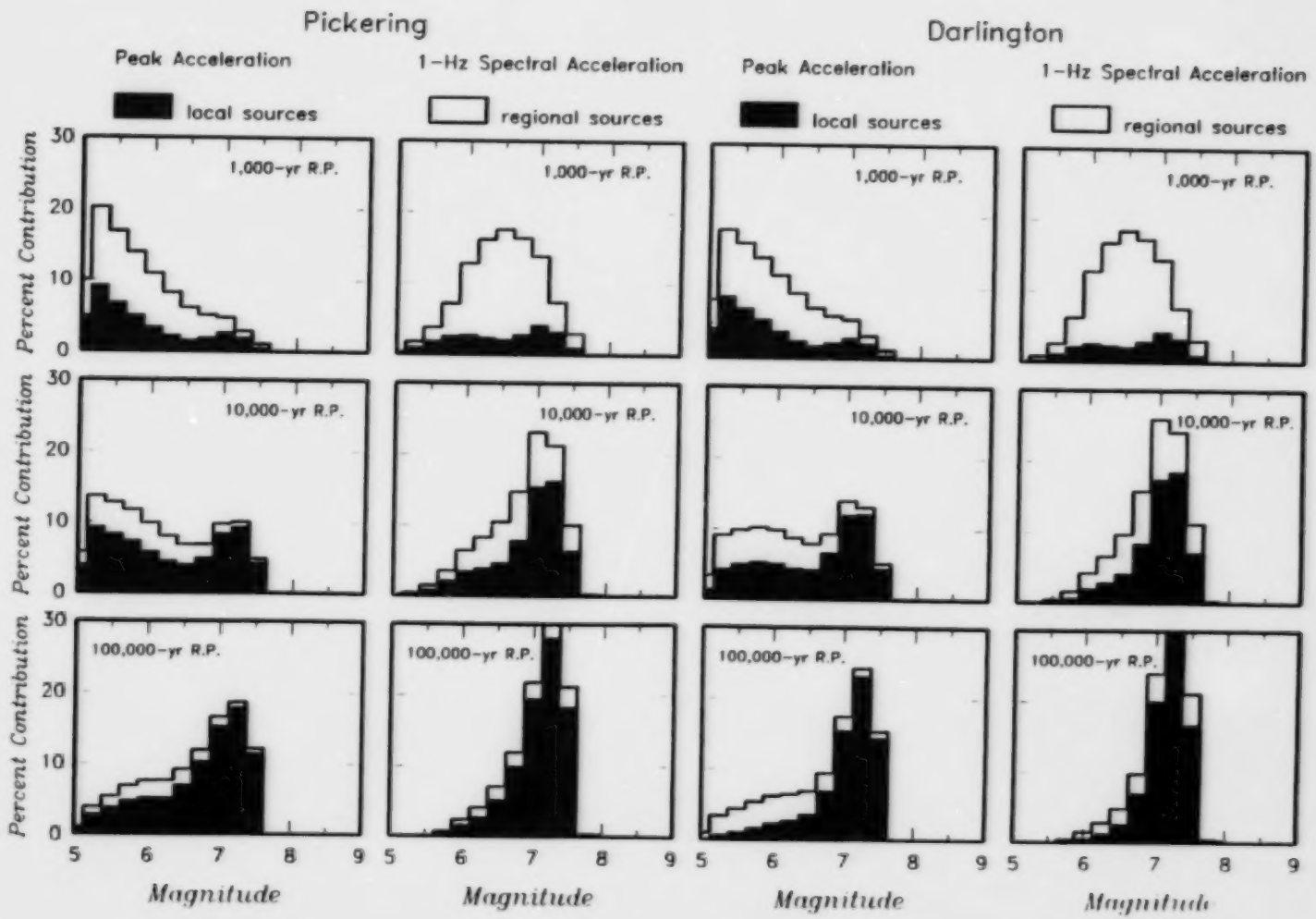

Figure 2-7 **Disaggregation of the hazard showing relative contributions of earthquakes of various magnitudes to the total hazard. Contributions are separated for local and regional sources.**

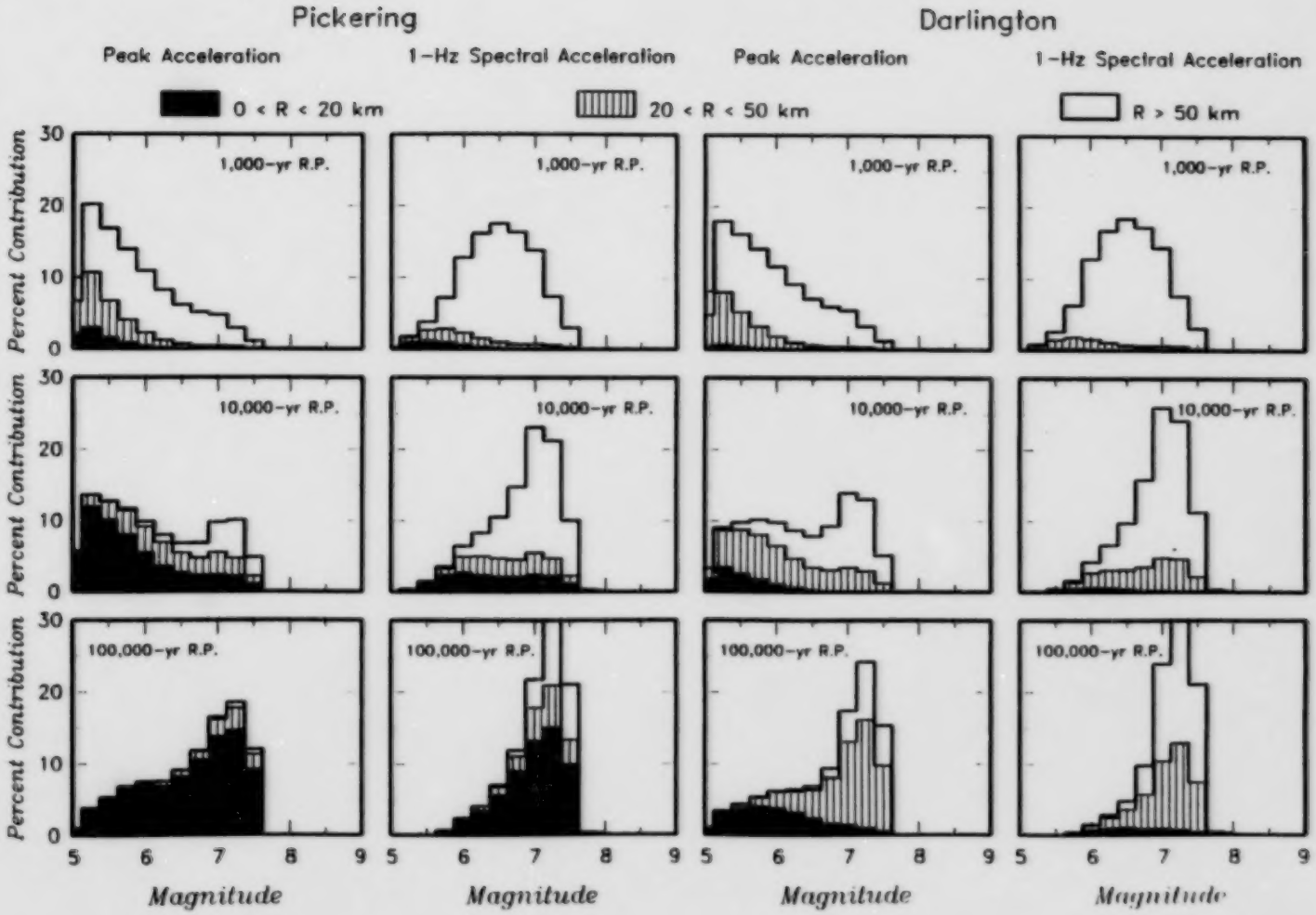

Figure 2-8 Disaggregation of the hazard showing relative contributions of earthquakes of various magnitudes to the total hazard. Contributions are separated into three distance intervals.

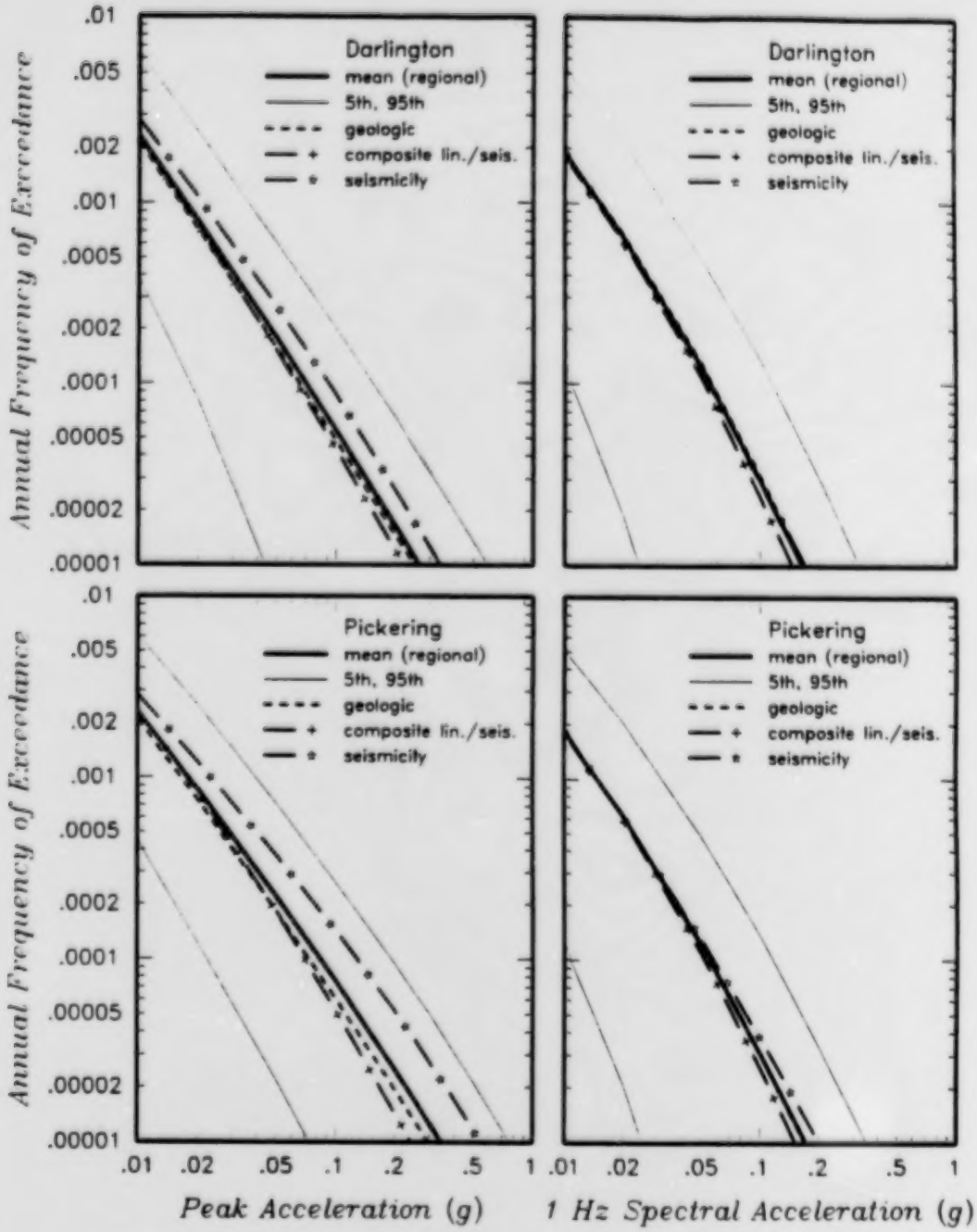

Figure 2-9 Effect of the alternative regional source modeling approaches on the hazard from regional sources only. The thick solid curves show the mean hazard from regional sources and the thin solid lines show the 5th and 95th percentile hazard curves for the regional sources.

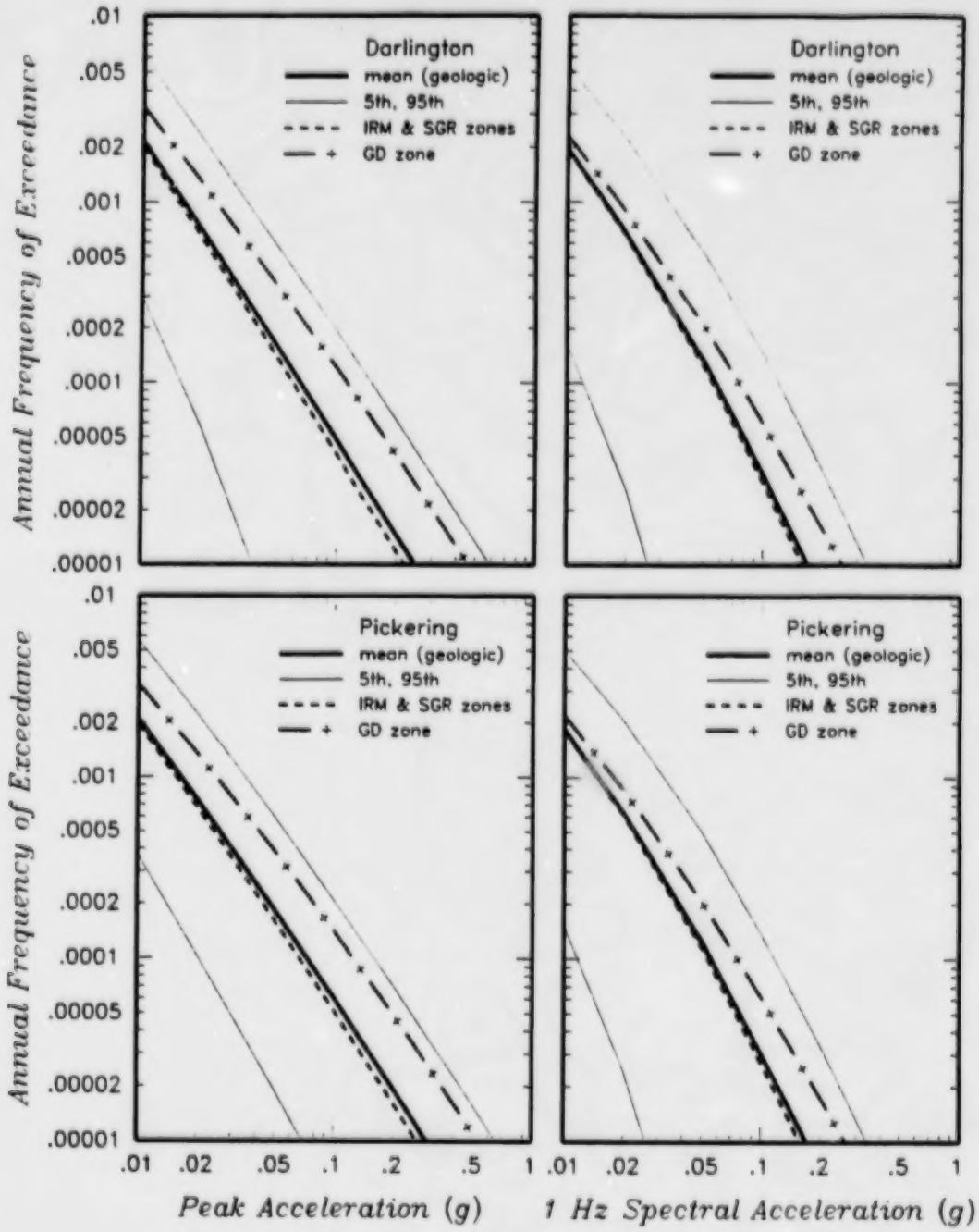

Figure 2-10 Effect of the considering the Iapetan rifted margin (IRM)/southern Grenville region (SGR) boundary to be significant (separate IRM and SGR regional sources) or not significant (a single Grenville domain [GD] regional source). The thick solid curves show the mean hazard from the geologic regional source model and the thin solid lines show the 5th and 95th percentile hazard curves for the geologic regional source model.

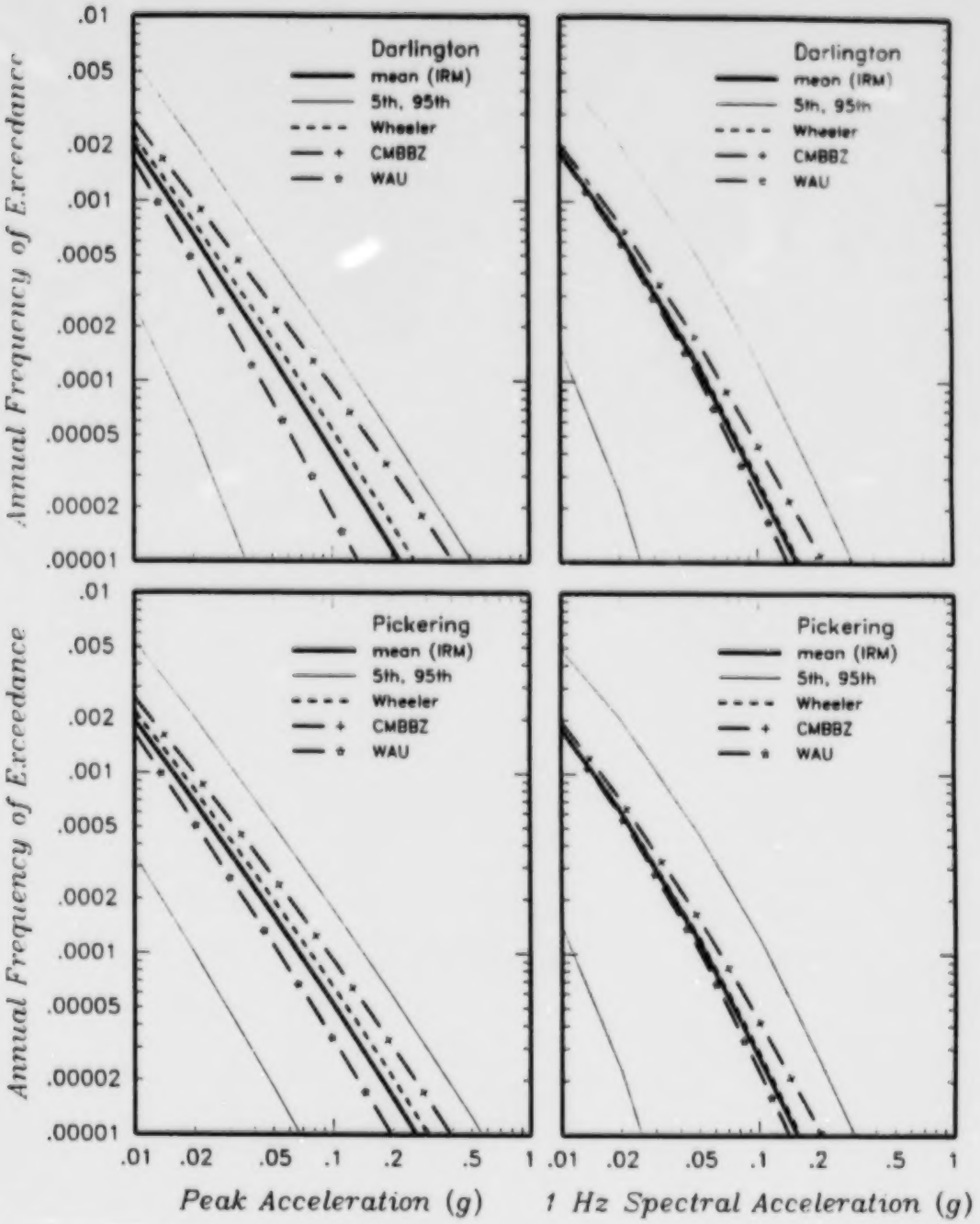

Figure 2-11 Effect of the alternative Iapetan rifted margin (IRM)/southern Grenville region (SGR) boundary locations on the hazard from the geologic source model with a IRM/SGR boundary (see Plates 1 through 9 of the Part 1 report). The thick solid curves show the mean hazard from the geologic regional model with an IRM/SGR boundary and the thin solid lines show the 5th and 95th percentile hazard curves for this case. The proposed boundaries are the location described by Wheeler (1995), at the Central Metasedimentary Belt boundary zone (CMBBZ), and at the western flank of the Adirondack uplift (WAU).

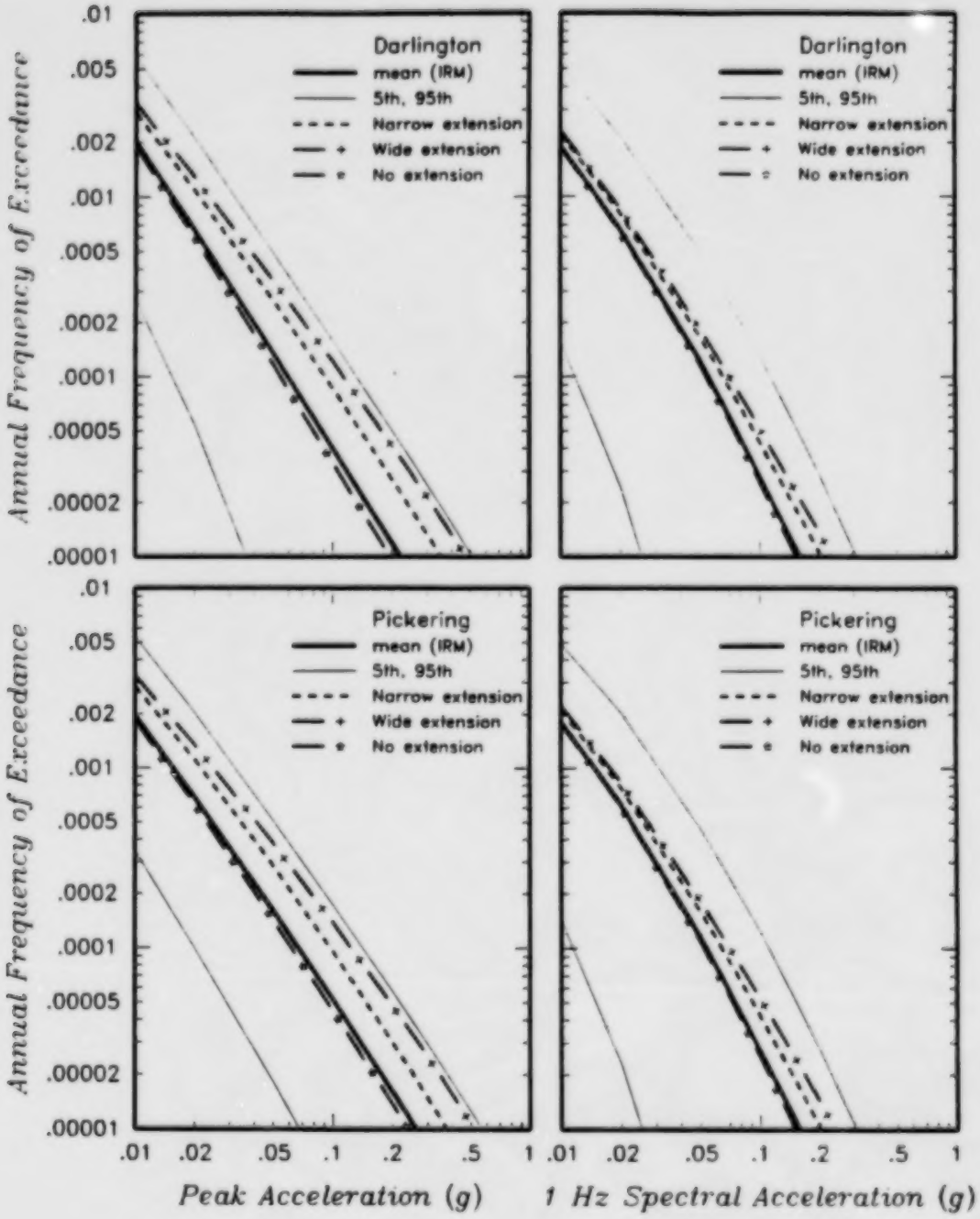

Figure 2-12 Effect of the considering a potential extension of the St. Lawrence rift system into the Lake Ontario region and the effect of alternative northern boundaries for such a source. The thick solid curves show the mean hazard from the geologic regional model with an IRM/SGR boundary and the thin solid lines show the 5th and 95th percentile hazard curves for this case.

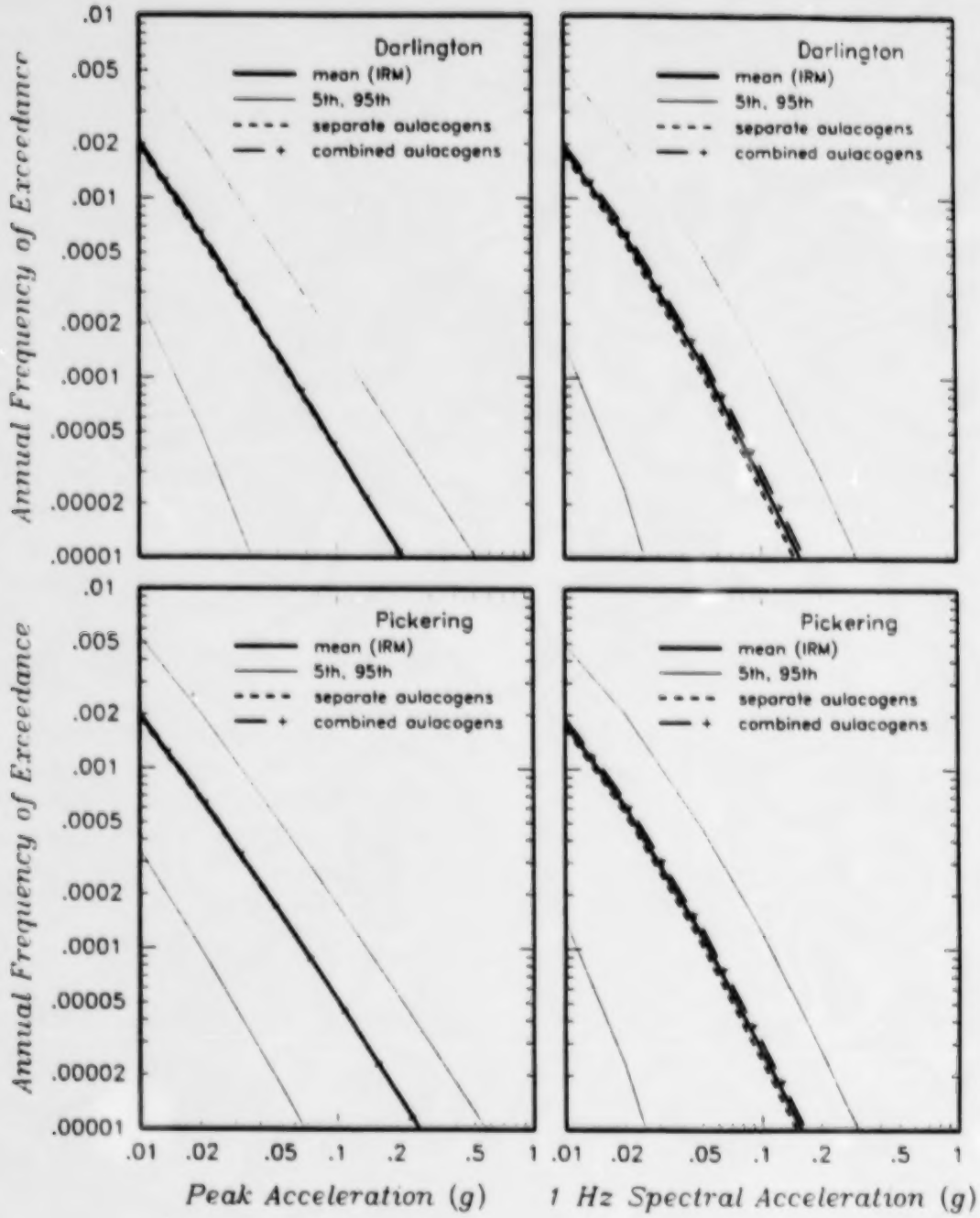

Figure 2-13 Effect of considering the aulacogens (Ottawa graben, Saguenay Graben, and the postulated St. Lawrence extension) as either separate sources (see Plates 1a through 9a of the Part 1 report) or as part of the Iapetan rifted margin (IRM) regional source (see Plates 1b through 9b of the Part 1 report). The thick solid curves show the mean hazard from the geologic regional model with an IRM/SGR boundary and the thin solid lines show the 5th and 95th percentile hazard curves for this case.

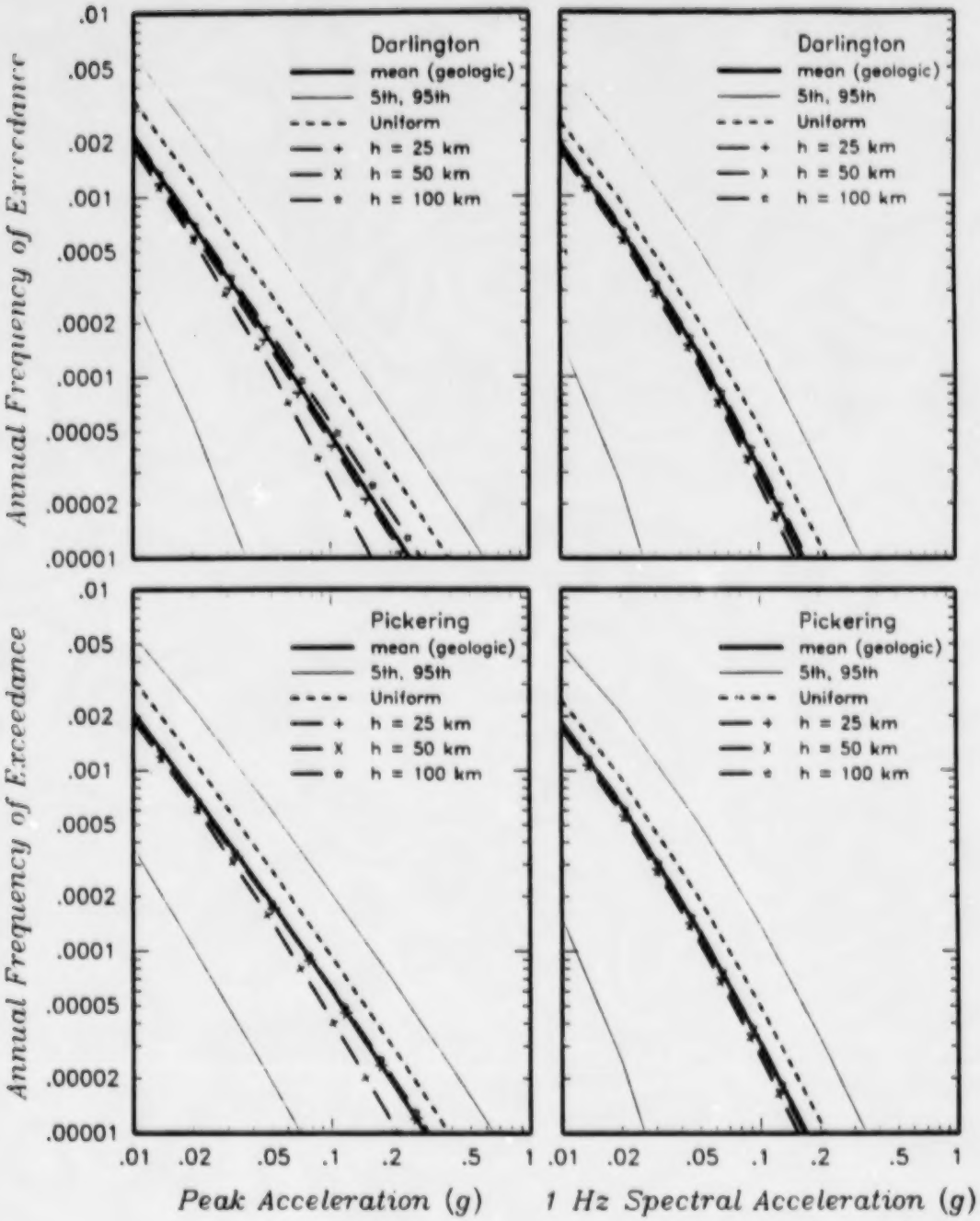

Figure 2-14 Effect of alternative spatial models on the hazard from the geologic regional source model only. The thick solid curves show the mean hazard from geologic regional source model and the thin solid lines show the 5th and 95th percentile hazard curves for this case. The parameter h is one standard deviation for the 2-D Gaussian kernel smoothing function.

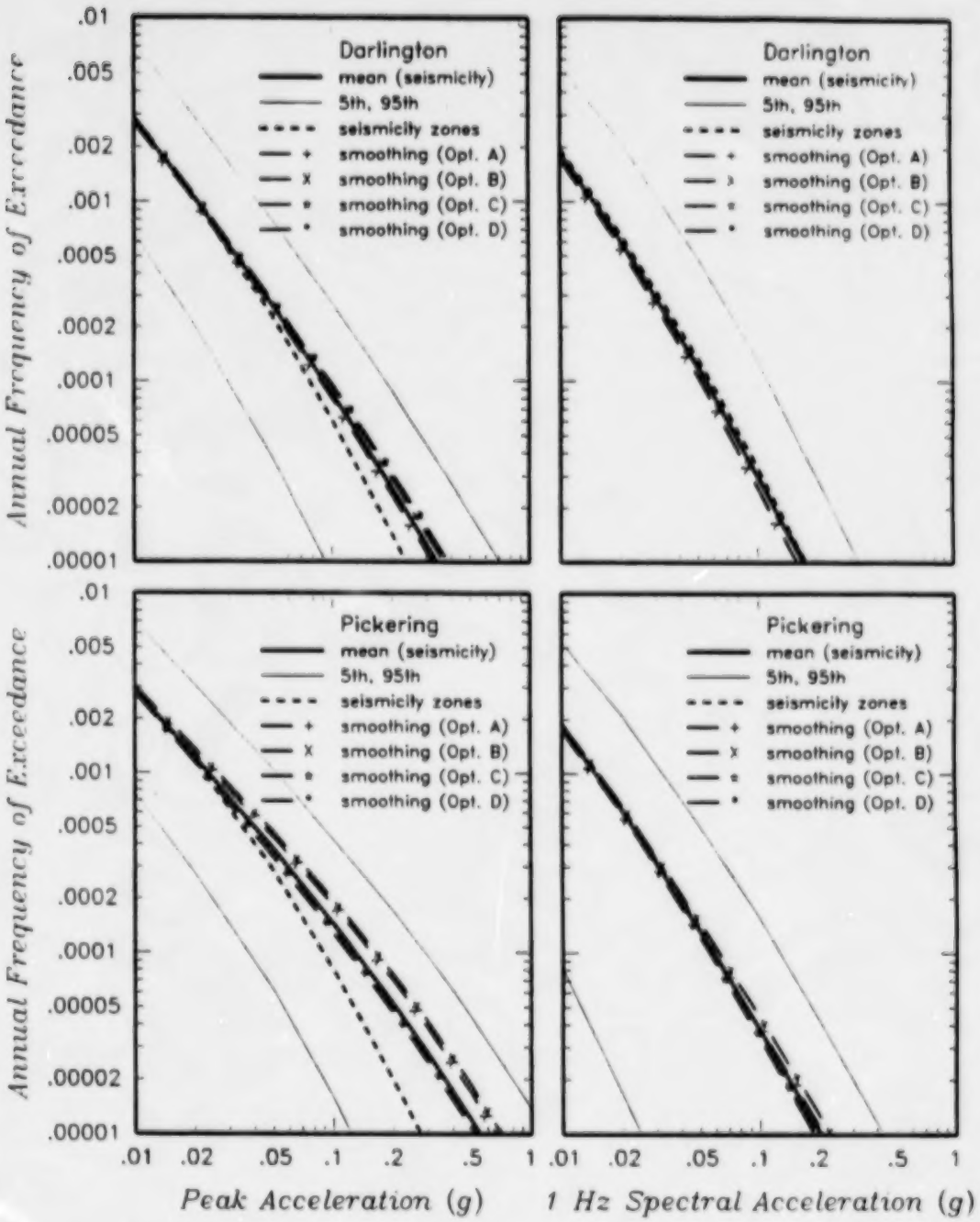

Figure 2-15 Effect of alternative source models used for the seismicity-based approach to regional source modeling. The thick solid curves show the mean hazard from the seismicity based regional source model and the thin solid lines show the 5th and 95th percentile hazard curves for that case. The source zone approach is compared to the four options for regional smoothing of seismicity using the approach developed by Veneziano and van Dyck (1985). Option A is no smoothing of seismicity rate, weak smoothing of *b*-value; Option B is weak smoothing of seismicity rate, weak smoothing of *b*-value; Option C is no smoothing of seismicity rate, moderate smoothing of *b*-value; and Option D is weak smoothing of seismicity rate, moderate smoothing of *b*-value.

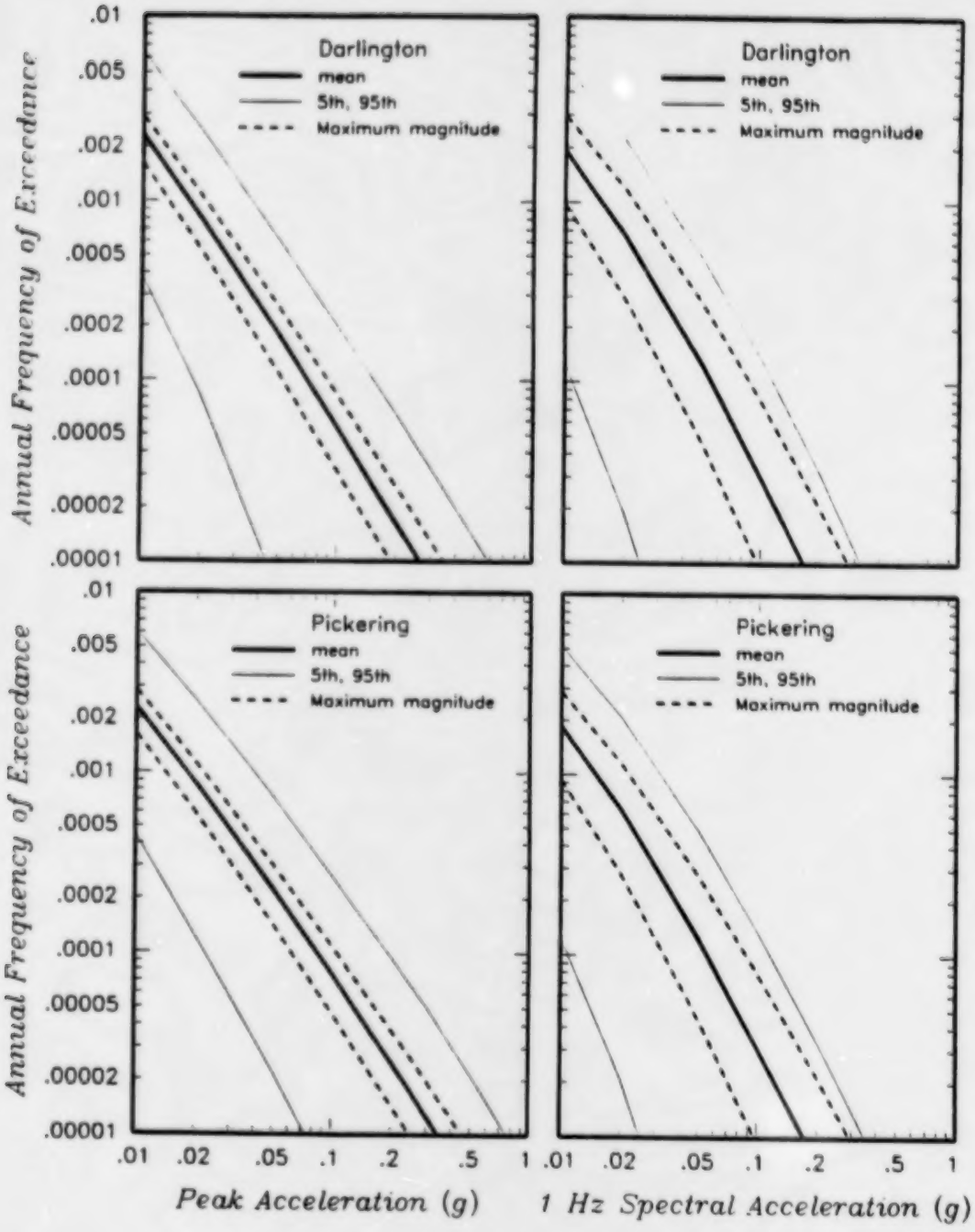

Figure 2-16 **Effect of variation in maximum magnitude on the computed hazard for the combined regional source model. The thick solid curves show the mean hazard from regional sources and the thin solid lines show the 5th and 95th percentile hazard curves for the regional sources. The dashed curves show the 5th and 95th percentile hazard curves considering only the uncertainty in maximum magnitude.**

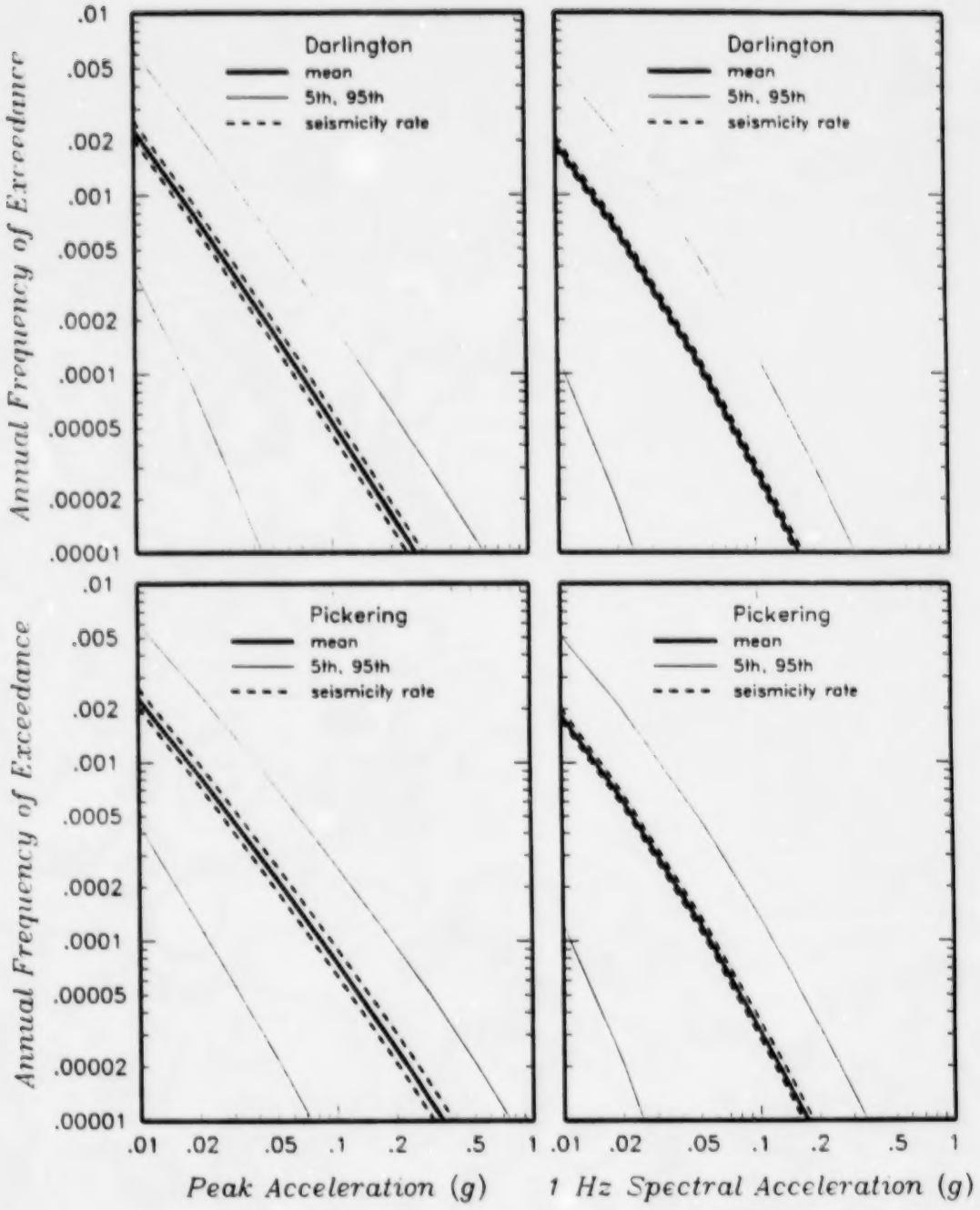

Figure 2-17 Effect of variation in seismicity rate on the computed hazard for the combined regional source model. The thick solid curves show the mean hazard from regional sources and the thin solid lines show the 5th and 95th percentile hazard curves for the regional sources. The dashed curves show the 5th and 95th percentile hazard curves considering only the uncertainty in seismicity rate (annual frequency of earthquakes with magnitudes m_b 3.3).

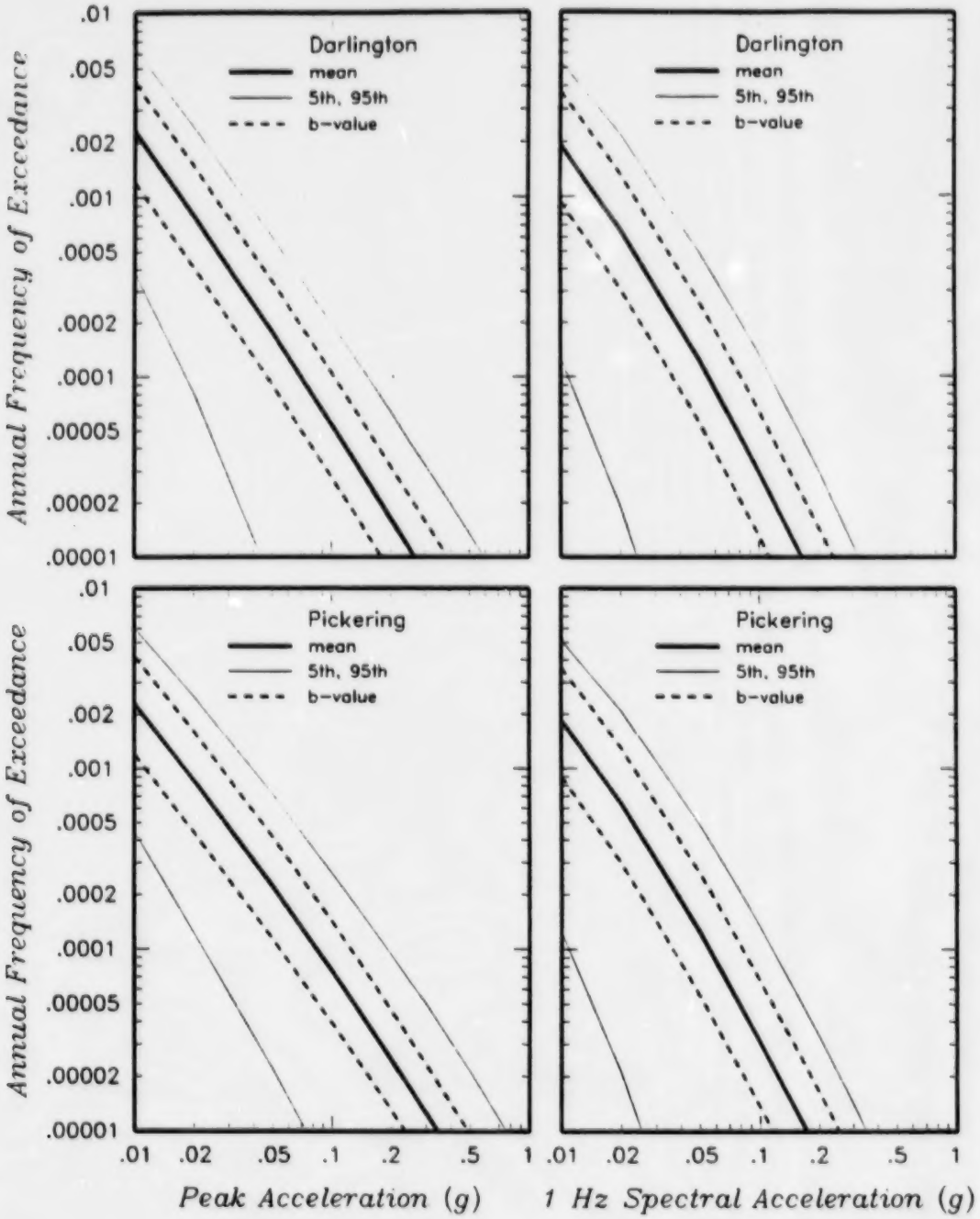

Figure 2-18 Effect of variation in *b*-value on the computed hazard for the combined regional source model. The thick solid curves show the mean hazard from regional sources and the thin solid lines show the 5th and 95th percentile hazard curves for the geologic regional source model. The dashed curves show the 5th and 95th percentile hazard curves considering only the uncertainty in *b*-value.

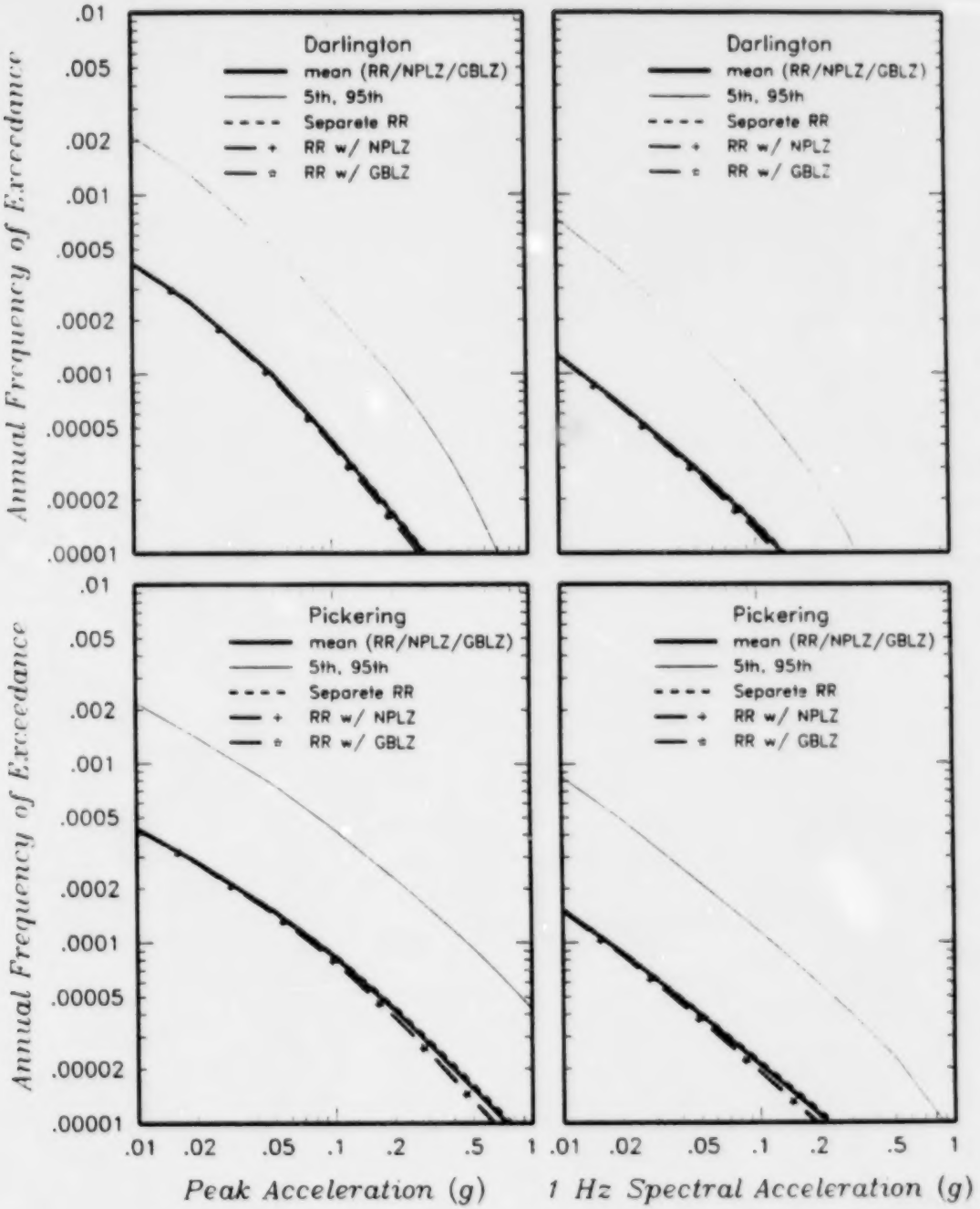

Figure 2-19 Effect of alternative assumptions for the association of the Rouge River (RR) fault with other structures [either the Niagara-Pickering linear zone (NPLZ) or the Georgian Bay linear zone (GBLZ)] on the computed hazard from these three local sources. The thick solid curves show the mean hazard from RR, NPLZ, and GBLZ local sources and the thin solid lines show the 95th percentile hazard curves for these local sources (the 5th-percentile hazard curves are at zero for the local sources).

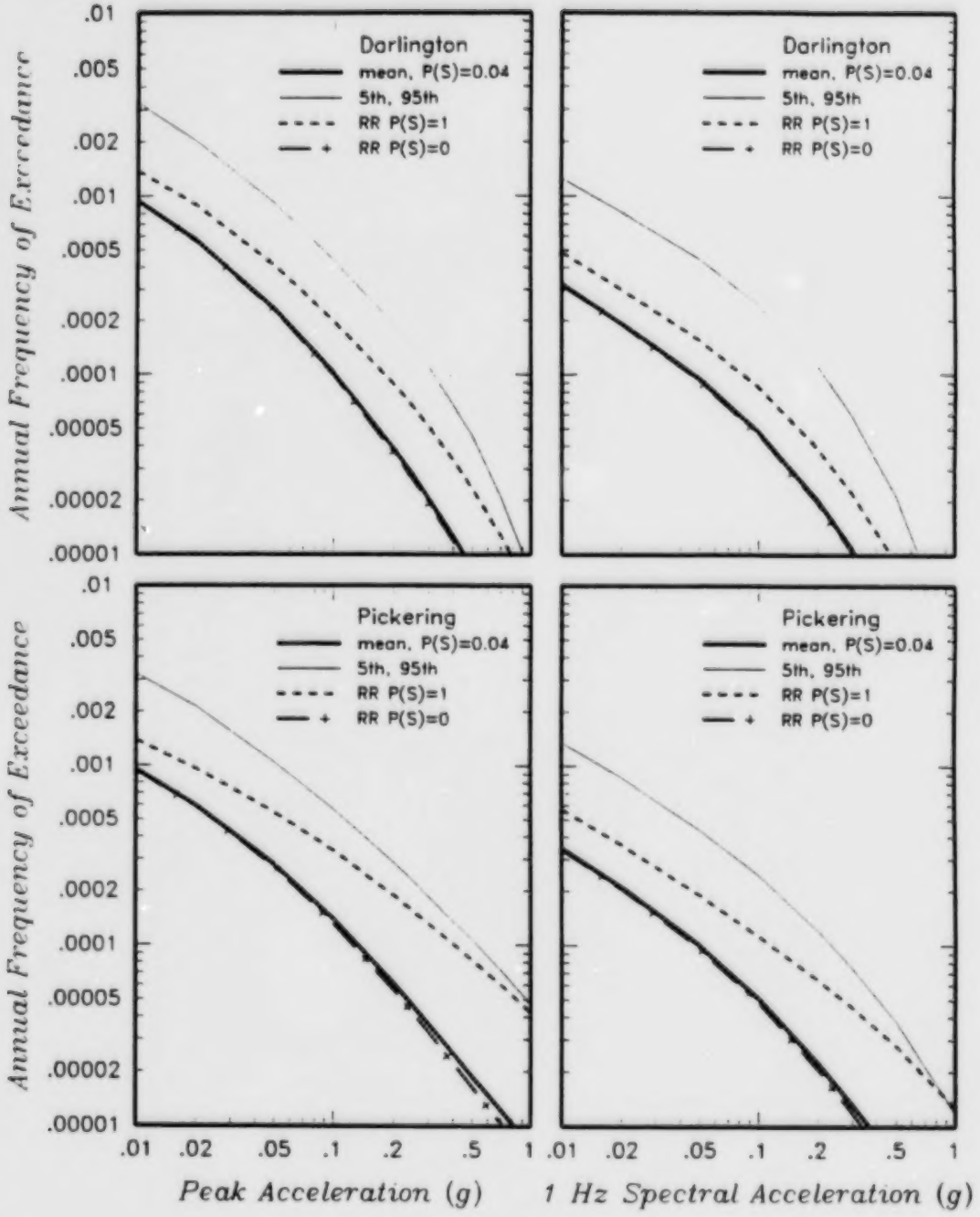

Figure 2-20a Effect of the assumption of whether the Rouge River (RR) fault is seismogenic [P(S)=1] or not seismogenic [P(S)=0] on the computed hazard for the local sources. The thick solid curves show the mean hazard from the local sources [RR P(S)=0.04] and the thin solid lines show the 95th percentile hazard curves for the local sources (the 5th-percentile hazard curves are at zero for the local sources).

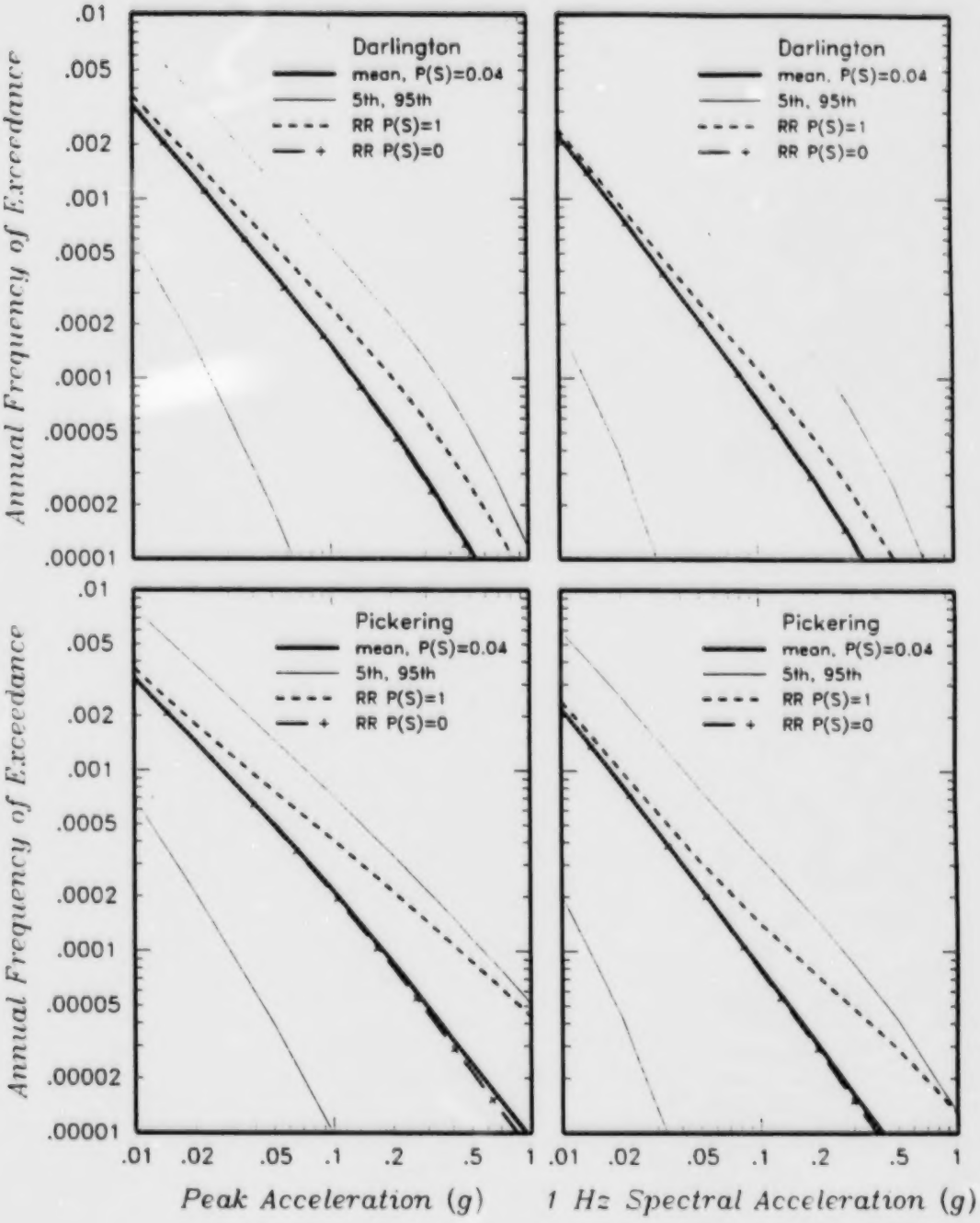

Figure 2-20b Effect of the assumption of whether the Rouge River (RR) fault is seismogenic [P(S)=1] or not seismogenic [P(S)=0] on the computed hazard for all sources. The thick solid curves show the mean hazard from all sources [RR P(S)=0.04] and the thin solid lines show the 5th and 95th percentile hazard curves for all sources.

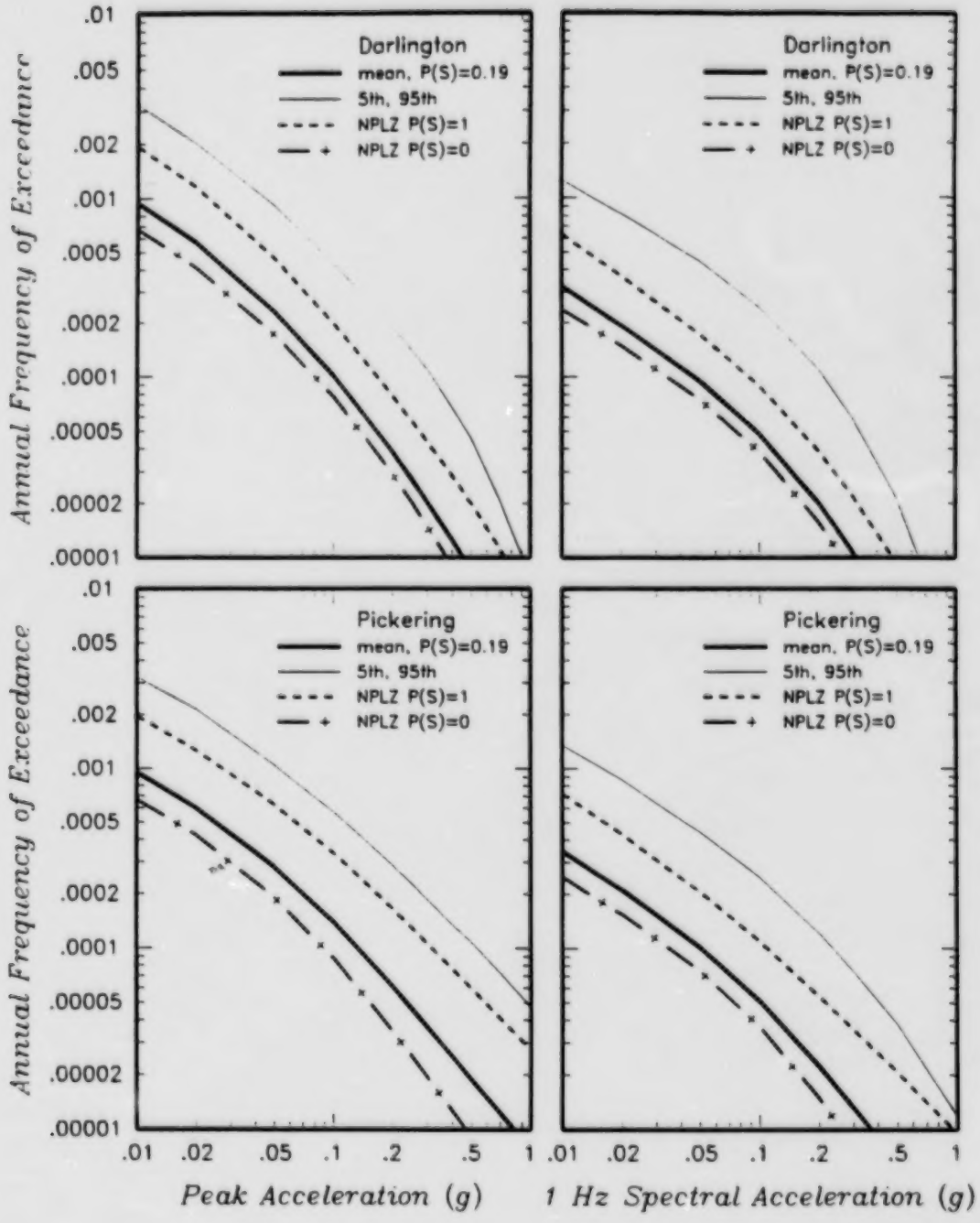

Figure 2-21a Effect of the assumption of whether the Niagara-Pickering linear zone (NPLZ) is seismogenic [P(S)=1] or not seismogenic [P(S)=0] on the computed hazard for the local sources. The thick solid curves show the mean hazard from the local sources [weighted average NPLZ P(S)=0.19] and the thin solid lines show the 95th percentile hazard curves for the local sources (the 5th-percentile hazard curves are at zero for the local sources).

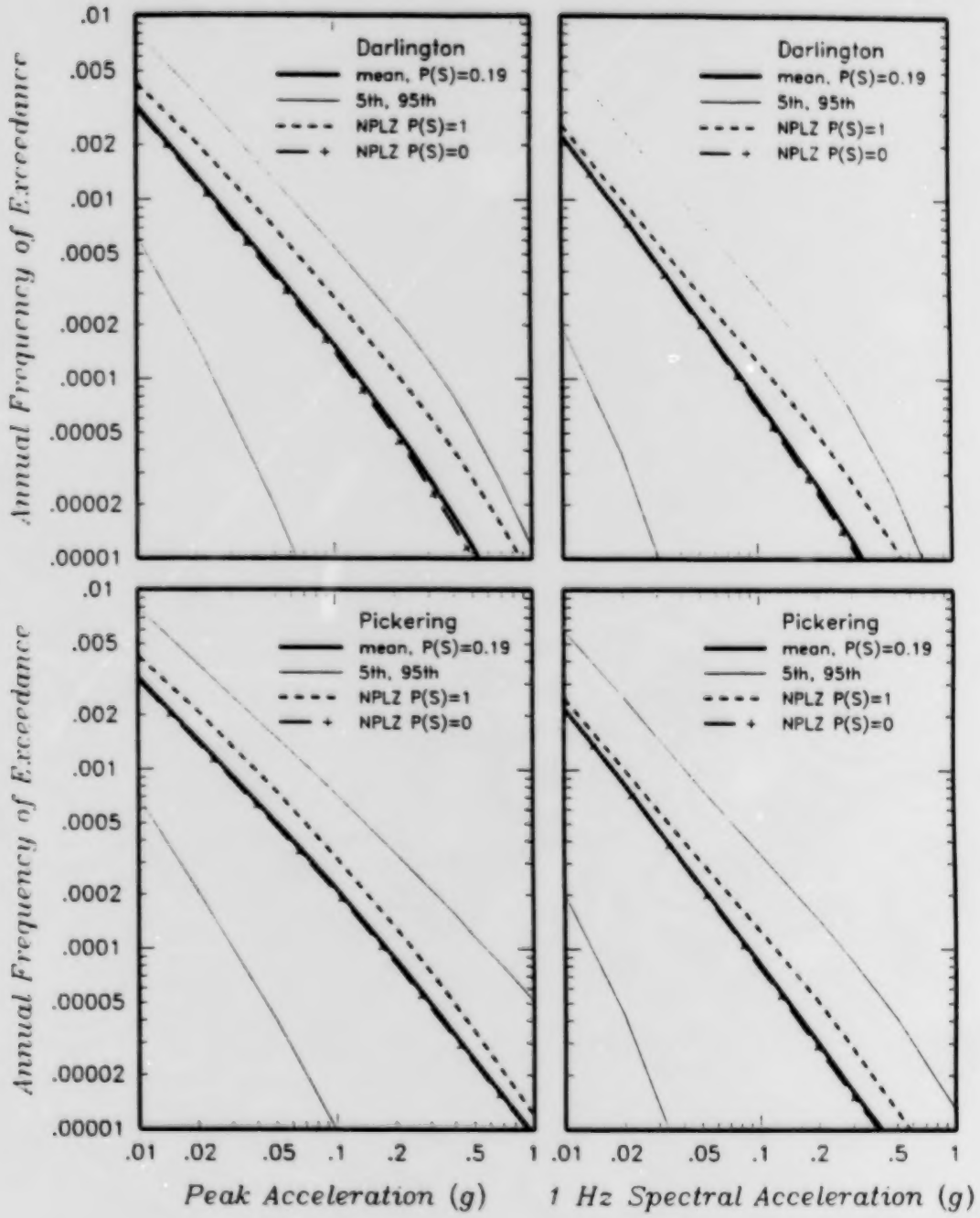

Figure 2-21b Effect of the assumption of whether the Niagara-Pickering linear zone (NPLZ) is seismogenic [P(S)=1] or not seismogenic [P(S)=0] on the computed hazard for all sources. The thick solid curves show the mean hazard from all sources [weighted average NPLZ P(S)=0.19] and the thin solid lines show the 5th and 95th percentile hazard curves for all sources.

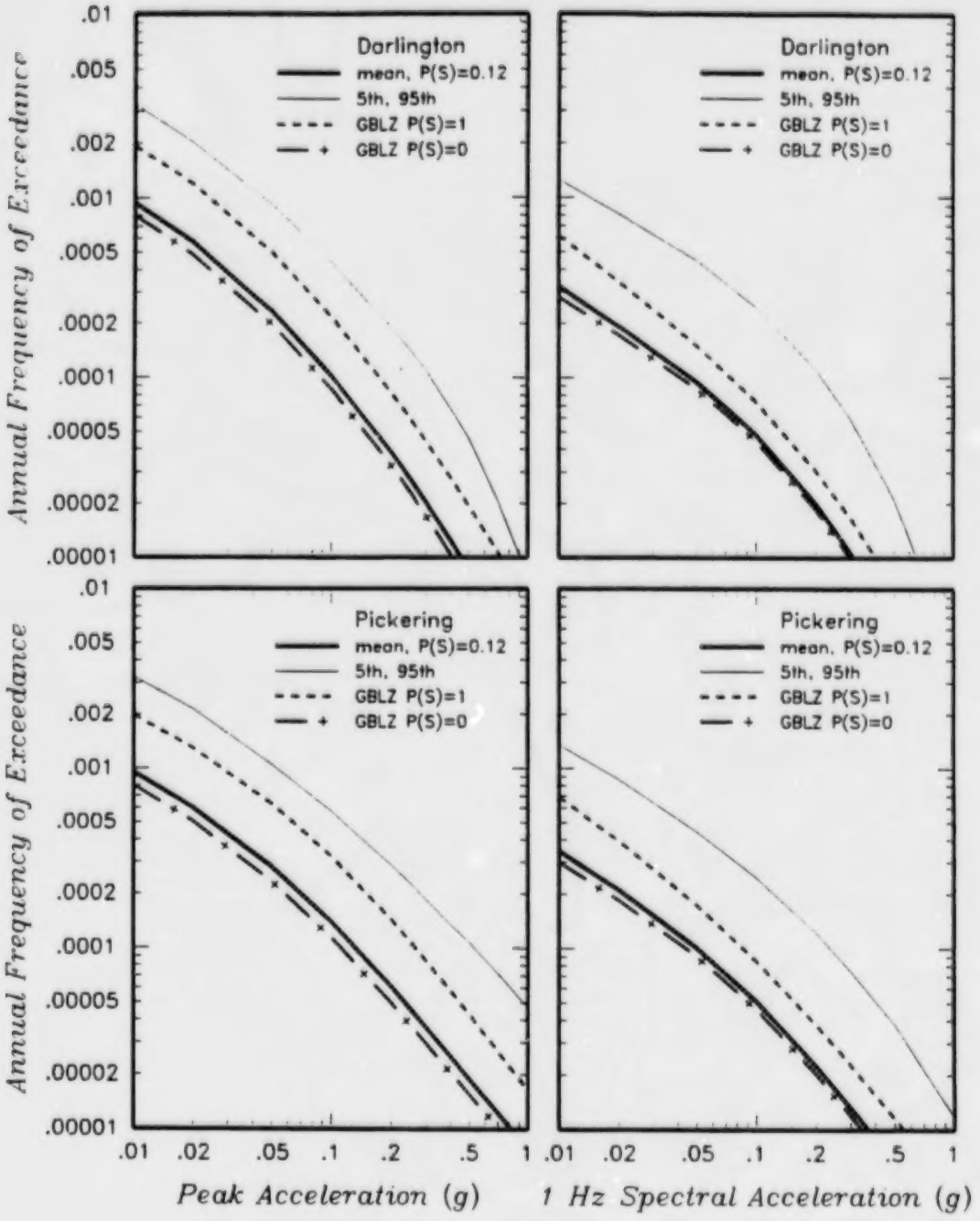

Figure 2-22a Effect of the assumption of whether the Georgian Bay linear zone (GBLZ) is seismogenic [P(S)=1] or not seismogenic [P(S)=0] on the computed hazard for the local sources. The thick solid curves show the mean hazard from the local sources [weighted average GBLZ P(S)=0.12] and the thin solid lines show the 95th percentile hazard curves for the local sources (the 5th-percentile hazard curves are at zero for the local sources).

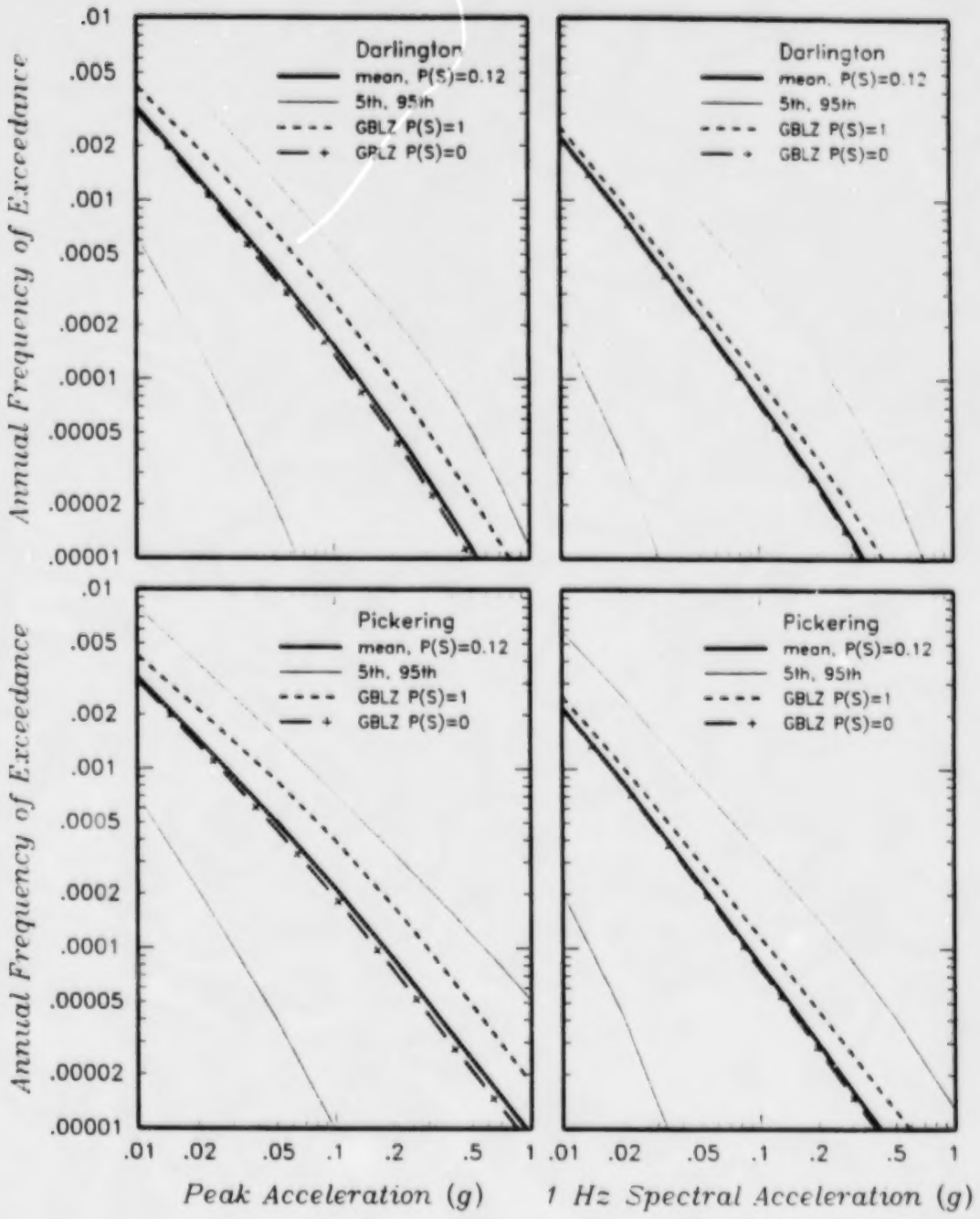

Figure 2-22b Effect of the assumption of whether the Georgian Bay linear zone (GBLZ) is seismogenic [P(S)=1] or not seismogenic [P(S)=0] on the computed hazard for all sources. The thick solid curves show the mean hazard from all sources [weighted average GBLZ P(S)=0.12] and the thin solid lines show the 5th and 95th percentile hazard curves for all sources.

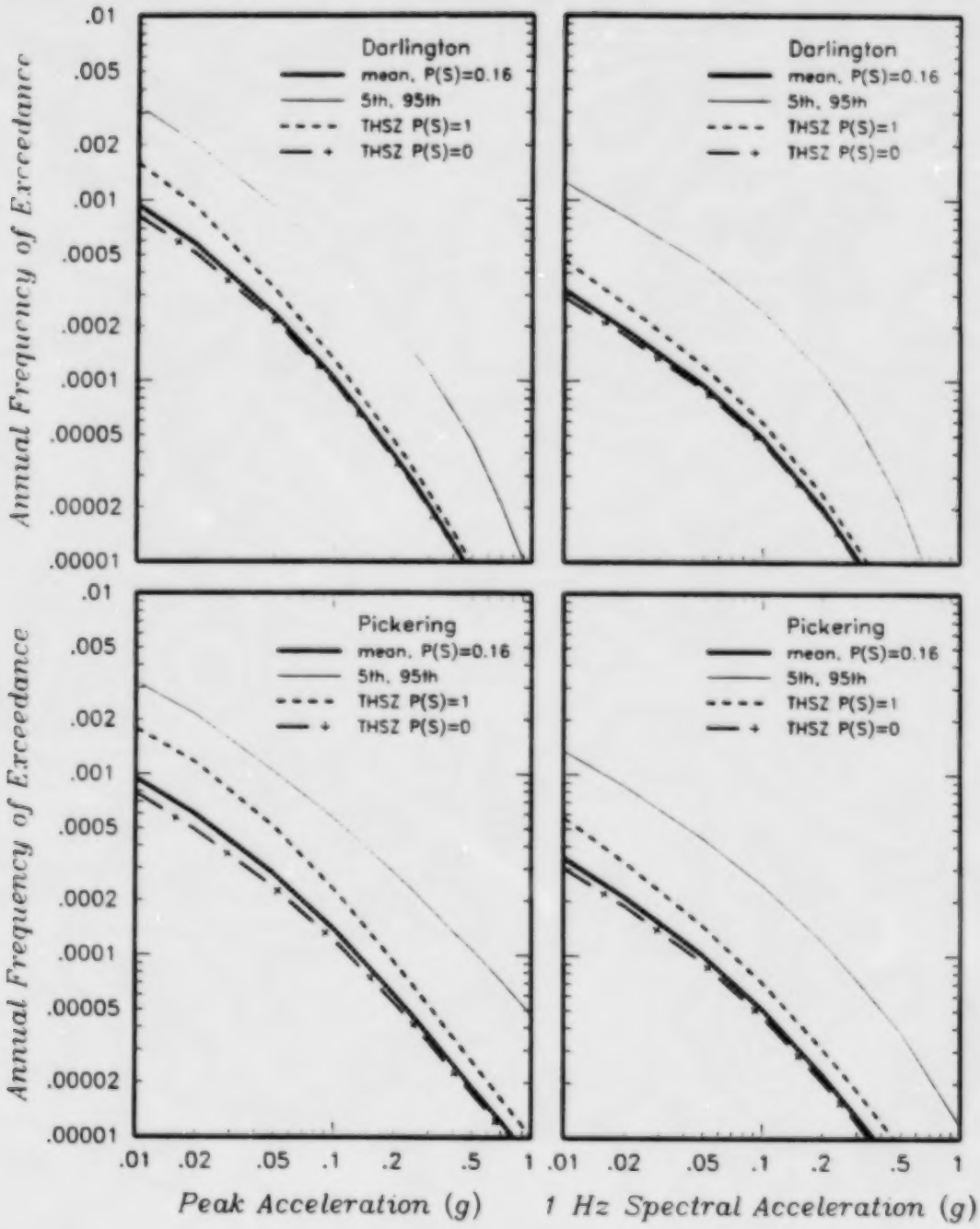

Figure 2-23a Effect of the assumption of whether the Toronto-Hamilton seismic zone (THSZ) is seismogenic [P(S)=1] or not seismogenic [P(S)=0] on the computed hazard for the local sources. The thick solid curves show the mean hazard from the local sources [THSZ P(S)=0.16] and the thin solid lines show the 95th percentile hazard curves for the local sources (the 5th-percentile hazard curves are at zero for the local sources).

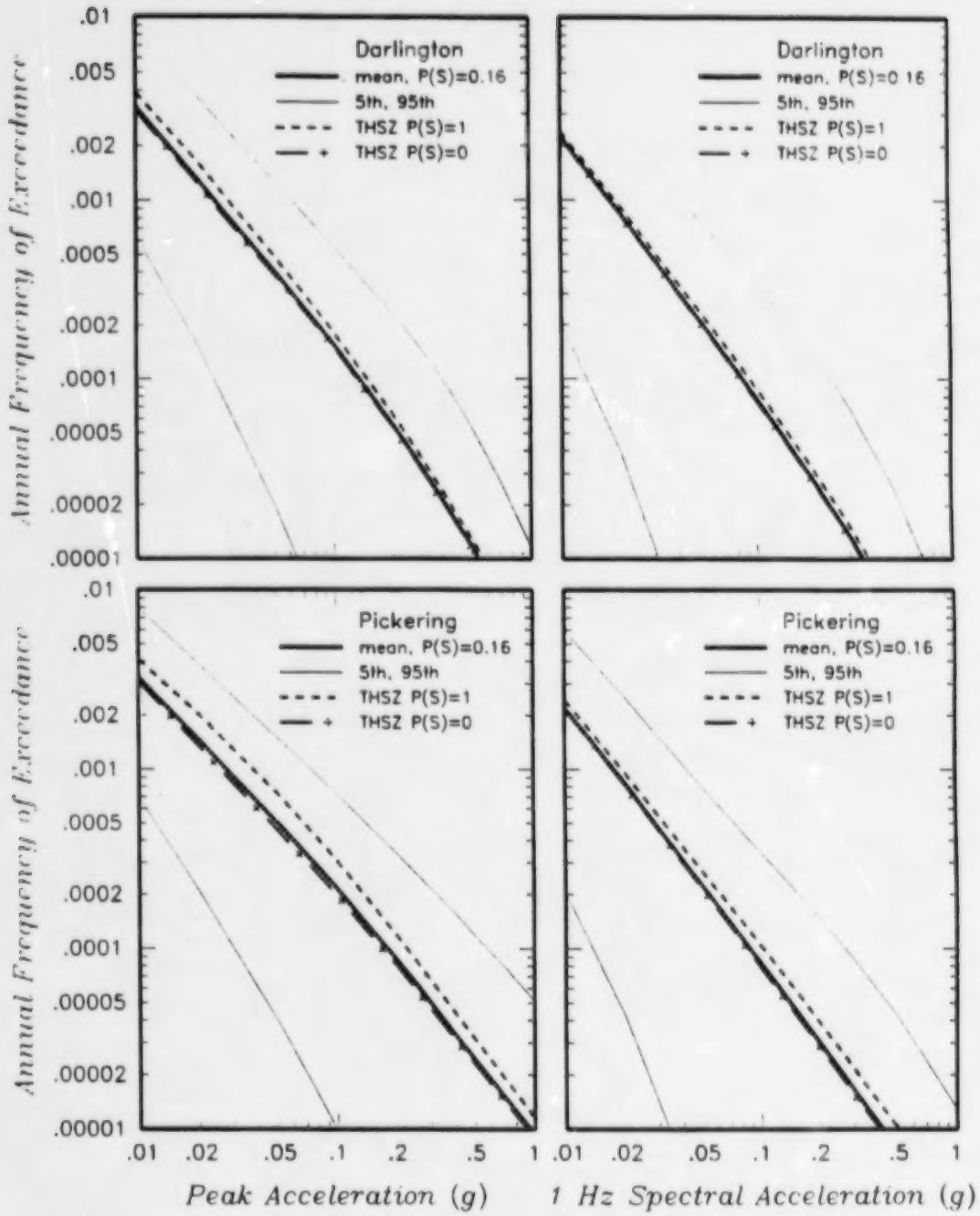

Figure 2-23b Effect of the assumption of whether the Toronto-Hamilton seismic zone (THSZ) is seismogenic [P(S)=1] or not seismogenic [P(S)=0] on the computed hazard for all sources. The thick solid curves show the mean hazard from all sources [THSZ P(S)=0.16] and the thin solid lines show the 5th and 95th percentile hazard curves for all sources.

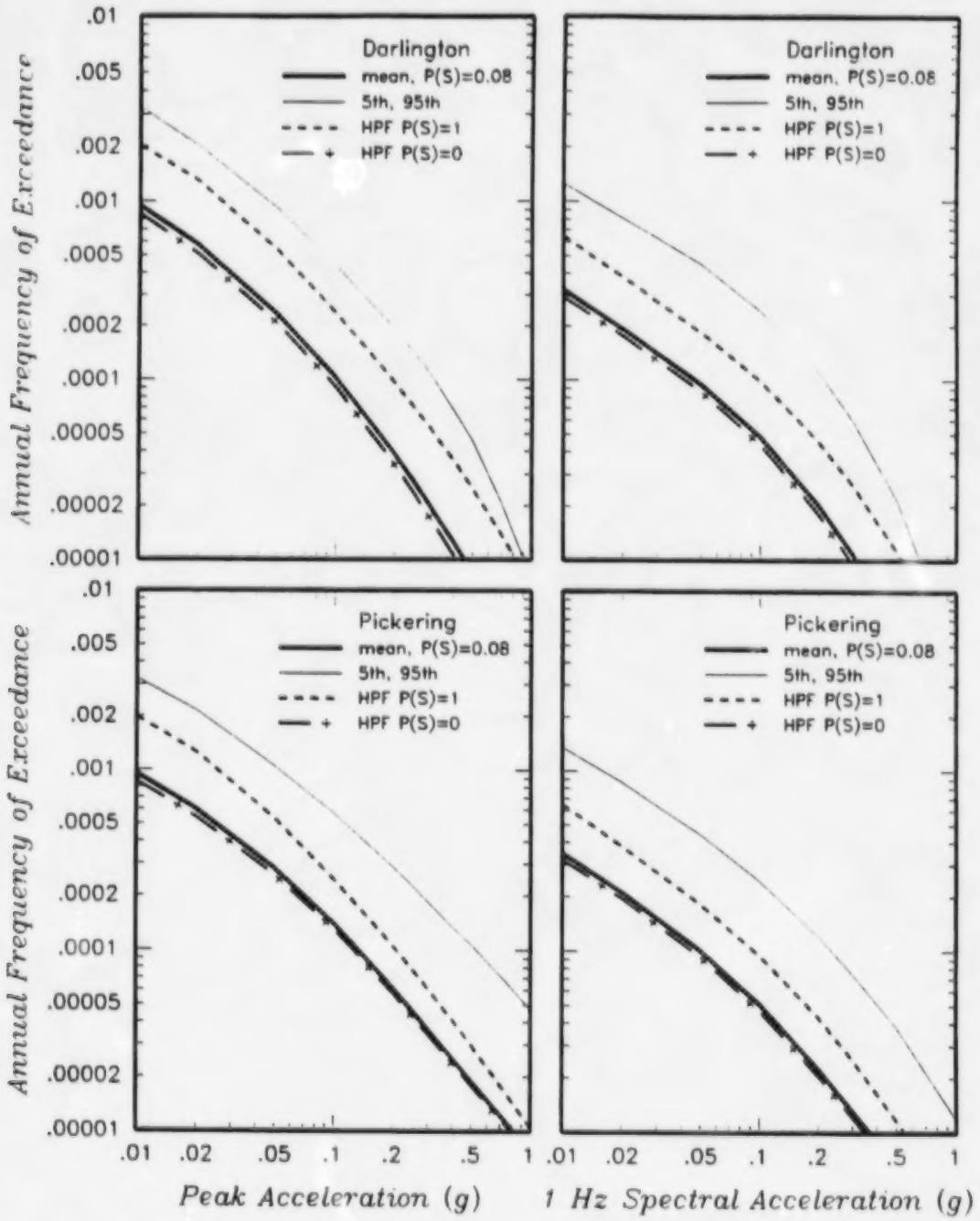

Figure 2-24a **Effect of the assumption of whether the Hamilton-Presqu'ile fault (HPF) is seismogenic [P(S)=1] or not seismogenic [P(S)=0] on the computed hazard for the local sources. The thick solid curves show the mean hazard from the local sources [HPF P(S)=0.08] and the thin solid lines show the 95th percentile hazard curves for the local sources (the 5th-percentile hazard curves are at zero for the local sources).**

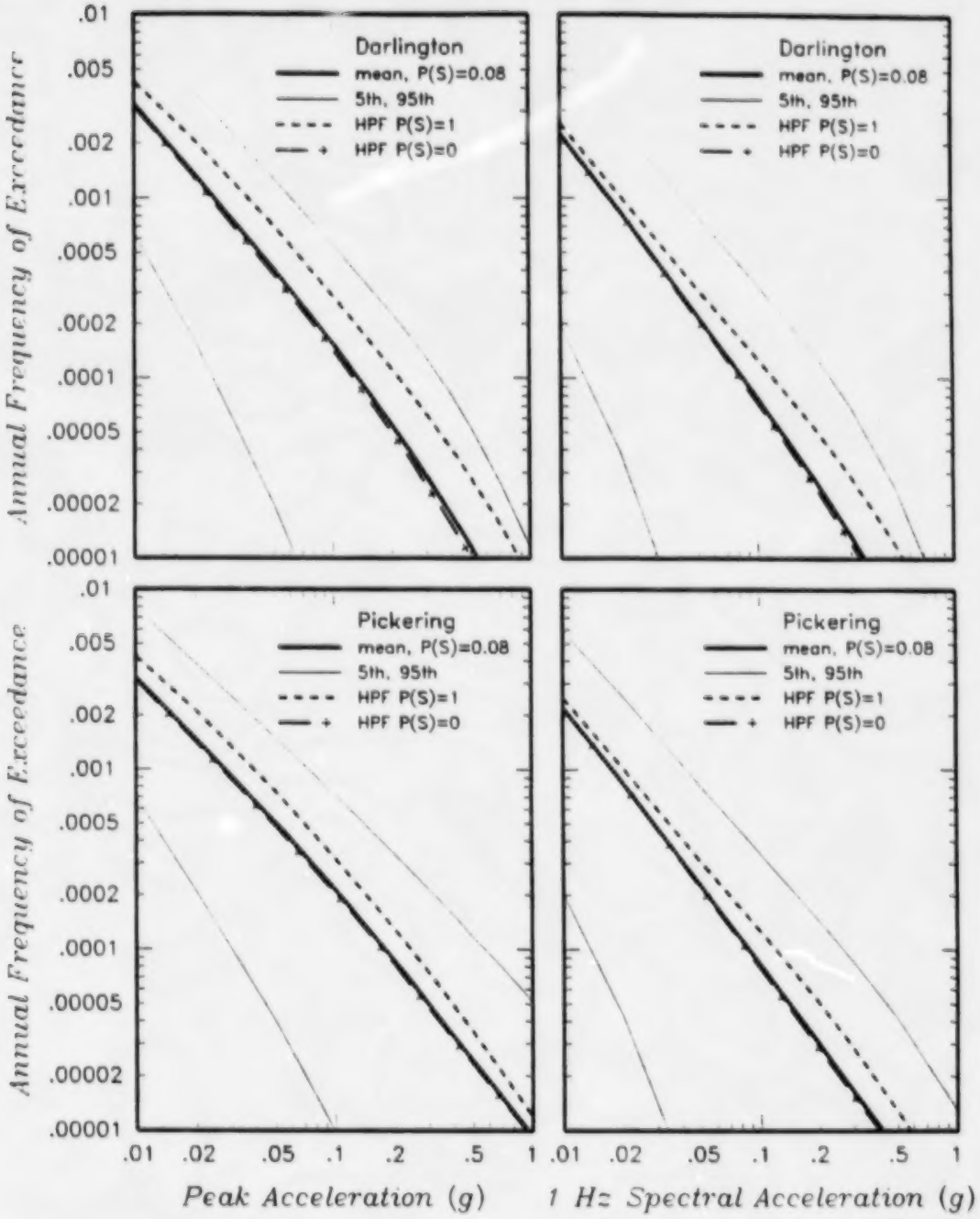

Figure 2-24b Effect of the assumption of whether the Hamilton-Presqu'ile fault (HPF) is seismogenic [P(S)=1] or not seismogenic [P(S)=0] on the computed hazard for all sources. The thick solid curves show the mean hazard from all sources [HPF P(S)=0.08] and the thin solid lines show the 5th and 95th percentile hazard curves for all sources.

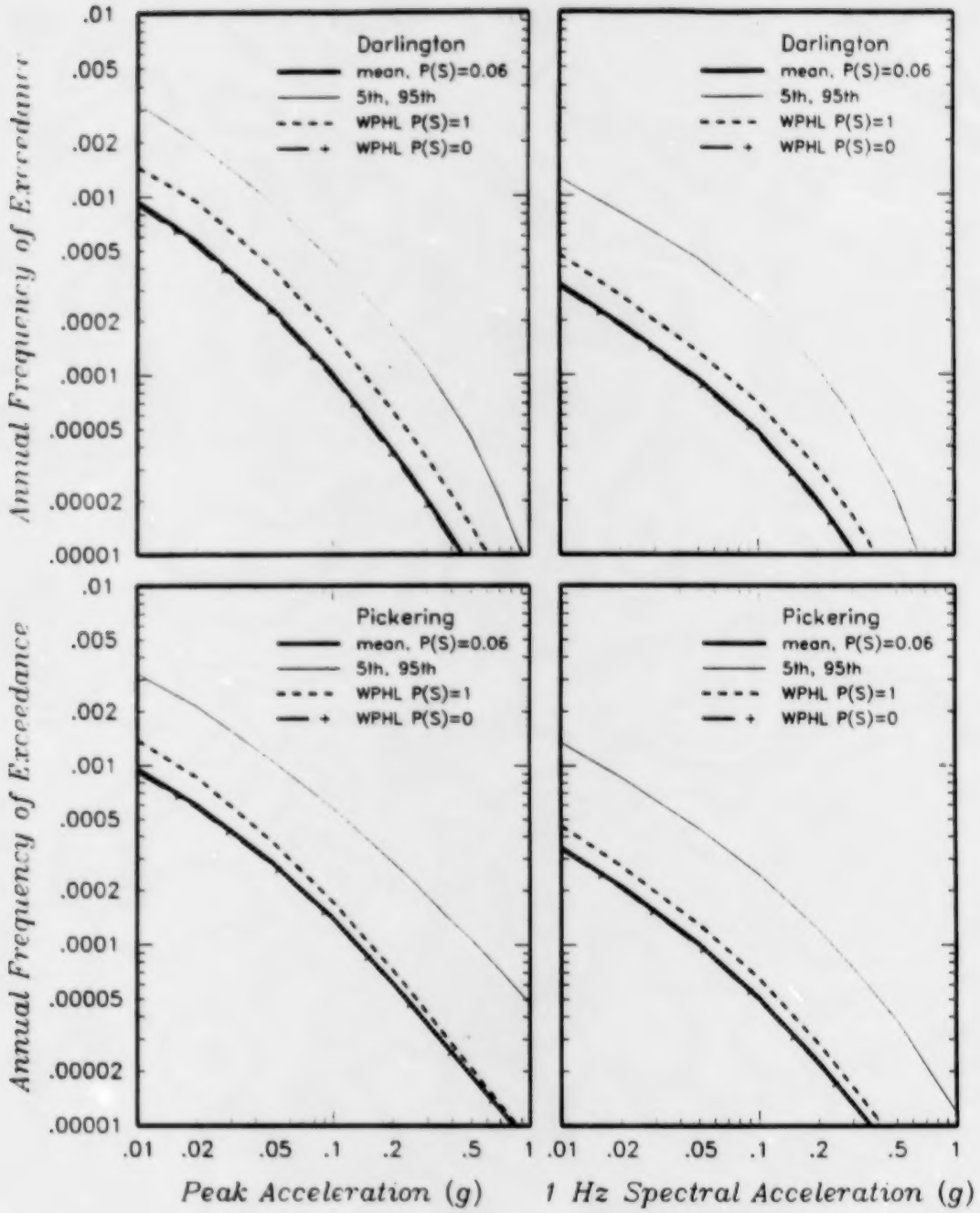

Figure 2-25a Effect of the assumption of whether the Wilson-Port Hope lineament (WPHL) is seismogenic [P(S)=1] or not seismogenic [P(S)=0] on the computed hazard for the local sources. The thick solid curves show the mean hazard from the local sources [WPHL P(S)=0.06] and the thin solid lines show the 95th percentile hazard curves for the local sources (the 5th-percentile hazard curves are at zero for the local sources).

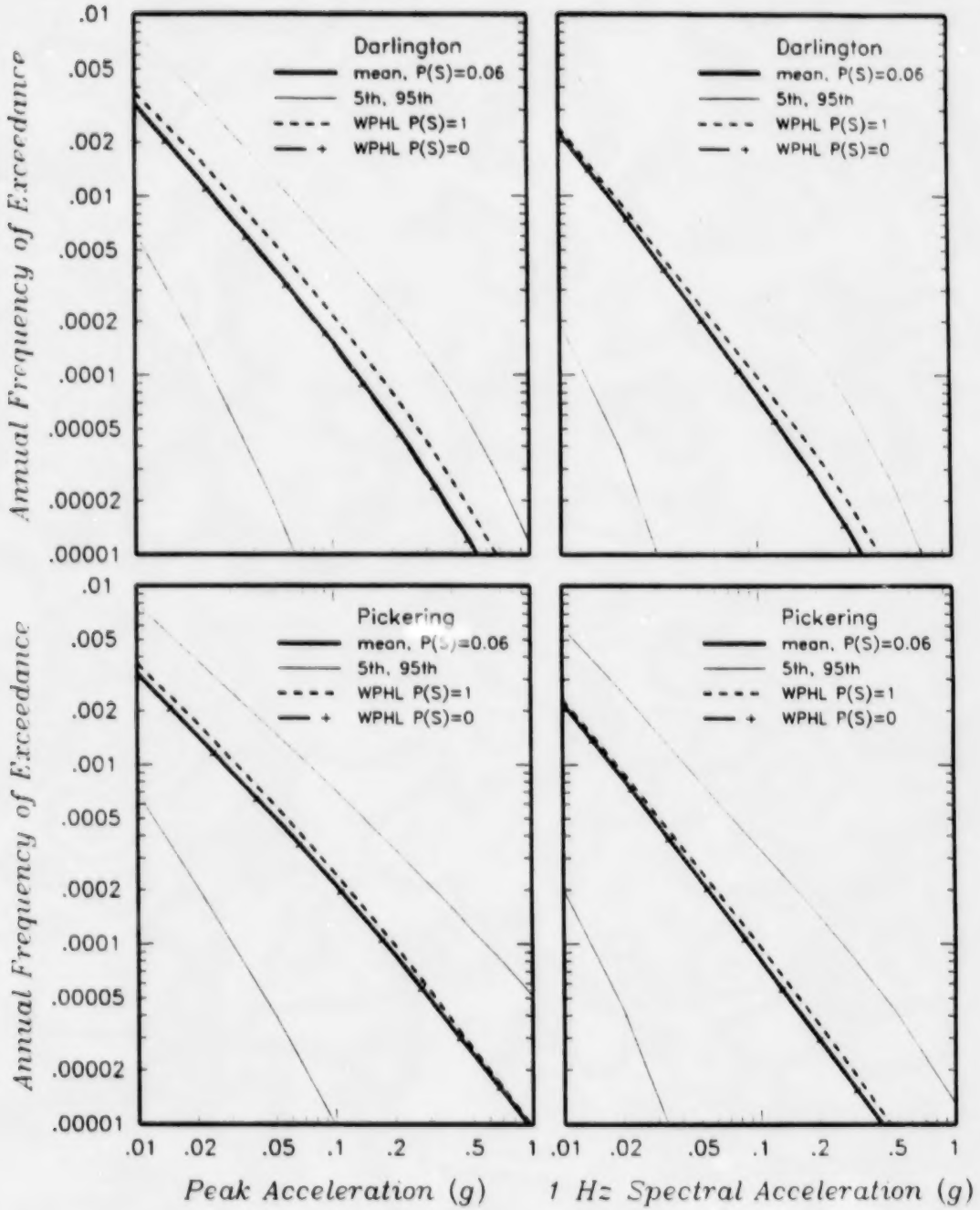

Figure 2-25b Effect of the assumption of whether the Wilson-Port Hope lineament (WPHL) is seismogenic [P(S)=1] or not seismogenic [P(S)=0] on the computed hazard for all sources. The thick solid curves show the mean hazard from all sources [WPHL P(S)=0.06] and the thin solid lines show the 5th and 95th percentile hazard curves for all sources.

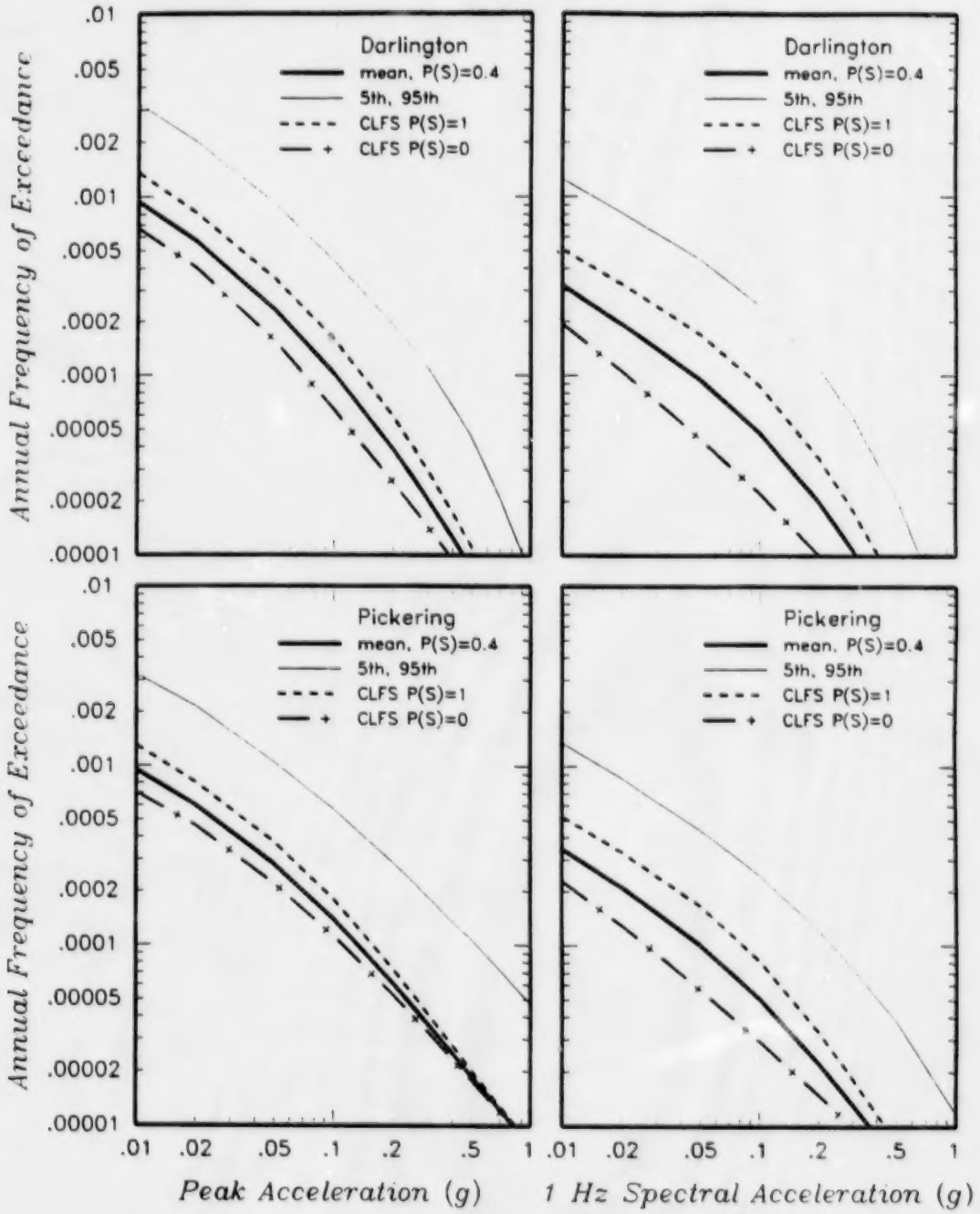

Figure 2-26a Effect of the assumption of whether or the Clarendon-Linden fault system (CLFS) is seismogenic [P(S)=1] or not seismogenic [P(S)=0] on the computed hazard for the local sources. The thick solid curves show the mean hazard from the local sources [CLFS P(S)=0.4] and the thin solid lines show the 95th percentile hazard curves for the local sources (the 5th-percentile hazard curves are at zero for the local sources).

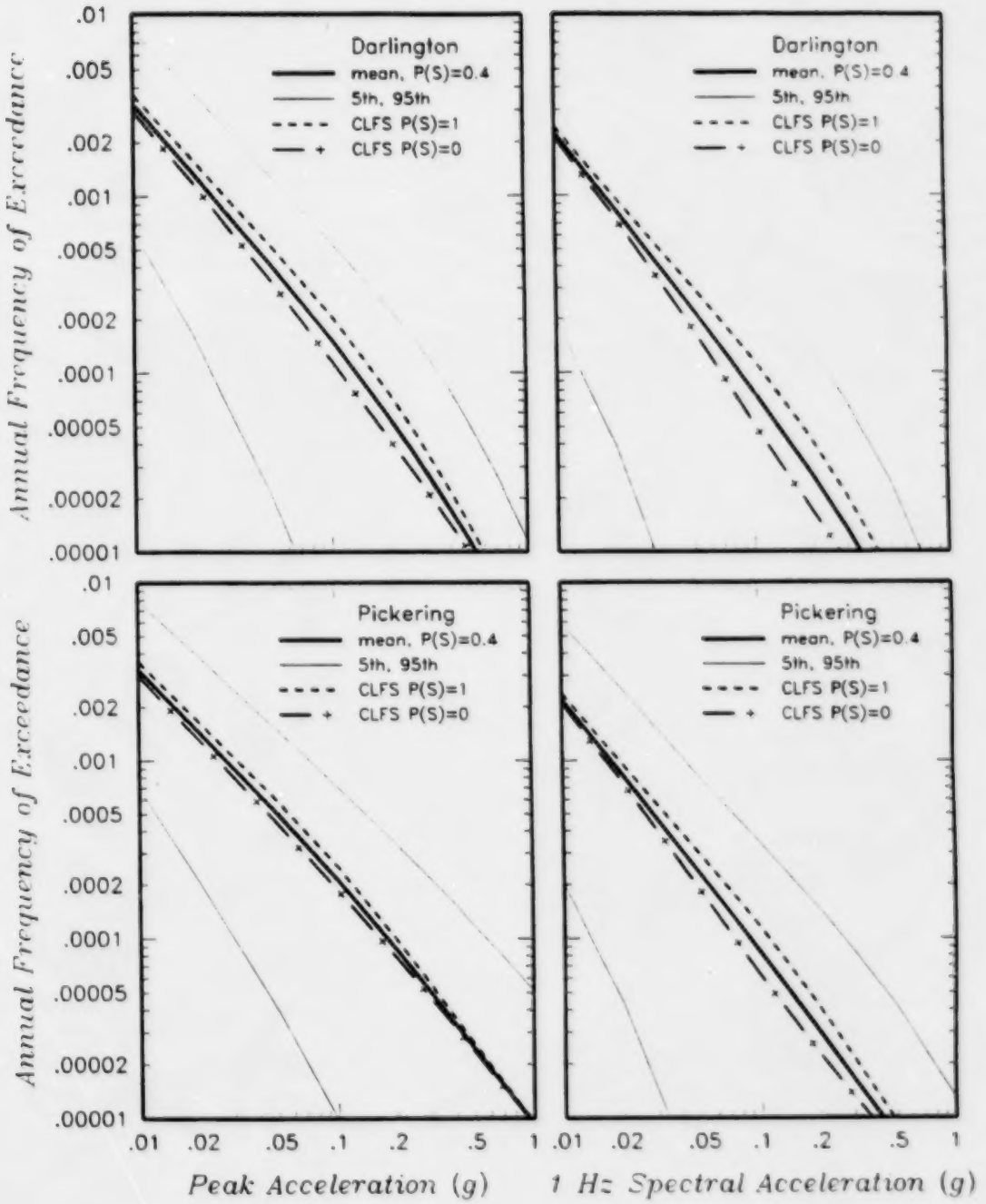

Figure 2-26b Effect of the assumption of whether or the Clarendon-Linden fault system (CLFS) is seismogenic [P(S)=1] or not seismogenic [P(S)=0] on the computed hazard for all sources. The thick solid curves show the mean hazard from all sources [CLFS P(S)=0.4] and the thin solid lines show the 5th and 95th percentile hazard curves for all sources.

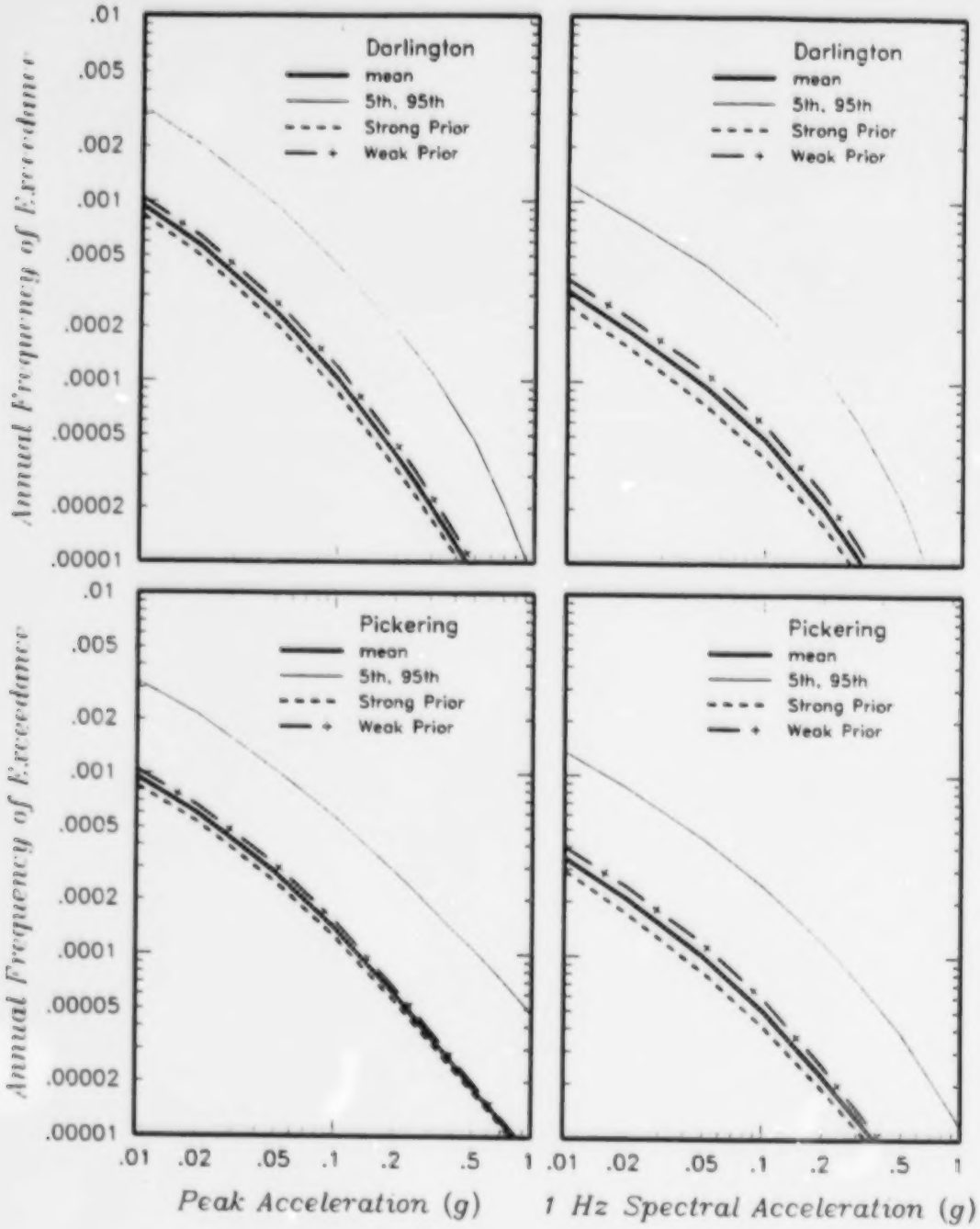

Figure 2-27 Effect of alternative weights on the use of a *b*-value prior in developing recurrence relationships for the local sources on the hazard from these sources. The thick solid curves show the mean hazard from the local sources and the thin solid lines show the 95th percentile hazard curves for the local sources (the 5th-percentile hazard curves are at zero for the local sources).

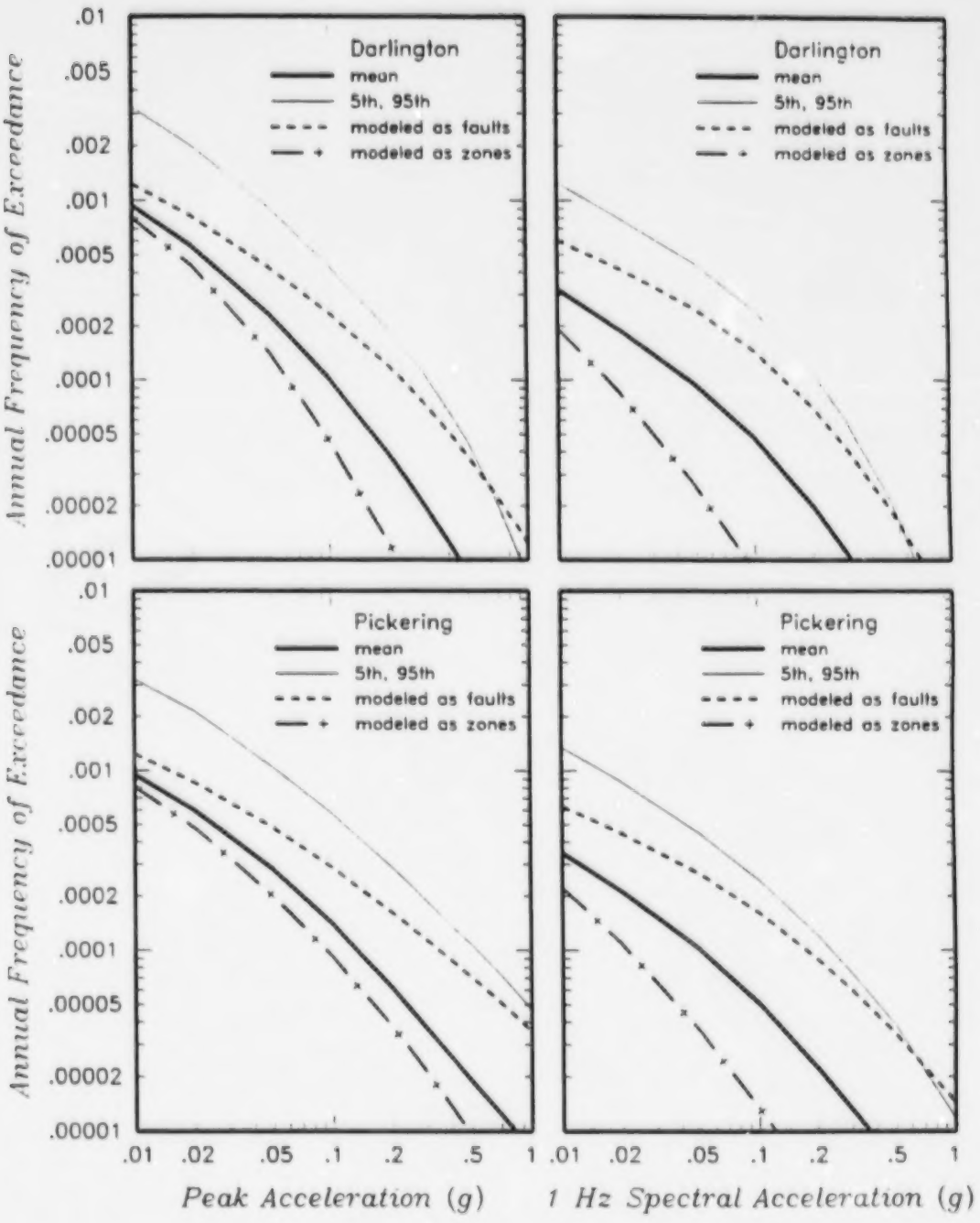

Figure 2-28 Effect of alternative assumptions for the local source behavior (fault versus zone) on the hazard from these sources. The thick solid curves show the mean hazard from the local sources and the thin solid lines show the 95th percentile hazard curves for the local sources (the 5th-percentile hazard curves are at zero for the local sources).

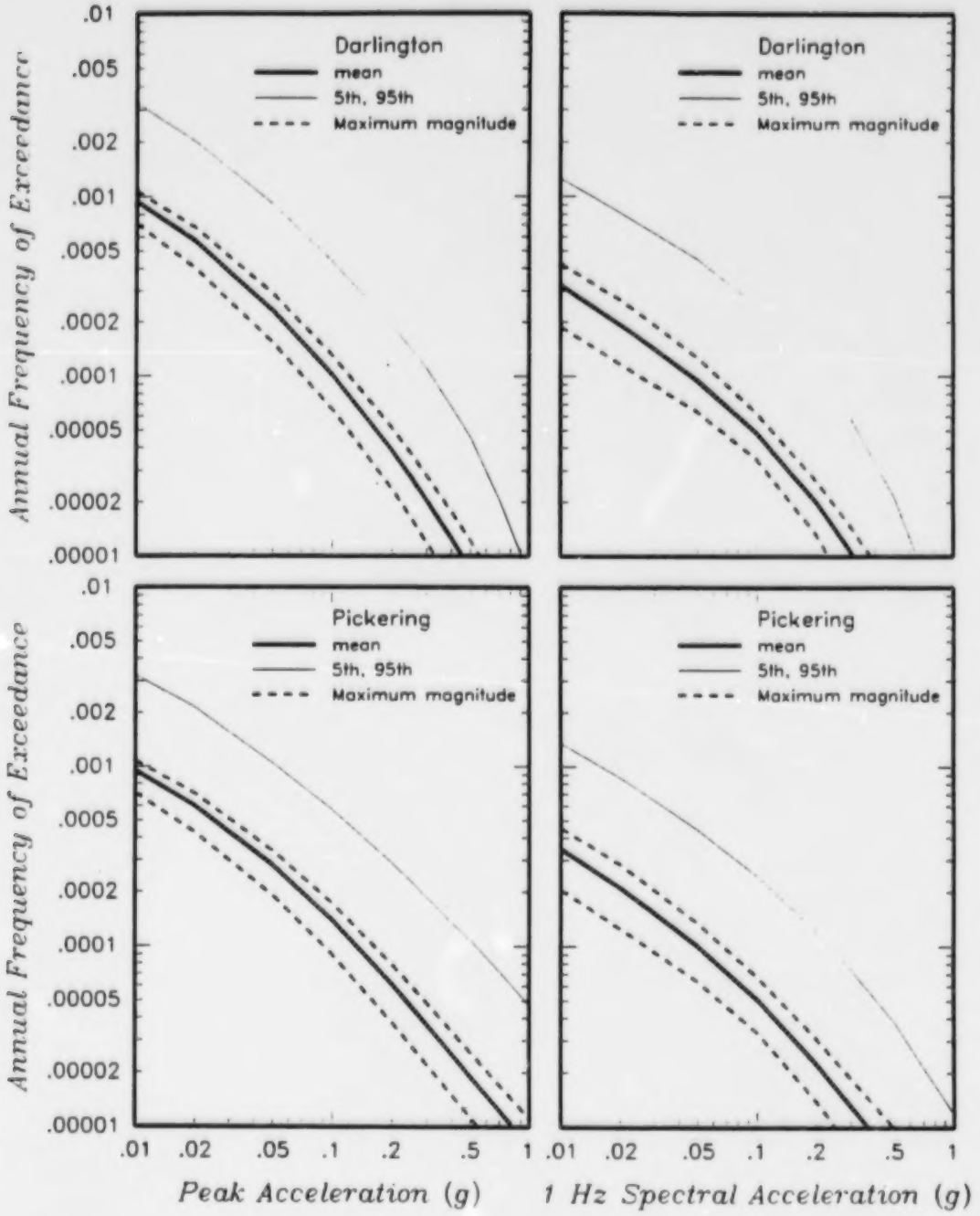

Figure 2-29 Effect of variation in maximum magnitude on the computed hazard for the combined local source model. The thick solid curves show the mean hazard from local sources and the thin solid lines show the 95th percentile hazard curves for the local sources (the 5th-percentile hazard curves are at zero for the local sources). The dashed curves show the 5th and 95th percentile hazard curves considering only the uncertainty in maximum magnitude.

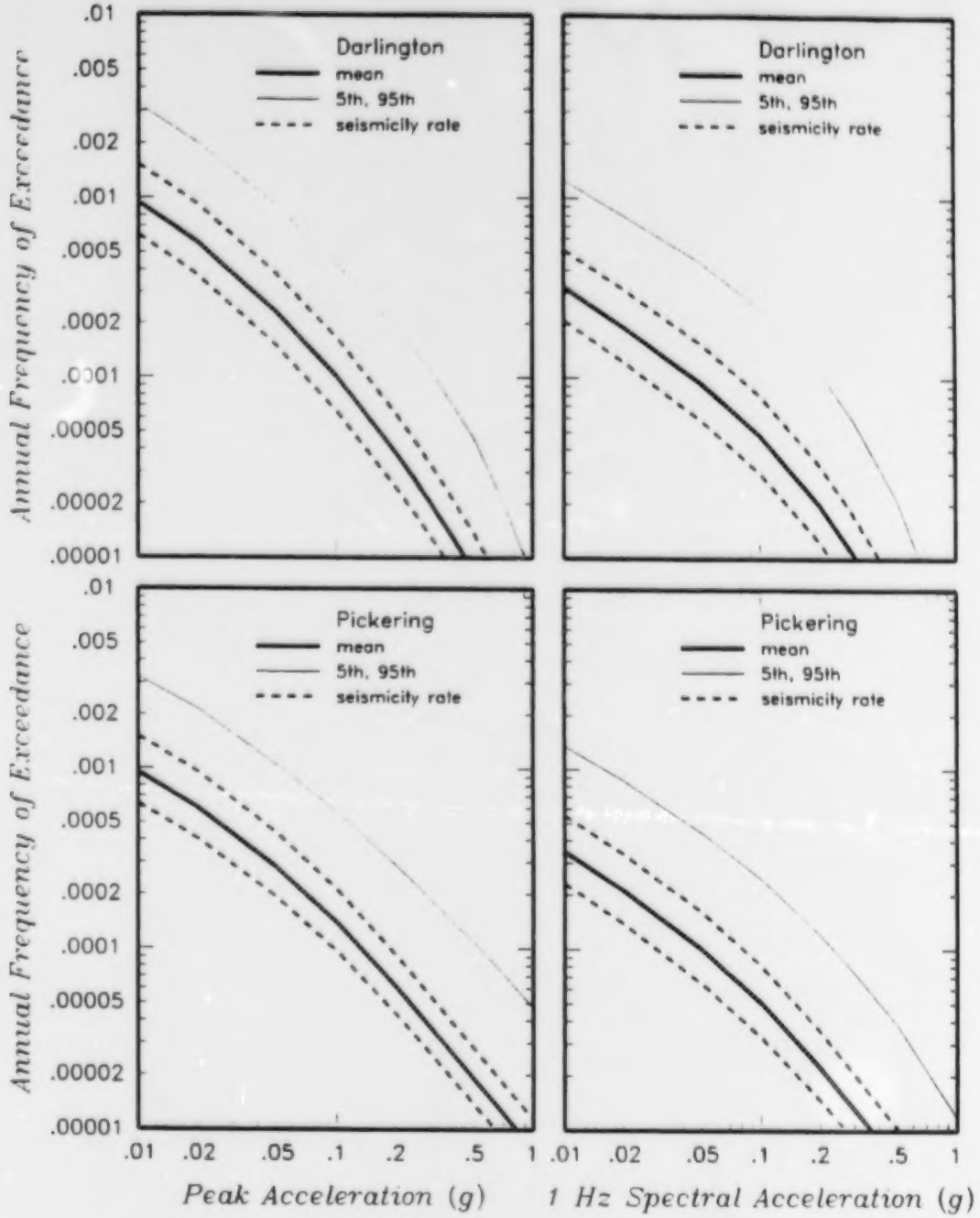

Figure 2-30 Effect of variation in seismicity rate on the computed hazard for the combined local source model. The thick solid curves show the mean hazard from local sources and the thin solid lines show the 95th percentile hazard curves for the local sources (the 5th-percentile hazard curves are at zero for the local sources). The dashed curves show the 5th and 95th percentile hazard curves considering only the uncertainty in seismicity rate (annual frequency of earthquakes with magnitudes m_b 3.3).

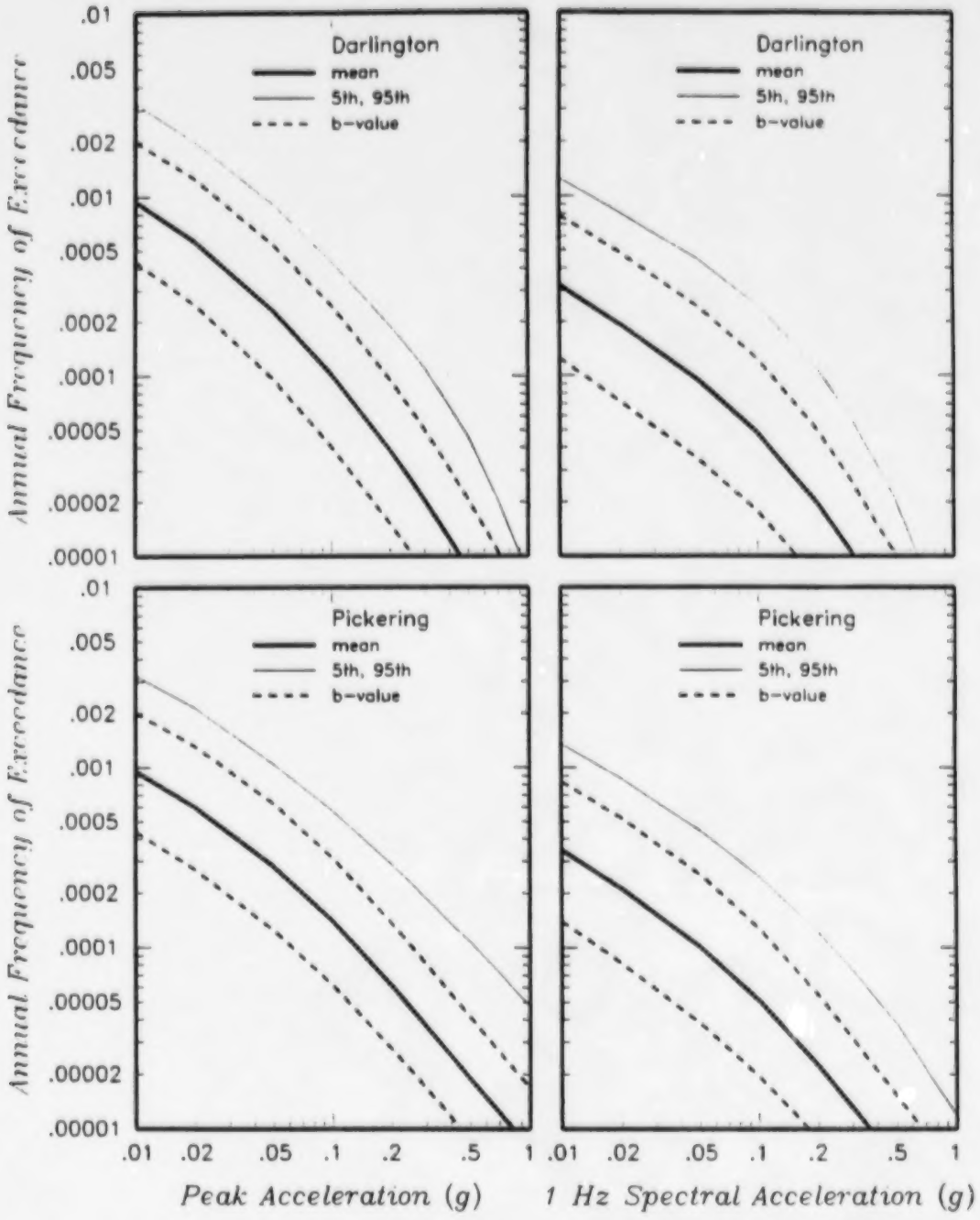

Figure 2-31 Effect of variation in *b*-value on the computed hazard for the combined local source model. The thick solid curves show the mean hazard from local source model and the thin solid lines show the 95th percentile hazard curves for the local sources (the 5th-percentile hazard curves are at zero for the local sources). The dashed curves show the 5th and 95th percentile hazard curves considering only the uncertainty in *b*-value.

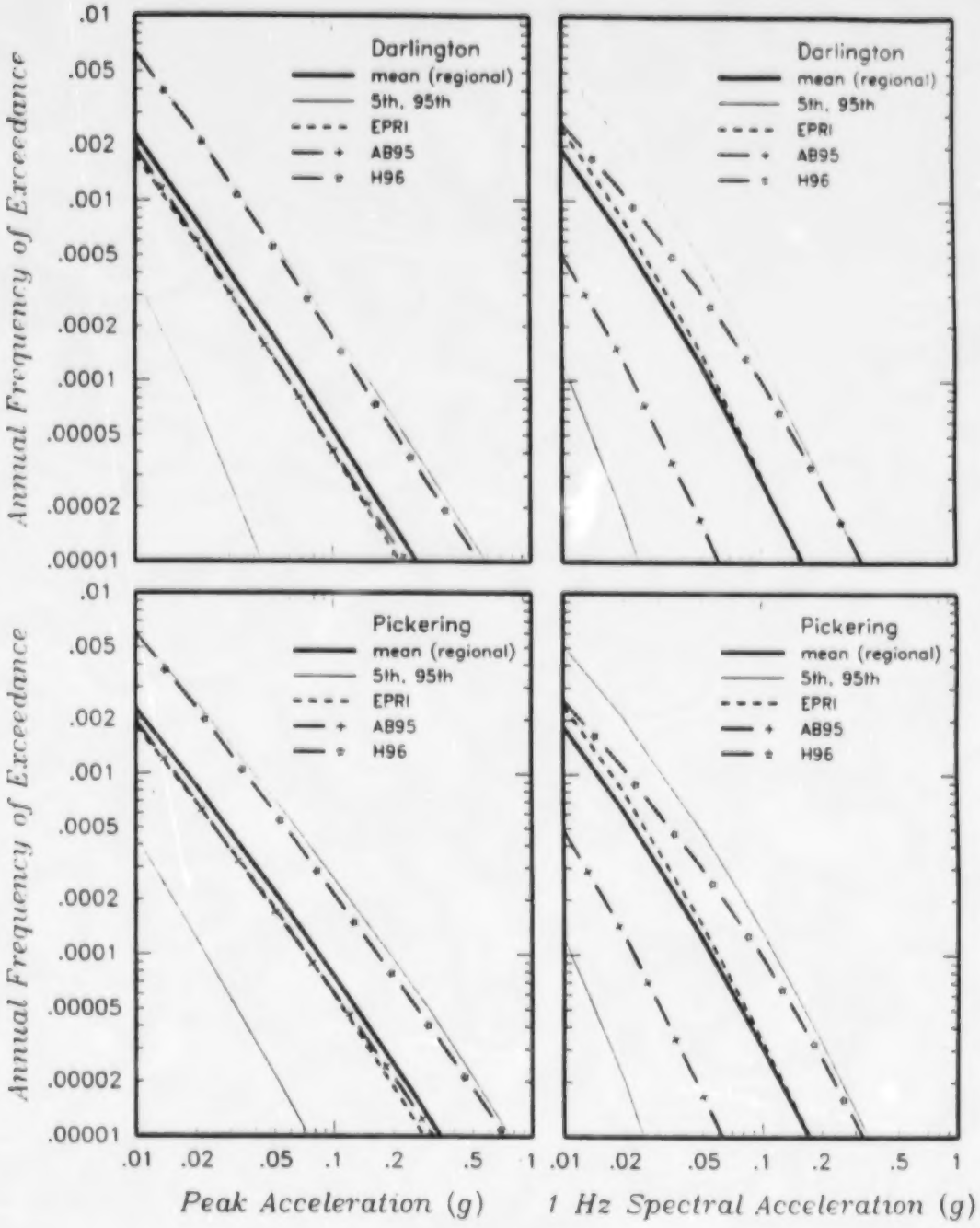

Figure 2-32a Effect of alternative attenuation relationships on the hazard from regional sources. The thick solid curves show the mean hazard from regional sources and the thin solid lines show the 5th and 95th percentile hazard curves for the regional sources. The attenuation models are EPRI - EPRI (1993), AB95 - Atkinson and Boore (1995), and H96 - source spectra based on Haddon (1996).

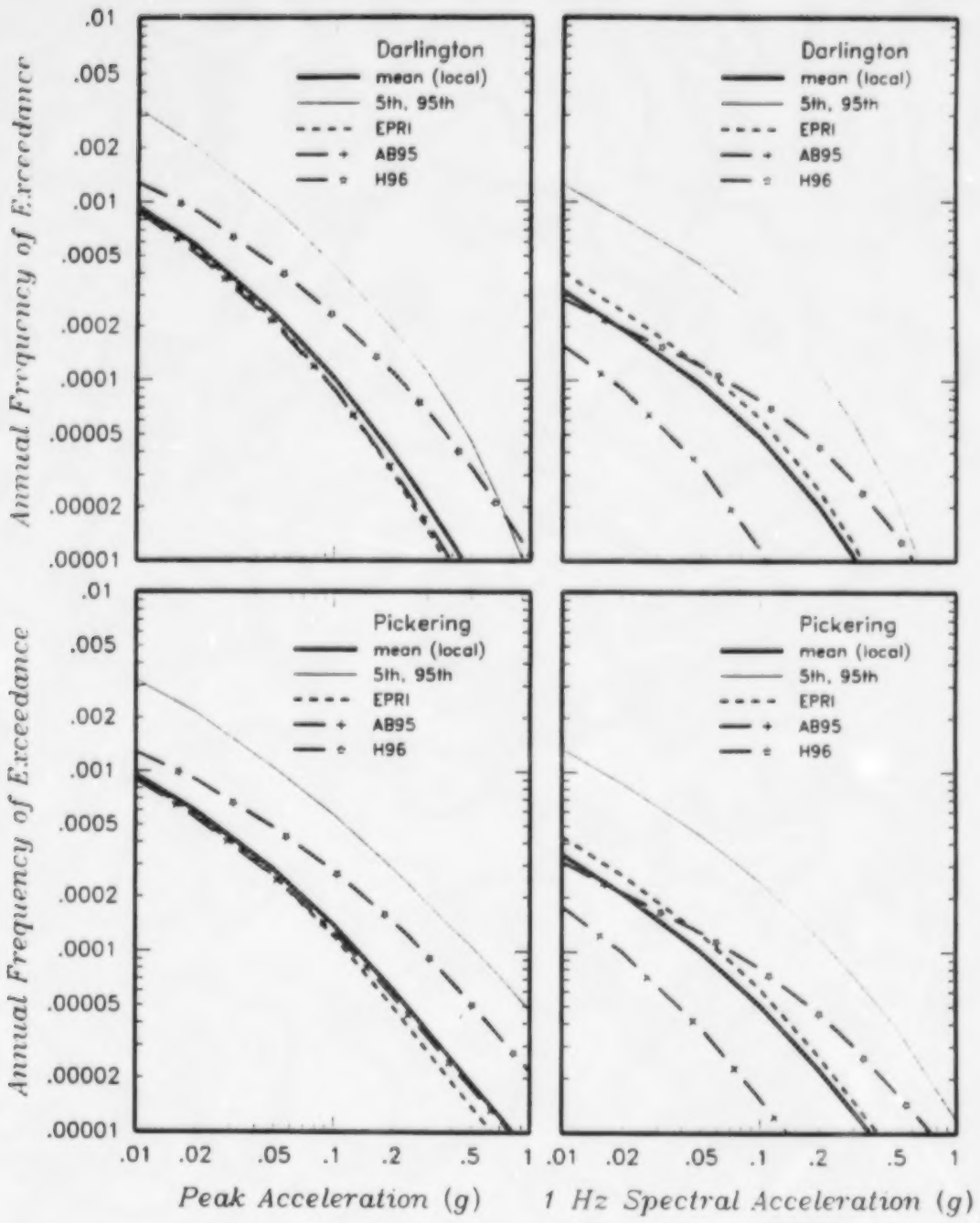

Figure 2-32b Effect of alternative attenuation relationships on the hazard from local sources. The thick solid curves show the mean hazard from local sources and the thin solid lines show the 95th percentile hazard curves for the local sources (the 5th-percentile hazard curves are at zero for the local sources). The attenuation models are EPRI - EPRI (1993), AB95 - Atkinson and Boore (1995), and H96 - source spectra based on Haddon (1996).

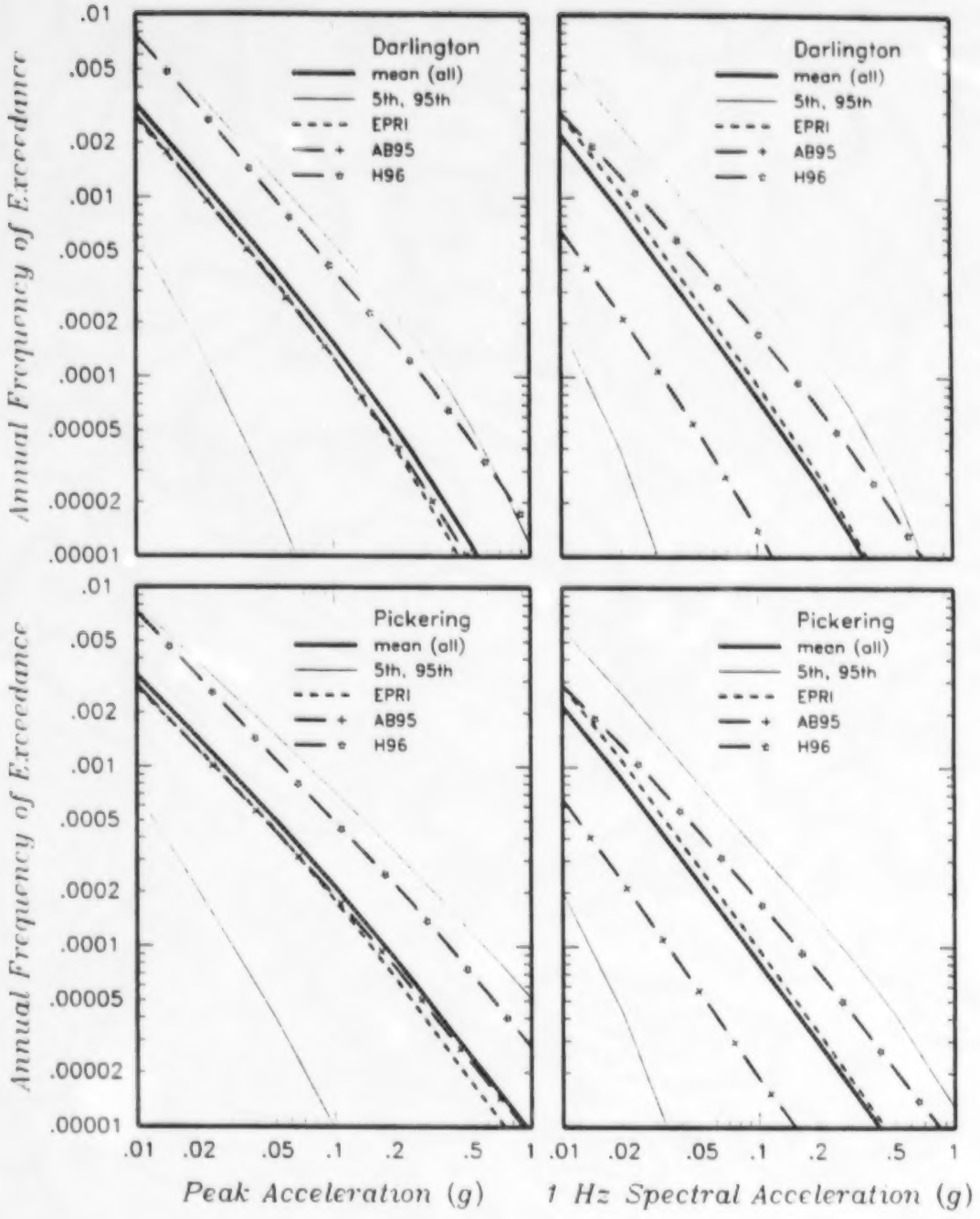

Figure 2-32c Effect of alternative attenuation relationships on the hazard from all sources. The thick solid curves show the mean hazard from all sources and the thin solid lines show the 5th and 95th percentile hazard curves for all sources. The attenuation models are EPRI - EPRI (1993), AB95 - Atkinson and Boore (1995), and H96 - source spectra based on Haddon (1996).

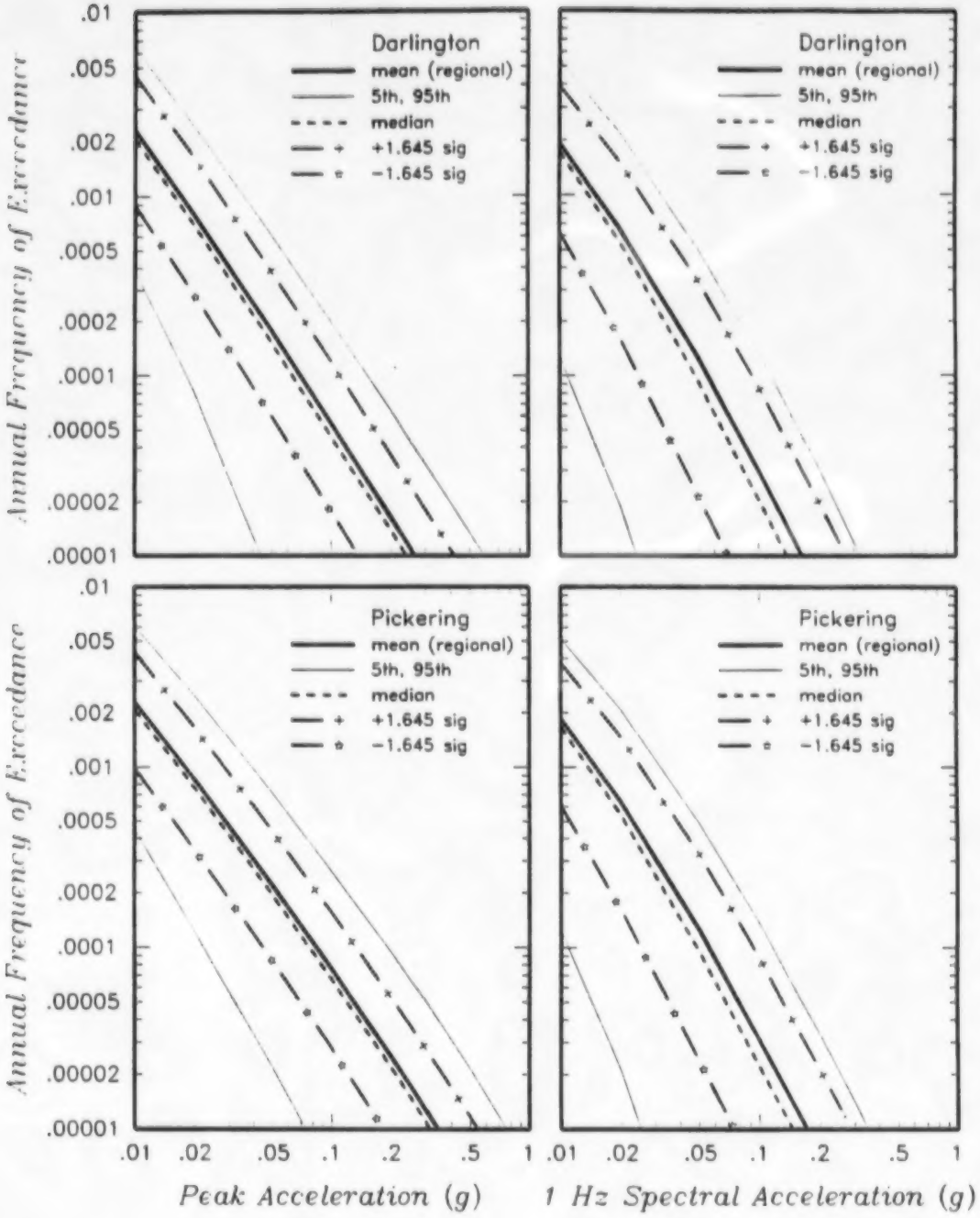

Figure 2-33a Effect of epistemic uncertainty in the attenuation relationships on the hazard from regional sources. The thick solid curves show the mean hazard from regional sources and the thin solid lines show the 5th and 95th percentile hazard curves for the regional sources.

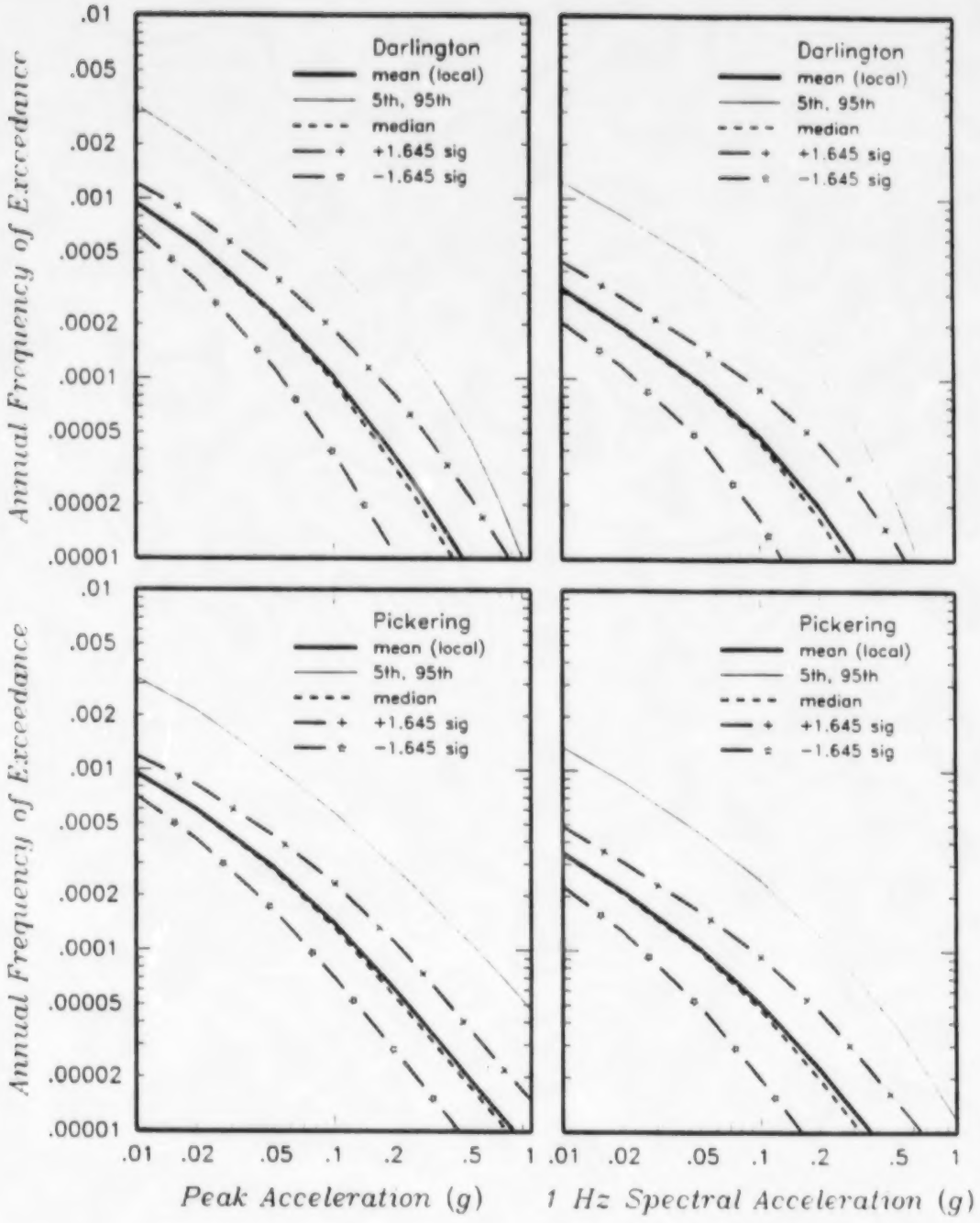

Figure 2-33b Effect of epistemic uncertainty in the attenuation relationships on the hazard from local sources. The thick solid curves show the mean hazard from local sources and the thin solid lines show the 95th percentile hazard curves for the local sources (the 5th-percentile hazard curves are at zero for the local sources).

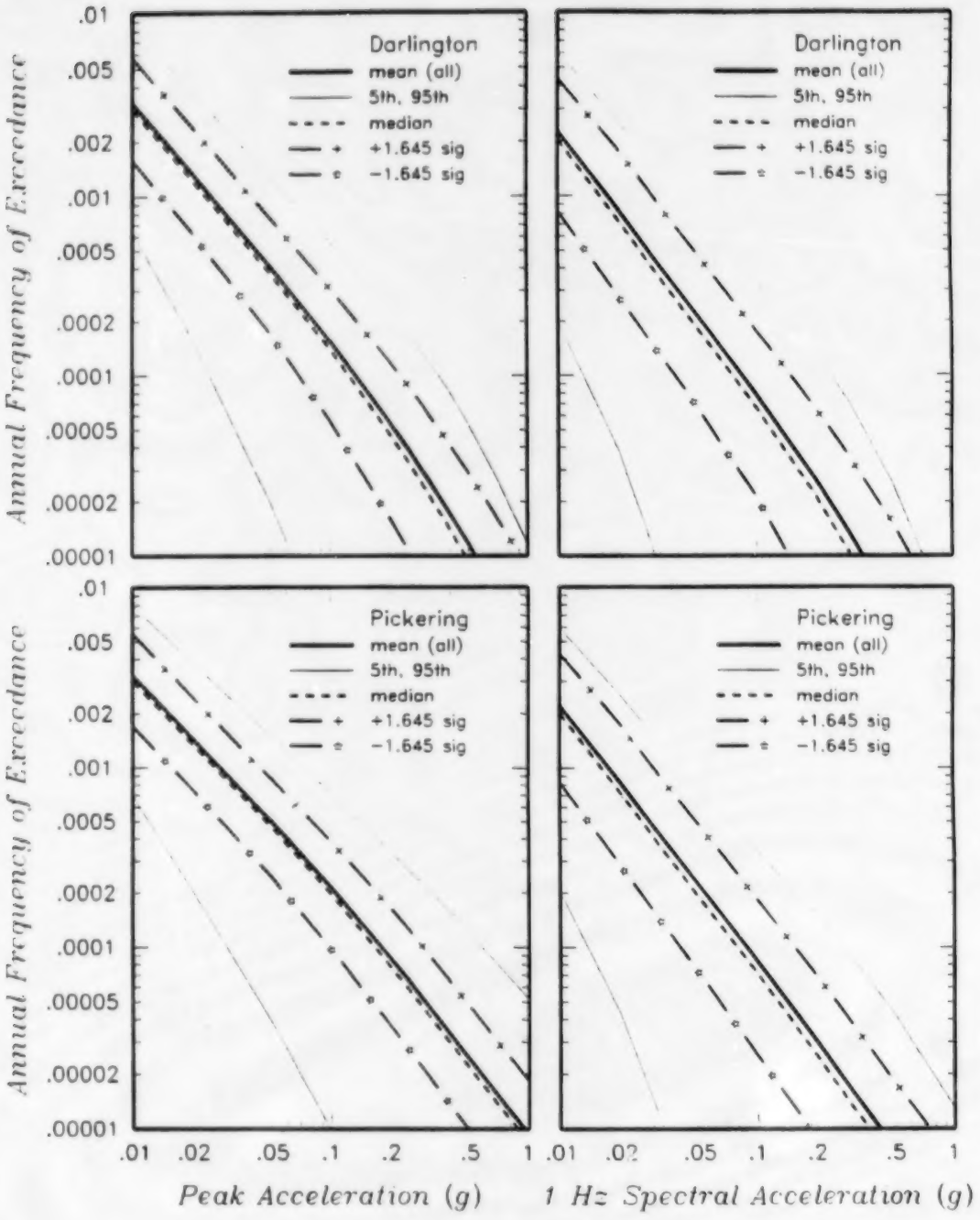

Figure 2-33c Effect of epistemic uncertainty in the attenuation relationships on the hazard from all sources. The thick solid curves show the mean hazard from all sources and the thin solid lines show the 5th and 95th percentile hazard curves for all sources.

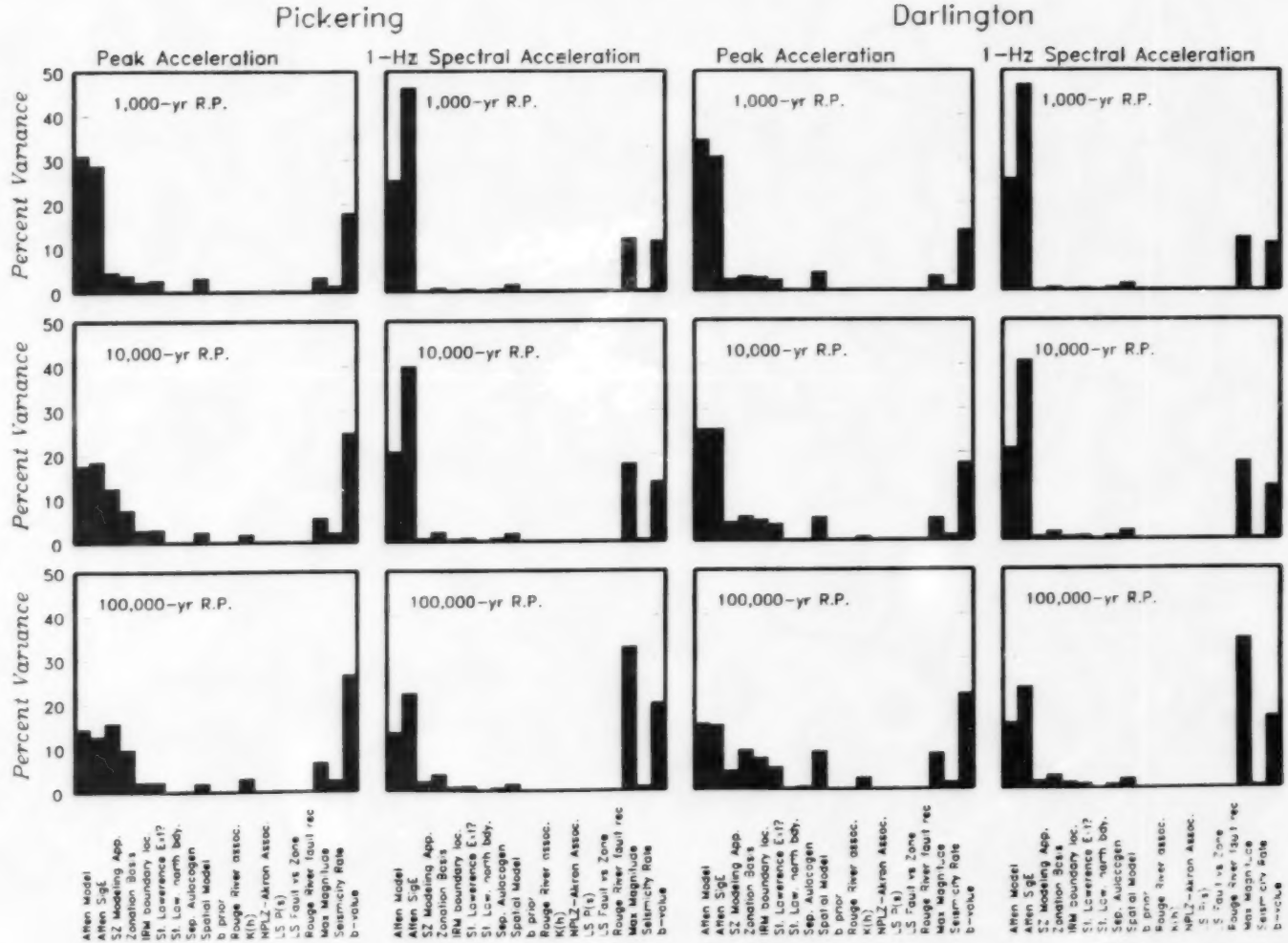

Figure 2-34 Disaggregation of the variance in the computed hazard from the regional sources into the relative contribution from the 19 levels of uncertainty in the overall logic tree uncertainty model for the PSHA.

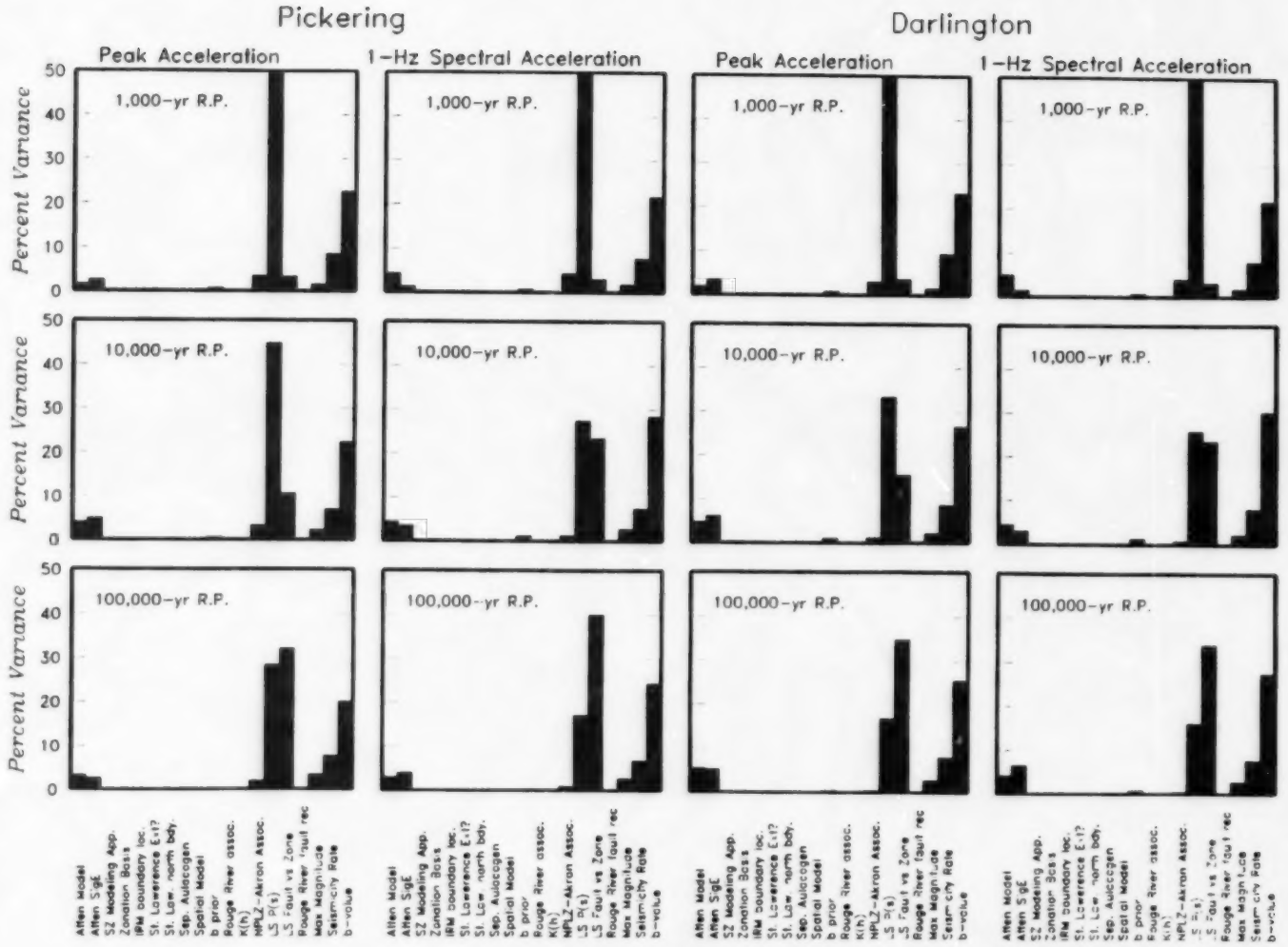

Figure 2-35 Disaggregation of the variance in the computed hazard from the local sources into the relative contribution from the 19 levels of uncertainty in the overall logic tree uncertainty model for the PSHA.

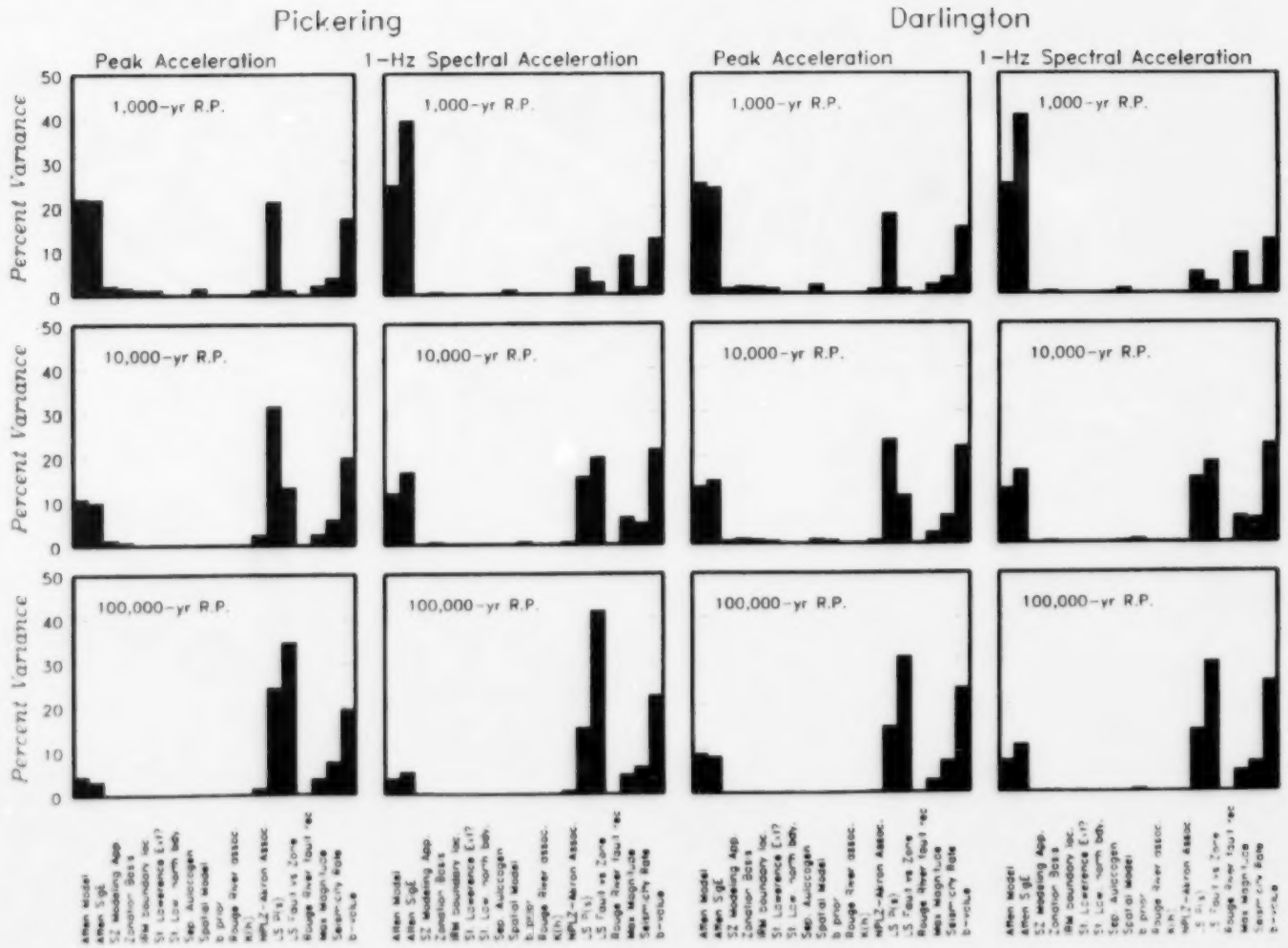

Figure 2-36 Disaggregation of the variance in the computed hazard from all sources into the relative contribution from the 19 levels of uncertainty in the overall logic tree uncertainty model for the PSHA.

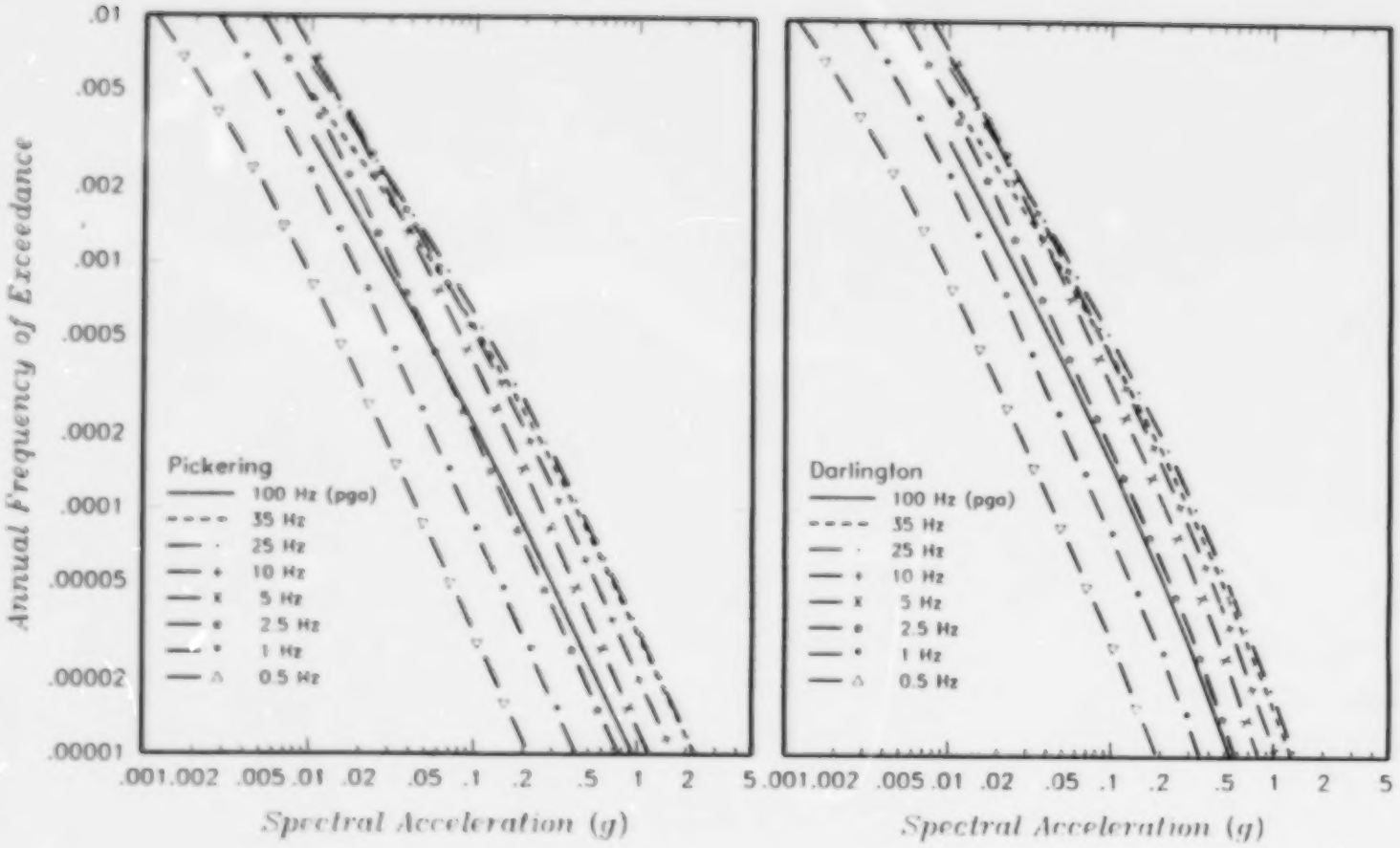

Figure 2-37 Mean hazard curves for the 8 spectral frequencies.

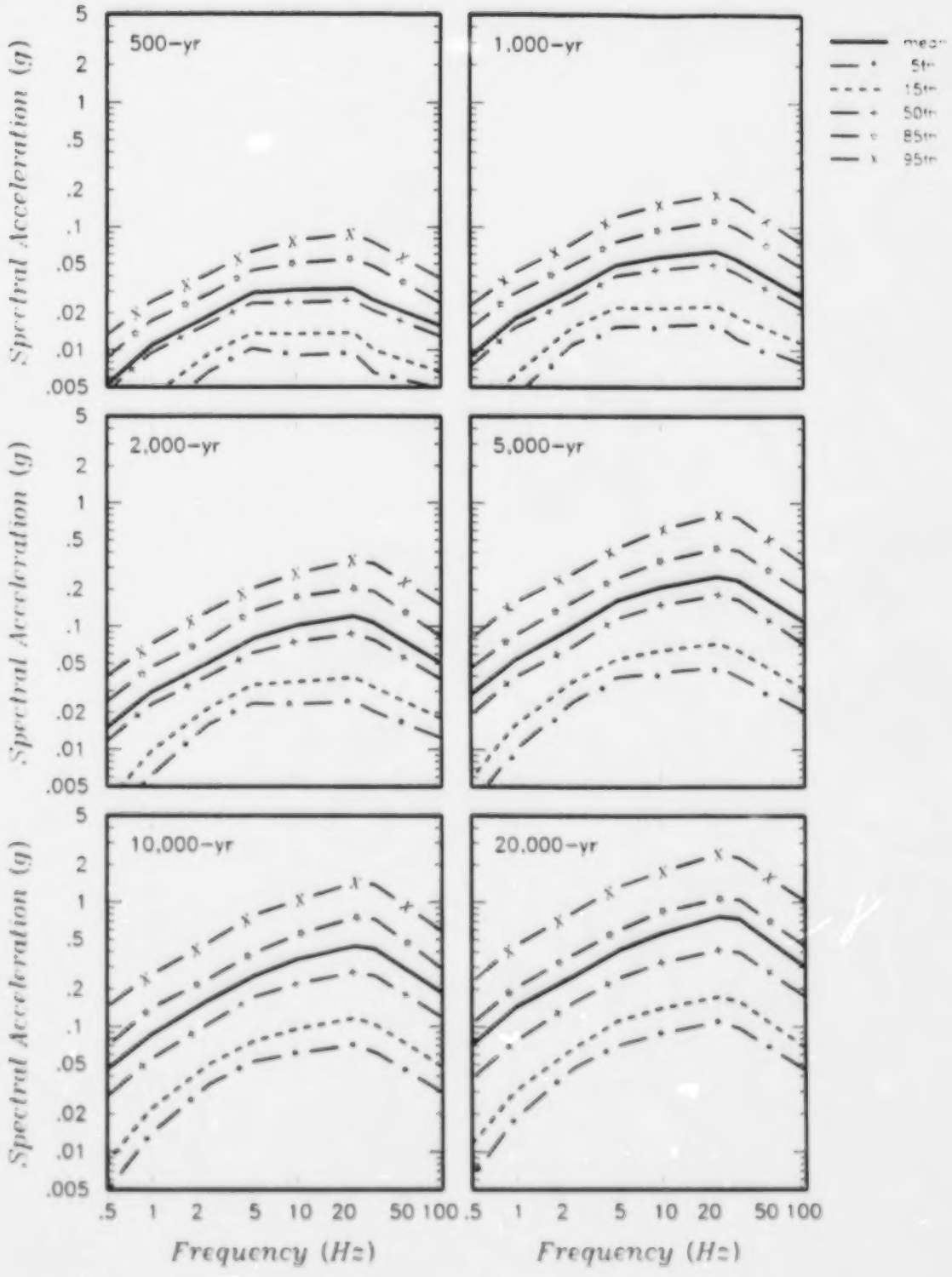

Figure 2-38 Equal-hazard spectra for the Pickering site

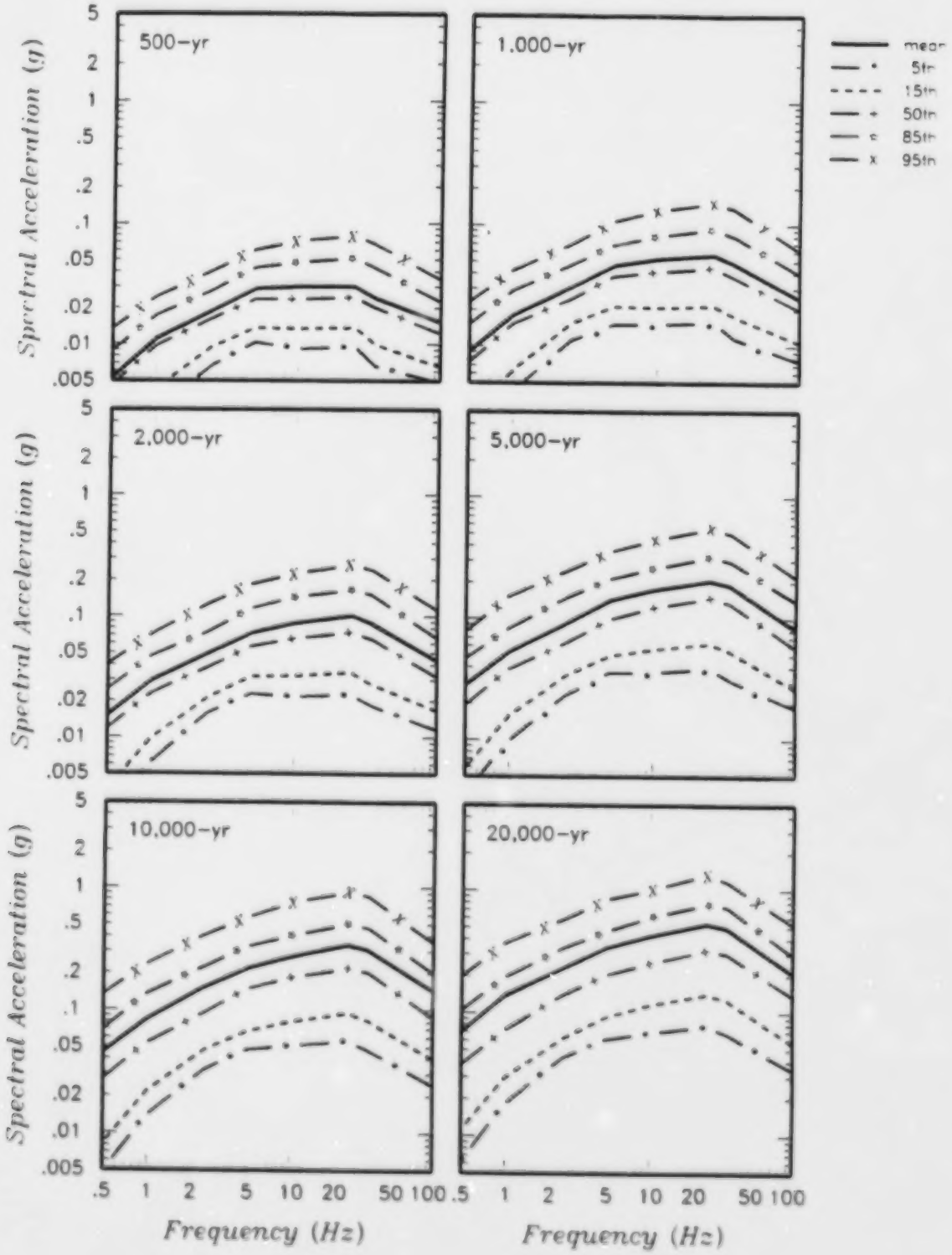

Figure 2-39 Equal-hazard spectra for the Darlington site.

3.0 REFERENCES

Adams, J., Weichert, D.H., Halchuk, S., and Basham, P.W., 1996, Trial seismic hazard maps of Canada - 1995: Final values for selected Canadian cities: Geological Survey of Canada, Open-File 3283, 97 p.

Atkinson, G.M., and Boore, D.M., 1995, Ground motion relations for eastern North America: Bulletin of the Seismological Society of America, v. 85, p. 11-27.

Atkinson, G.M., and Boore, D.M., 1997, Some comparisons between recent ground-motion relations: Seismological Research Letters, v. 68, n. 1, p. 29-40.

Cornell, C.A., 1968, Engineering seismic risk analysis: Bulletin of the Seismological Society of America, v. 58, p. 1583-1606.

Cornell, C.A., 1971, Probabilistic analysis of damage to structures under seismic loads: *in* Dynamic Waves in Civil Engineering,Howells, D.A. , Haigh, I.P., and Taylor, C. (eds.), John Wiley, London.

Electric Power Research Institute (EPRI), 1993, Guidelines for determining design basis ground motions: Electric Power Research Institute Report EPRI TR-102293, 5 v.

Haddon, R.A.W., 1996, Earthquake source spectra in eastern North America: Bulletin of the Seismological Society of America, v. 86, p. 1300-1313.

SSHAC, 1996, Probabilistic seismic hazard analysis: a consensus methodology: Senior Seismic Hazard Analysis Committee (R. Budnitz, G. Apostolokis, D. Boore, L. Cluff, K. Coppersmith, A. Cornell, P. Morris), U.S. Department of Energy, U.S. Nuclear Regulatory Commission, Electric Power Research Institute.

Toro, G.R., Abrahamson, N.A., and Schneider, J.F., 1997, Model of strong ground motions from earthquakes in central and eastern North America: best estimates and uncertainties: Seismological Research Letters, v. 68, n. 1, p. 41-57.

Veneziano, D., and van Dyck, J., 1985, Analysis of earthquake catalogs for incompleteness and recurrence rates: Seismic Hazard Methodology for Nuclear Facilities in the Eastern United States, EPRI Research Project N. P101-29, EPRI/SOG Draft 85-1, v.2, Appendix A, April 30.

Wheeler, R.L., 1995, Earthquakes and the cratonward limit of Iapetan faulting in eastern North America: Geology, v. 23, no. 2, p. 105-108.

APPENDIX A
MAXIMUM MAGNITUDE AND EARTHQUAKE RECURRENCE

This appendix presents estimates of the earthquake recurrence parameters and the maximum magnitude for the seismic source zones that are described in Sections 3 and 4 of the Part 1 report. Geometry of these sources are shown on Plates 1 through 15 of the Part 1 report. The results presented in this appendix are based on approaches that follow closely those presented in EPRI (1988) and Johnson and others (1994) and are described in Section 5.1.1 and Section 5.2 of the Part 1 report.

A.1 MAXIMUM MAGNITUDE

The maximum magnitude earthquake defines the upper truncation to earthquake recurrence relationships (m_u of Equation (A-1) below). Given the rare occurrence of maximum earthquakes and the lack of recognized surface expression or well defined seismicity patterns associated with most seismic sources in the central and eastern United States, the assessment of the maximum earthquake is difficult and previous studies have relied on approaches that commonly provide non-rigorous and non-unique solutions. The recently completed stable continental regions (SCR) earthquake project (Johnson and others, 1994) specifically addressed this problem and developed worldwide data bases that could be used to develop scientifically-supportable assessments of maximum earthquake magnitude for seismic sources in the central and eastern United States for use in probabilistic seismic hazard analysis. In this section, we present the probabilistic distribution of maximum magnitude that incorporates uncertainties of the assessment using the procedure in Johnson and others (1994). Detailed formulations of their approach are given in Chapters 5 and 6 of Johnson and others (1994).

Inputs into the assessment of maximum magnitude for each of the source zones are provided in Table A-1. The resulting distribution of maximum magnitude is re-normalized and discretized at intervals of 0.5 unit to obtain a discrete distribution centered on one-half

magnitude values (Figure A-1). This discrete distribution is used in the seismic hazard calculations.

A.2 EARTHQUAKE CATALOG ANALYSIS

A.2.1 Earthquake Recurrence Model

The earthquake occurrence in a given source zone is assumed to be a stationary, but not necessarily homogeneous, Poisson process. A truncated exponential rate-density function $\lambda(m_b, x)$ is used and it is expressed as:

$$\lambda(m, x) = \alpha(m^0, x) \frac{e^{-\beta(x)(m-m^0)}}{1 - e^{-\beta(x)(m^u-m^0)}}, \quad m^0 \le m \le m^u \qquad \text{(A-1)}$$

The recurrence parameter $\alpha(m^0,x)$ is the expected number of earthquakes with magnitude $\geq m^0$ per year per km^2 at location x; parameter $\beta(x) = ln(10)b(x)$, where $b(x)$ is the Gutenberg and Richter (1954) b-value at location x; and m^u is the maximum magnitude. We also include in our recurrence parameter estimation: (1) use of the rate-consistent body-wave magnitude, m_b^* (see Section A.2.2 below); (2) identification of dependent events by local cluster analysis; and (3) incorporation of the probability of earthquake detection into the recurrence model so incompletely reported data may also be used. The development of these items is discussed in the sections below. A more detailed description of the methodology can be found in EPRI (1988).

A.2.2 Magnitude Conversion

The catalog being analyzed in this study is described in Section 5.2.1 of Part I. Typically, the size of an earthquake is reported on a variety of scales. A single size measure must be used, however, in the analysis of earthquake clustering, record incompleteness, and recurrence rates. In the EPRI study (1988), m_b was chosen as the standard measure. The m_b values given in the catalog were converted from one of the three size measures: MMI (maximum Modified Mercalli Intensity), MMI/FA (Felt Area), and reliable instrumental

magnitudes, in the order of increasing preference. Conversion between MMI and m_b and between MMI/FA and m_b are based on the relations developed by Sibol and others (1987).

The catalog obtained from the Geological Survey of Canada lists the magntiude for most of the earthquakes prior to 1960 in terms of local Richter magnitude, M_L. However, many of these M_L values were estimated from MMI. Figure A-2 shows a plot of the M_L magnitudes in the catalog as a function of time before January 1, 1997. The horizontal dotted lines denote M_L magnitudes that correspond to unit MMI values. Most of the M_L values prior to about 1950 fall on these values. Therefore, the m_b estimates for these magnitudes were obtained by first converting the M_L magnitudes mack into the unit MMI values and then using the MMI-m_b relationships provided in Sibol and others (1987).

EPRI's study (1988) demonstrated that when m_b is estimated through conversion from other size measures, the statistical uncertainty on the m_b conversion introduces bias in the estimated recurrence parameters. An estimator m_b^* (called the uniform magnitude) is derived in such a manner that m_b^* leads to the same recurrence rate as the "true" m_b. When m_b is estimated from MMI or MMI/FA, m_b^* is defined as:

$$m_b^* = E[m_b] + \frac{1}{2} \ln(10)\ b\ \sigma_{m_b}^2 \qquad \text{(A-2)}$$

where $E[m_b]$ and σ_{mb}^2 are the mean value and variance of m_b given MMI or MMI/FA (See Tables 3 and 6 of Sibol and others, 1987). The influence of the assumed b-value on m_b^* is minimal and, thus, a single value of 1.00 is used for the purpose of calculating m_b^*. When $E[m_b]$ is determined directly from instrumental data, m_b^* is given by

$$m_b^* = E[m_b] - \frac{1}{2} \ln(10)\ b\ \sigma_{m_b}^2 \qquad \text{(A-3)}$$

Because σ_{mb}^2 in this case is very small (≈ 0.2), m_b^* is very close to $E[m_b]$.

A.2.3 Identification of Main Events and Dependent Events

The earthquake recurrence model applied in this study assumes earthquake occurrence is a Poisson process. However, it is well known that actual earthquakes tend to occur in clusters of short duration and over a small region in space. The earthquakes in a cluster could be causally or physically related to a parent (main) earthquake. Examples of such clustering phenomena are foreshocks and aftershocks. The mathematical formulation used in this (and most) hazard analysis is based on an assessment of the frequency of occurrence of main earthquakes and it is thus necessary to remove dependent events from the earthquake catalog used in the recurrence estimation.

In the EPRI study (1988), a local cluster analysis was used to identify dependent events. In the analysis, the spatial-temporal extent of a cluster is first identified; then, the largest earthquake in the cluster is classified as main earthquake and the remaining members of the cluster as dependent events. The cluster region is estimated as the largest spatial-temporal window (surrounding the main event) in which the seismicity rate is statistically different from the background rate. The shape and size of a cluster thus varies from one cluster to another.

We applied this local cluster analysis to the earthquake catalog. Results from our analysis show few changes from the previous designation given in the EPRI's catalog. Distribution of the identified mainshocks are shown on the Plates in the Part 1 report.

A.2.4 Catalog Incompleteness and Earthquake Recurrence Model

The earthquake sequence in a historical catalog is normally nonstationary in time due to incomplete reporting of earthquakes. One approach of dealing with incomplete reporting is to estimate the recurrence rate based on the seismic activity during a time period over which earthquakes can be considered completely reported in the catalog (e.g. Weichert, 1980). This approach requires that earthquakes occurred in the period of incomplete reporting not be used. The completeness period is usually determined by a method based on the stability of observed recurrence rate in a magnitude interval as a function of time before the present (Stepp, 1972). The point in time at which the rate begins to steadily

diminish with increasing time before the present indicates the time before which the catalog may be incomplete. This method requires a certain degree of judgment at very low and very high magnitudes.

In this study, a general recurrence model developed by EPRI (1988) was adopted so that incompletely reported data may also be used for the estimation of recurrence rate. For convenience, the symbol * of m_b^* will be omitted in the following discussion, with the understanding that m_b^* is being used.

The basic component of EPRI's model is the use of probability of earthquake detection to account for the reduction of observed rate due to incomplete reporting. The rate of the "catalog" earthquake is the product of the true rate $\lambda(m_b, \mathbf{x})$ and the probability of detection $P_D(x, m_b, t)$, which is defined as the probability that an earthquake of given magnitude m_b, origin time t, and epicenter x is reported in the catalog. Probability of detection improves with larger magnitude events and recent origin times. $P_D(x, m_b, t)$ equals to 1.0 means complete reporting

For this study, we used the discretization scheme developed for the EPRI (1988) study. To assess the completeness of the EPRI catalog, $P_D(x, m_b, t)$ in central and eastern United States (CEUS) was discretized in the EPRI study by partitioning the (x, m_b, t) space into six magnitude intervals $\{(m_{i-1}, m_i), i=1,6\}$, thirteen incompleteness regions delineated by thirteen polygons $\{R_k, k=1,13\}$, and six observing periods $\{t_j, j=1,6\}$ (see Table A-2). Incompleteness regions relevant to the study area of this analysis are shown in Figure A-3. Probability of detection inside each sub-volume is assumed to be constant. The definitions of the thirteen incompleteness regions are entirely based on the demographic and instrumental evolution and boundaries of the regional catalogs in CEUS and are independent of the definitions of seismic source zones or seismicity.

To allow for spatial variation of recurrence parameters, a given source zone may be subdivided by meridian lines into subzones (indexed by the integer l) independent of the incompleteness region. Each subzone has its own constant recurrence rate-density. From Equation (A-1), the truncated exponential rate density for earthquakes in the i-th magnitude interval (m_{i-1}, m_i) and subzone l is then given by the expression:

$$\lambda_{il} = \alpha_l(m_o) \frac{e^{-\beta_l (m_{i-1}-m_o)} - e^{-\beta_l (m_i-m_o)}}{1 - e^{-\beta_l (m_u-m_o)}} \qquad \text{(A-4)}$$

Note the definitions for α_l and β_l ($= ln(10)\ b_l$) in the above equation follow the conventions adopted in most publications (e.g. Weichert (1980)), but are different from those used in EPRI's study (1988). In EPRI's notation, the rate-density for the i-th magnitude interval is expressed as

$$\lambda_{il} = e^{\alpha_l - \beta_l (i-1)} \qquad \text{(A-5)}$$

where α_l is now the logarithm of the expected number of earthquakes per year per squared equatorial degree in the first magnitude interval ($3.3 \le m_b < 3.9$); β_l is equal to $0.6\ ln(10)\ b_l$, where 0.6 is the length of the magnitude interval in Table A-2. Conversions of EPRI's recurrence parameters to the accumulative rate and the b-value as defined in Equation (A-1) are always made before being presented in this Appendix.

For the i-th magnitude interval and the j-th observing period, the probability of "observing" n_{ijkl} events in an area A_{kl} common to the l-th subzone and the k-th incompleteness region is

$$Prob(N=n_{ijkl}) = \frac{(\lambda_{il} P_{D_{ijk}} A_{kl} t_j)^{n_{ijkl}} e^{-\lambda_{il} P_{D_{ijk}} A_{kl} t_j}}{n_{ijkl}!} \quad \text{(A-6)}$$

To estimate the true recurrence rate and the probability of detection, a likelihood function for the entire catalog is formed, including earthquakes that occurred during the period of incomplete reporting. The logarithm of the likelihood function is

$$\begin{aligned} \ln L = & \left[\sum_{l=1}^{L} \sum_{k=1}^{13} \sum_{j=1}^{6} \sum_{i=1}^{6} n_{ijkl} \ln(\lambda_{il} P_{D_{ijk}} A_{kl} t_j) - \lambda_{il} P_{D_{ijk}} A_{kl} t_j - \ln(n_{ijkl}!) \right] \\ & - \frac{W_\alpha}{2} \sum_{l=1}^{L} (\alpha_l - \bar{\alpha}_l)^2 - \frac{W_\beta}{2} \sum_{l=1}^{L} (\beta_l - \bar{\beta}_l)^2 \\ & - \frac{W_P}{2} \sum_{i=1}^{6} \sum_{j=1}^{6} (P_{D_{ijk}} - \bar{P}_{D_{ijk}})^2 - \frac{W_{\beta'}}{2} \sum_{l=1}^{L} (\beta_l - \beta_l^P)^2 \end{aligned} \quad \text{(A-7)}$$

The second and third terms of the likelihood function impose smoothness on α and β as a function of space and the fourth term on P_D as a function of magnitude and time. The last term in Equation (A-7) represents the contribution from the β-prior distribution, where β^P_l is the prior for β. Variables $\bar{P}_{Dijk}$, $\bar{\alpha}_P$ and $\bar{\beta}_l$ are local averages and W_α, W_β, and W_p are user-specified coefficients that adjust the degree of variation (smoothness) of α, β, and P_D, respectively, with respect to these local averages. One can maximize Equation (A-7) to jointly estimate the parameters $\{\alpha_l, \beta_l, P_{Dijk}\}$ most likely to represent the Poisson process and the recording history that produces the observed catalog. A more detailed discussion of this likelihood function is provided by EPRI (1988) and Geomatrix (1995).

Probabilities of detection for the entire CEUS were estimated jointly with the recurrence parameters in EPRI's study (1988) using subzones of one-degree cell (their base case analysis. Re-evaluation of P_D subjecting to the same conditions as EPRI's analysis were made (Geomatrix, 1996) using the NCEER91 catalog only. Differences between the new estimates and the old estimates obtained by EPRI's study are small. We have assumed these estimates are also applicable to this study. Values of P_D for incompleteness regions

relevant to the study area are tabulated in Table A-3. Also shown in Table A-3 are the default time intervals (solid lines) used in our estimation of the recurrence relation.

A.2.5 Estimation of Recurrence Parameters in a Homogeneous Source Zone

The assumption of homogeneous rate density is made for seismic source zones and local faults. Recurrence parameters for the local fault source is estimated from the observed seismicity in an area surrounding the fault as described in Section 5.3 of the previous report. The homogeneous rate density assumption leads to a much simpler likelihood function than Equation **(A-7)**. With the homogeneity assumption, $L=1$, and index l is dropped; the second and third terms in **(A-7)** are always zero. In order to reduce computational effort, we fix the incompleteness parameters P_D to the values determined earlier by Geomatrix (1996) (Table A-3). Fixing P_D is also necessitated by the difficulty in estimating P_D for a small area. The penalty term associated with P_D is thus a constant and can be ignored. Equation **(A-7)** is thus reduced to the likelihood function of Weichert (1980), with extensions to include the probability of detection and a stabilizing prior on b-value (EPRI, 1988; Geomatrix, 1995). The likelihood function is expressed as:

$$\ln L \propto \left[\sum_{k=1}^{13} \sum_{i=1}^{6} \sum_{j=1}^{6} n_{ijk} \ln(\lambda_i P_{D\,ijk} A_k t_j) - \lambda_i P_{D\,ijk} A_k t_j \right] - \frac{W_{\beta}{}^{p}}{2} (\beta - \beta^{p})^2 \qquad \textbf{(A-8)}$$

Because of the sparse seismicity in some of the source area, a prior b-value of 0.9 representing the average b-value in the northeastern US (Jacob and others, 1994; Frankel, 1995) is imposed with a weight coefficient of 5.0 (i.e. $\beta^{p} = 0.9\ ln(10)$ and $W_{\beta}{}^{p} = 5.0$ in Equation **(A-8)**. This b-prior has little effect on the final b-value estimate where observed seismicity is high, but it helps to constrain and stabilize b-value estimates in cases where there are insufficient observations to give a reliable estimate. However, as discussed in Section 5.3, for the local sources, a strong b-prior of 0.94 representing the average of the estimated b-values of the surrounding source zones is used. The weight coefficient used for these local sources are higher by a factor of 8.

Table A-4 tabulates the maximum likelihood estimates of the recurrence parameters for these homogeneous source zones. The associated estimation uncertainty is given as the standard error σ_a and σ_b in Table A-4. The contribution of this estimation uncertainty to the uncertainty of seismic hazard is incorporated into the logic via a set of 25 recurrence relations that cover the range of two standard errors centered at the maximum likelihood solution. Each of these 25 relations is given a weight proportional to the likelihood that it actually generates the observed seismicity.

A.2.6 Estimation of Recurrence Parameters in an Inhomogeneous Source Zone - EPRI's Approach

The treatment of the study area as an inhomogeneous source zone is discussed in Section ? of the previous report, in which a model that relies entirely on historical seismicity is proposed as an alternative to the geology-based source model. For this seismicity-based model (Plate 12), the entire study area is divided into subzones of one-degree cells and each subzone has its own recurrence parameters. To jointly estimate the recurrence parameters, Equation (A-7) is maximized by the algorithm described in EPRI (1988) with the probability of detection fixed at the values listed in Table A-3. Four smoothing conditions are selected for analysis, where (W_a, W_b) = (0, 25), (5, 25), (0, 50), and (5, 50). The two selected values of W_a correspond to no smoothing (W_a=0) and weak smoothing (W_a=5) on α_i, whereas W_b values of 25 and 50 represent weak and moderate smoothing, respectively, on b_i. Because the b-value is a more stable quantity, a higher level of smoothing is adopted for b_i than for α_i, as was recommended by EPRI (1988). As for the homogeneous case, a b-prior of 0.9 is applied. The resulting maximum likelihood estimates for the four smoothing are shown in Figure A-4.

Uncertainty in estimating cell-by-cell seismicity parameters was incorporated into the seismic hazard calculations by a set of 100 recurrence relations. These relations are the results of 100 artificial catalogs generated by the bootstrapping technique (EPRI, 1988).

Each relation is given the same weight. An example of the distribution of these 100 relations is given in Figure A-5.

REFERENCES

Electric Power Research Institute (EPRI), 1988, Seismic hazard methodology for the central and eastern United States - EPRI Report NP-4726, vols. 1-10

Frankel, A., 1995, Mapping seismic hazard in the central and eastern United States, submitted to Seismological Research Letters.

Geomatrix, 1995, Seismic design mapping, State of Oregon, Report to the Oregon Department of Transportation.

Gutenburg, B., Richter, C.F., 1954, Seismicity of the Earth and Associated Phenomena, Princeton University Press, Princeton, N.J., 273 p.

Johnston, A.C., Coppersmith, K.J., Kanter, L.R., and Cornell, C.A., 1994, The earthquakes of stable continental regions, Volume 1; Assessment of large earthquake potential: Final report submitted to Electric Power Research Institute (EPRI), TR-102261-V1.

Seeber, A., and Armbruster, J.G., 1991, The NCEER-91 Earthquake Catalog: Improved intensity-based magnitudes and recurrence relations for U.S. earthquakes east of New Madrid, Technical Report NCEER-91-0021, National Center for Earthquake Engineering Research, Buffalo, New York.

Sibol, M.S., Bollinger, G.A., and Birch, J.B., 1987, Estimation of magnitudes in central and eastern North America using intensity and felt area, Bulletin of Seismological Society of America, v. 77, p. 1635-1654.

Stepp, J.C., 1972, Analysis of the completeness of the earthquake hazard sample in the Puget Sound area and its effect on statistical estimates of earthquake hazard, Proceedings for International Conference on Microzonation for Safer Construction Research Application 2, Seattle, Washington, p. 897-909.

Weichert, D.H., 1980, Estimation of the earthquake recurrence parameters for unequal observation periods for different magnitudes, Bulletin Seismological Society of America, v. 70, p. 1337-1346.

GEOMATRIX

TABLE A-1
MAXIMUM MAGNITUDE ASSESSMENT PARAMETERS

Description of Source	Ref. Plate	Source Zone Abbreviation	Indicator Variables										Predicted Mean	No. of Events wt.	Historical Maximum Mag. (m_{max})
			Domain Type			Basement Age			Stress Regime		Activity Log	Bounding Crust Type				
			Margin (X_1)	Margin (X_2)	Rift (X_3)	Meso zoic (X_4)	Paleo zoic (X_5)	Pre-Camb (X_6)	Comp. (X_7)	Ext. (X_8)	(Rate) (X_9)	Oceanic (X_{10})	Continental (X_{11})	Mw	Mw>4.5	
Northern Adirondacks	13	ADR	1.0	0.0	0.0	0.0	1.0	0.0	1.0	0.0	0.644	0.0	1.0	5.44	1	5.6
Atlantic Offshore Background	13	AOBH	0.0	1.0	0.0	1.0	0.0	0.0	1.0	0.0	-0.311	1.0	0.0	6.24	1	7.0
Anna, Ohio	13	AOH	0.0	0.0	1.0	0.0	0.0	1.0	1.0	0.0	1.501	0.0	1.0	6.30	3	5.1
Bas Saint Laurent	13	BSL	0.0	1.0	0.0	0.0	1.0	0.0	1.0	0.0	1.210	0.0	1.0	5.92	0	4.7
Champlain	13	CHA	1.0	0.0	0.0	0.0	1.0	0.0	1.0	0.0	1.106	0.0	1.0	5.58	1	5.2
Charlevoix	13	CHV	0.0	1.0	0.0	0.0	1.0	0.0	1.0	0.0	2.427	0.0	1.0	6.31	10	7.0
Cochrane	13	COC	0.0	0.0	1.0	0.0	1.0	0.0	1.0	0.0	0.237	0.0	1.0	5.48	0	4.4
Gatineau	13	GAT	0.0	0.0	0.0	1.0	0.0	0.0	1.0	0.0	1.241	0.0	0.0	6.72	2	5.5
Montreal	13	MNT	0.0	0.0	1.0	0.0	1.0	0.0	1.0	0.0	1.101	0.0	1.0	5.75	4	5.8
Northern Appalachians	13	NAN	0.0	0.0	0.0	0.0	1.0	0.0	1.0	0.0	0.584	0.0	0.0	6.09	6	7.0
Niagara Attica Trend	13	NAT	0.0	0.0	0.0	0.0	0.0	1.0	1.0	0.0	1.057	0.0	0.0	6.66	1	5.5
Ontario Background	13	OBGH	0.0	0.0	0.0	0.0	0.0	1.0	1.0	0.0	0.019	0.0	0.0	6.33	5	5.5
Pembroke	13	PEM	0.0	0.0	1.0	0.0	1.0	0.0	1.0	0.0	0.849	0.0	1.0	5.67	0	4.7
Passamaquoddy Bay	13	PMQ	0.0	0.0	0.0	0.0	1.0	0.0	1.0	0.0	1.543	0.0	0.0	6.39	2	5.9
Saguenay	13	SAG	0.0	0.0	1.0	0.0	1.0	0.0	1.0	0.0	0.716	0.0	1.0	5.63	0	3.8
Southeast Canada Background	13	SEB	0.0	0.5	0.0	0.0	0.5	0.5	1.0	0.0	0.371	0.0	0.5	6.04	1	6.5
South Shore Lake Erie	13	SLE	0.0	0.0	0.0	0.0	0.0	1.0	1.0	0.0	0.790	0.0	0.0	6.57	1	5.3
TAD	13	TAD	0.0	1.0	0.0	0.0	1.0	0.0	1.0	0.0	0.727	0.0	1.0	5.76	0	3.5
Timiskaming	13	TIM	0.0	0.0	1.0	0.0	1.0	0.0	1.0	0.0	1.406	0.0	1.0	5.85	1	5.6
Trois-rivieres	13	TRR	0.0	1.0	0.0	0.0	1.0	0.0	1.0	0.0	0.715	0.0	1.0	5.76	0	4.5

TABLE A-1 (Continued)
MAXIMUM MAGNITUDE ASSESSMENT PARAMETERS

Description of Source	Ref. Plate	Source Zone Abbreviation	Indicator Variables[2]											Predicted Mean	No. of Events wt.	Historical Maximum Mag. (m_{max})
			Domain Type			Basement Age			Stress Regime		Activity Log	Bounding Crust Type				
			Margin	Margin *	Rift	Meso zoic	Paleo zoic	Pre-Camb	Comp.	Ext.	(Rate)	Oceanic	Continental	Mw	Mw>4.5	
			(X_1)	(X_2)	(X_3)	(X_4)	(X_5)	(X_6)	(X_7)	(X_8)	(X_9)	(X_{10})	(X_{11})			
Adirondak	11	ADIRONDA	0.0	1.0	0.0	0.0	1.0	0.0	1.0	0.0	0.931	0.0	1.0	5.83	5	5.8
Maniwaki	11	MANIWAKI	0.0	0.0	0.0	0.0	0.0	1.0	1.0	0.0	1.100	0.0	0.0	6.67	2	5.5
Niagara	11	NIAGARA	0.0	0.0	0.0	0.0	0.0	1.0	1.0	0.0	0.632	0.0	0.0	6.52	1	5.5
Ottawa	11	OTTAWA	0.0	0.0	1.0	0.0	1.0	0.0	1.0	0.0	0.689	0.0	1.0	5.62	1	5.6
Rochester	11	ROCHESTE	0.0	0.0	0.0	0.0	0.0	1.0	1.0	0.0	-0.415	0.0	0.0	6.19	0	4.8
Central Craton, w/. OG	1A	CC-A	0.0	0.0	0.0	0.0	0.0	1.0	1.0	0.0	0.259	0.0	0.0	6.40	3	5.1
Central Craton, w/o OG	10	CC-B	0.0	0.0	0.0	0.0	0.0	1.0	1.0	0.0	0.239	0.0	0.0	6.40	3	5.1
Central Craton (A), w/. Narrow SLE	4A	CC_N	0.0	0.0	0.0	0.0	0.0	1.0	1.0	0.0	-0.328	0.0	0.0	6.22	0	4.8
Central Cradon (A), w/ Wide SLE	7A	CC_W	0.0	0.0	0.0	0.0	0.0	1.0	1.0	0.0	-0.303	0.0	0.0	6.22	0	4.8
Extended continental Crust	10	ECC	0.5	0.5	0.0	1.0	0.0	0.0	1.0	0.0	0.465	1.0	0.0	6.34	13	7.0
Grenville Domain	10	GD	0.0	0.5	0.0	0.0	0.5	0.5	1.0	0.0	0.452	0.0	0.5	6.07	23	7.0
Great Meteor Hotspot	10	GMH	0.0	0.0	0.0	1.0	0.0	0.0	1.0	0.0	1.244	0.0	0.0	6.72	2	5.5
Iapetan Rifted Margin	1A	IRM-A	0.0	1.0	0.0	0.0	1.0	0.0	1.0	0.0	0.598	0.0	1.0	5.72	16	7.0
Iapetan Rifted Margin	2A	IRM-B	0.0	1.0	0.0	0.0	1.0	0.0	1.0	0.0	0.557	0.0	1.0	5.71	17	7.0
Iapetan Rifted Margin	3A	IRM-C	0.0	1.0	0.0	0.0	1.0	0.0	1.0	0.0	0.640	0.0	1.0	5.73	16	7.0
Iapetan Rifted Margin	1B	IRM-A2	0.0	1.0	0.0	0.0	1.0	0.0	1.0	0.0	0.607	0.0	1.0	5.72	19	7.0
Iapetan Rifted Margin	2B	IRM-B2	0.0	1.0	0.0	0.0	1.0	0.0	1.0	0.0	0.570	0.0	1.0	5.71	20	7.0
Iapetan Rifted Margin	3B	IRM-C2	0.0	1.0	0.0	0.0	1.0	0.0	1.0	0.0	0.643	0.0	1.0	5.74	19	7.0
Iapetan Rifted Margin	4B	IRM-A3	0.0	1.0	0.0	0.0	1.0	0.0	1.0	0.0	0.658	0.0	1.0	5.74	23	7.0
Iapetan Rifted Margin	5B	IRM-B3	0.0	1.0	0.0	0.0	1.0	0.0	1.0	0.0	0.690	0.0	1.0	5.75	24	7.0
Iapetan Rifted Margin	6B	IRM-C3	0.0	1.0	0.0	0.0	1.0	0.0	1.0	0.0	0.684	0.0	1.0	5.75	24	7.0
Iapetan Rifted Margin	7B	IRM-A4	0.0	1.0	0.0	0.0	1.0	0.0	1.0	0.0	0.653	0.0	1.0	5.74	23	7.0
Iapetan Rifted Margin	8B	IRM-B4	0.0	1.0	0.0	0.0	1.0	0.0	1.0	0.0	0.619	0.0	1.0	5.73	24	7.0
Iapetan Rifted Margin	9B	IRM-C4	0.0	1.0	0.0	0.0	1.0	0.0	1.0	0.0	0.652	0.0	1.0	5.74	24	7.0
Northern Appalachians	10	NAZ	0.0	0.0	0.0	0.0	1.0	0.0	1.0	0.0	0.435	0.0	0.0	6.04	1	5.5
Northern Grenville	10	NGR	0.0	0.0	0.0	0.0	0.0	1.0	1.0	0.0	0.683	0.0	0.0	6.54	2	5.5
Ottawa Graben	1A	OG	0.0	0.0	1.0	0.0	1.0	0.0	1.0	0.0	0.694	0.0	1.0	5.62	2	5.8

GEOMATRIX

TABLE A-1 (Continued)
MAXIMUM MAGNITUDE ASSESSMENT PARAMETERS

Description of Source	Ref. Plate	Source Zone Abbreviation	Indicator Variables: Domain Type			Basement Age			Stress Regime		Activity Log	Bounding Crust Type		Predicted Mean	No. of Events wt.	Historical Maximum Mag. (m_{max})
			Margin	Margin *	Rift	Meso zoic	Paleo zoic	Pre-Camb	Comp.	Ext.	(Rate)	Oceanic	Continental	Mw	Mw>4.5	
			(X_d)	(X_d)	(X_d)	(X_d)	(X_d)	(X_d)	(X_d)	(X_d)	(X_d)	(X_{rd})	(X_{rd})			
Sagueney Graben	1A	SG	0.0	0.0	1.0	0.0	1.0	0.0	1.0	0.0	0.800	0.0	1.0	5.66	1	6.5
Southern Grenville (A)	1A	SGR-A	0.0	0.0	0.0	0.0	0.0	1.0	1.0	0.0	0.010	0.0	0.0	6.32	4	5.5
Southern Grenville (B)	2A	SGR-B	0.0	0.0	0.0	0.0	0.0	1.0	1.0	0.0	0.022	0.0	0.0	6.33	3	5.3
Southern Grenville (C)	3A	SGR-C	0.0	0.0	0.0	0.0	0.0	1.0	1.0	0.0	0.008	0.0	0.0	6.32	4	5.5
Southern Grenville (A), w/ Norrow SLE	4A	SGR_N-A	0.0	0.0	0.0	0.0	0.0	1.0	1.0	0.0	-0.418	0.0	0.0	6.19	3	5.5
Southern Grenville (B), w/ Narrow SLE	5A	SGR_N-B	0.0	0.0	0.0	0.0	0.0	1.0	1.0	0.0	-2.477	0.0	0.0	5.53	2	5.3
Southern Grenville (C) w/ Narrow SLE	6A	SGR_N-C	0.0	0.0	0.0	0.0	0.0	1.0	1.0	0.0	-0.535	0.0	0.0	6.15	2	5.3
Southern Grenville (A), w/ Wide SLE	7A	SGR_W-A	0.0	0.0	0.0	0.0	0.0	1.0	1.0	0.0	-0.418	0.0	0.0	6.19	3	5.5
Southern Grenville (B), w/ Wide SLE	8A	SGR_W-B	0.0	0.0	0.0	0.0	0.0	1.0	1.0	0.0	-0.472	0.0	0.0	6.17	2	5.3
Southern Grenville (C), w/ Wide SLE	9A	SGR_W-C	0.0	0.0	0.0	0.0	0.0	1.0	1.0	0.0	-0.596	0.0	0.0	6.13	2	5.3
St. Lawrence Extension (A) - Narrow	4A	SLE-N-A	0.0	0.0	1.0	0.0	1.0	0.0	1.0	0.0	0.922	0.0	1.0	5.70	4	5.3
St. Lawrence Extension (B) - Narrow	5A	SLE-N-B	0.0	0.0	1.0	0.0	1.0	0.0	1.0	0.0	1.087	0.0	1.0	5.75	4	5.3
St. Lawrence Extension (C) - Narrow	6A	SLE-N-C	0.0	0.0	1.0	0.0	1.0	0.0	1.0	0.0	0.820	0.0	1.0	5.66	5	5.5
St. Lawrence Extension (A) - Wide	7A	SLE-W-A	0.0	0.0	1.0	0.0	1.0	0.0	1.0	0.0	0.738	0.0	1.0	5.64	4	5.3
St. Lawrence Extension (B) - Wide	8A	SLE-W-B	0.0	0.0	1.0	0.0	1.0	0.0	1.0	0.0	0.887	0.0	1.0	5.68	4	5.3
St. Lawrence Extension (C) - Wide	9A	SLE-W-C	0.0	0.0	1.0	0.0	1.0	0.0	1.0	0.0	0.676	0.0	1.0	5.62	5	5.5

\# Value of 0.5 indicates a weight of 0.5 is assigned to this assessment.

mb is converted to Mw using the relations given in Atkinson and Boore (1995).

TABLE A-2
DEFINITIONS OF MAGNITUDE INTERVALS AND OBSERVING PERIODS

i	Magnitude Interval
1	3.3 - 3.9
2	3.9 - 4.5
3	4.5 - 5.1
4	5.1 - 5.7
5	5.7 - 6.3
6	6.3 - 7.0

j	Observing Period
1	1625 - 1779
2	1780 - 1859
3	1860 - 1909
4	1910 - 1949
5	1950 - 1974
6	1975 -

GEOMATRIX

Table A-3
Estimates of Probability of Detection

ZONE : 4

m_b* \ Observing Period	1	2	3	4	5	6
3.60	0.00	0.10	0.51	1.00	1.00	1.00
4.20	0.00	0.18	0.70	1.00	1.00	1.00
4.80	0.00	0.25	1.00	1.00	1.00	1.00
5.40	0.00	0.79	1.00	1.00	1.00	1.00
6.00	0.62	0.90	1.00	1.00	1.00	1.00
6.60	0.93	1.00	1.00	1.00	1.00	1.00

ZONE : 5

m_b* \ Observing Period	1	2	3	4	5	6
3.60	0.07	0.24	0.56	1.00	1.00	1.00
4.20	0.07	0.49	0.56	1.00	1.00	1.00
4.80	0.55	0.75	1.00	1.00	1.00	1.00
5.40	1.00	1.00	1.00	1.00	1.00	1.00
6.00	1.00	1.00	1.00	1.00	1.00	1.00
6.60	1.00	1.00	1.00	1.00	1.00	1.00

ZONE : 6

m_b* \ Observing Period	1	2	3	4	5	6
3.60	0.05	0.28	0.90	1.00	1.00	1.00
4.20	0.05	0.62	0.90	1.00	1.00	1.00
4.80	0.68	1.00	1.00	1.00	1.00	1.00
5.40	0.92	1.00	1.00	1.00	1.00	1.00
6.00	0.98	1.00	1.00	1.00	1.00	1.00
6.60	1.00	1.00	1.00	1.00	1.00	1.00

ZONE : 7

m_b* \ Observing Period	1	2	3	4	5	6
3.60	0.00	0.13	0.17	0.70	1.00	1.00
4.20	0.00	0.13	0.72	0.93	1.00	1.00
4.80	0.23	0.55	0.94	0.99	1.00	1.00
5.40	0.93	0.97	0.99	1.00	1.00	1.00
6.00	0.99	1.00	1.00	1.00	1.00	1.00
6.60	1.00	1.00	1.00	1.00	1.00	1.00

ZONE : 8

m_b* \ Observing Period	1	2	3	4	5	6
3.60	0.00	0.00	0.00	0.00	0.40	1.00
4.20	0.00	0.00	0.00	0.00	0.47	1.00
4.80	0.00	0.00	0.00	0.00	0.91	1.00
5.40	0.00	0.24	0.24	0.61	1.00	1.00
6.00	0.00	0.25	0.77	0.97	1.00	1.00
6.60	0.00	0.25	0.90	1.00	1.00	1.00

TABLE A-3 (Continued)

ZONE : 9

m_b° \ Observing Period	1	2	3	4	5	6
3.60	0.00	0.03	0.16	0.41	1.00	1.00
4.20	0.00	0.03	0.23	1.00	1.00	1.00
4.80	0.00	0.03	0.57	1.00	1.00	1.00
5.40	0.00	0.03	0.85	1.00	1.00	1.00
6.00	0.00	0.05	0.96	1.00	1.00	1.00
6.60	0.00	0.13	1.00	1.00	1.00	1.00

ZONE : 10

m_b° \ Observing Period	1	2	3	4	5	6
3.60	0.01	0.06	0.27	0.52	0.79	1.00
4.20	0.01	0.06	0.27	1.00	1.00	1.00
4.80	0.06	0.17	0.38	1.00	1.00	1.00
5.40	0.41	0.99	1.00	1.00	1.00	1.00
6.00	0.86	1.00	1.00	1.00	1.00	1.00
6.60	0.96	1.00	1.00	1.00	1.00	1.00

ZONE : 11

m_b° \ Observing Period	1	2	3	4	5	6
3.60	0.00	0.00	0.00	0.00	0.88	1.00
4.20	0.00	0.00	0.00	0.32	1.00	1.00
4.80	0.00	0.00	0.00	0.38	1.00	1.00
5.40	0.00	0.00	0.00	0.68	1.00	1.00
6.00	0.00	0.00	0.02	0.93	1.00	1.00
6.60	0.00	0.00	0.11	1.00	1.00	1.00

ZONE : 12

m_b° \ Observing Period	1	2	3	4	5	6
3.60	0.02	0.25	0.51	1.00	1.00	1.00
4.20	0.14	0.63	0.83	1.00	1.00	1.00
4.80	0.70	1.00	1.00	1.00	1.00	1.00
5.40	0.94	1.00	1.00	1.00	1.00	1.00
6.00	0.99	1.00	1.00	1.00	1.00	1.00
6.60	1.00	1.00	1.00	1.00	1.00	1.00

TABLE A-4
MAXIMUM LIKELIHOOD ESTIMATES OF RECURRENCE PARAMETERS FOR SEISMIC SOURCES

Seismic Source	Ref. Plate	Abbreviation	Area	m_o	$\alpha(\pm\sigma_\alpha)$	$b(\pm\sigma_b)$
NORTHERN ADIRONDACKS	13	ADR	2.46	3.30	0.202(±0.036)	0.989(±0.120)
ATLANTIC OFFSHORE BACKGROUND	13	AOBH	8.94	3.30	0.089(±0.040)	1.006(±0.183)
ANNA, OHIO	13	AOH	0.85	3.30	0.122(±0.032)	0.706(±0.128)
BAS SAINT LAURENT	13	BSL	1.30	3.30	0.557(±0.091)	1.059(±0.126)
CHAMPLAIN	13	CHA	0.93	3.30	0.122(±0.029)	0.871(±0.129)
CHARLEVOIX	13	CHV	0.38	3.30	0.712(±0.091)	0.793(±0.071)
COCHRANE	13	COC	2.45	3.30	0.076(±0.038)	0.982(±0.186)
GATINEAU	13	GAT	2.61	3.30	1.010(±0.111)	1.024(±0.086)
MONTREAL	13	MNT	1.14	3.30	0.345(±0.050)	1.038(±0.108)
NORTHERN APPALACHIANS	13	NAN	18.36	3.30	1.706(±0.130)	1.078(±0.066)
NIAGARA ATTICA TREND	13	NAT	1.18	3.30	0.118(±0.028)	0.920(±0.136)
ONTARIO BACKGROUND	13	OBGH	35.93	3.30	0.473(±0.062)	1.185(±0.118)
PEMBROKE	13	PEM	2.21	3.30	0.282(±0.059)	0.984(±0.140)
PASSAMAQUODDY BAY	13	PMQ	0.57	3.30	0.149(±0.042)	0.807(±0.134)
SAGUENAY	13	SAG	0.76	3.30	0.074(±0.030)	0.989(±0.178)
SOUTHEAST CANADA BACKGROUND	13	SEB	24.63	3.30	1.084(±0.121)	0.990(±0.086)
SOUTH SHORE LAKE ERIE	13	SLE	0.96	3.30	0.112(±0.028)	1.016(±0.146)
TAD	13	TAD	0.47	3.30	0.038(±0.022)	0.950(±0.188)
TIMISKAMING	13	TIM	0.31	3.30	0.082(±0.034)	0.875(±0.171)
TROIS-RIVIERES	13	TRR	1.48	3.30	0.222(±0.041)	1.077(±0.133)
ADIRONDAK	11	ADIRONDA	3.74	3.30	0.693(±0.071)	1.020(±0.080)
MANIWAKI	11	MANIWAKI	4.18	3.30	1.130(±0.120)	1.018(±0.084)
NIAGARA	11	NIAGARA	3.45	3.30	0.146(±0.034)	0.941(±0.134)
OTTAWA	11	OTTAWA	3.81	3.30	0.304(±0.064)	0.963(±0.132)
ROCHESTER	11	ROCHESTE	10.12	3.30	0.106(±0.030)	1.072(±0.163)
CENTRAL CRATON, W/. OG	1A	CC-A	21.66	3.30	0.557(±0.085)	0.935(±0.109)
CENTRAL CRATON, W/O OG	10	CC-B	22.56	3.30	0.560(±0.085)	0.936(±0.109)
CENTRAL CRATON (A), W/. NARROW SLE	4A	CC_N	20.68	3.30	0.387(±0.072)	1.140(±0.144)
CENTRAL CRATON (A), W/. WIDE SLE	7A	CC_W	20.15	3.30	0.365(±0.070)	1.122(±0.145)
EXTENDED CONTINENTAL CRUST	10	ECC	26.02	3.30	1.409(±0.110)	0.989(±0.062)
GRENVILLE DOMAIN	10	GD	72.35	3.30	3.650(±0.178)	0.988(±0.040)
GREAT METEOR HOTSPOT	10	GMH	2.56	3.30	0.999(±0.110)	1.025(±0.086)
IAPETAN RIFTED MARGIN	1A	IRM-A	32.03	3.30	1.932(±0.120)	0.953(±0.048)
IAPETAN RIFTED MARGIN	2A	IRM-B	36.37	3.30	1.999(±0.122)	0.955(±0.047)
IAPETAN RIFTED MARGIN	3A	IRM-C	28.61	3.30	1.825(±0.117)	0.941(±0.049)
IAPETAN RIFTED MARGIN	1B	IRM-A2	37.56	3.30	2.498(±0.141)	0.969(±0.044)
IAPETAN RIFTED MARGIN	2B	IRM-B2	41.89	3.30	2.553(±0.142)	0.970(±0.044)
IAPETAN RIFTED MARGIN	3B	IRM-C2	34.14	3.30	2.400(±0.139)	0.960(±0.045)
IAPETAN RIFTED MARGIN	4B	IRM-A3	42.63	3.30	2.818(±0.149)	0.945(±0.041)
IAPETAN RIFTED MARGIN	5B	IRM-B3	45.13	3.30	2.855(±0.150)	0.925(±0.040)
IAPETAN RIFTED MARGIN	6B	IRM-C3	41.52	3.30	2.823(±0.149)	0.941(±0.040)
IAPETAN RIFTED MARGIN	7B	IRM-A4	44.73	3.30	2.920(±0.152)	0.946(±0.040)
IAPETAN RIFTED MARGIN	8B	IRM-B4	47.73	3.30	2.907(±0.151)	0.950(±0.040)
IAPETAN RIFTED MARGIN	9B	IRM-C4	44.46	3.30	2.907(±0.151)	0.948(±0.040)
NORTHERN APPALACHIANS	10	NAZ	17.52	3.30	1.540(±0.127)	1.099(±0.073)
NORTHERN GRENVILLE	10	NGR	15.84	3.30	1.617(±0.146)	1.014(±0.074)

TABLE A-4 (Continued)

MAXIMUM LIKELIHOOD ESTIMATES OF RECURRENCE PARAMETERS FOR SEISMIC SOURCES

Seismic Source	Ref. Plate	Abbreviation	Area	m_o	$\alpha(\pm\sigma_\alpha)$	$b(\pm\sigma_b)$
OTTAWA GRABEN	1A	OG	4.65	3.30	0.619(±0.085)	1.062(±0.107)
SAGUENEY GRABEN	1A	SG	0.88	3.30	0.057(±0.026)	0.870(±0.168)
SOUTHERN GRENVILLE (A)	1A	SGR-A	22.39	3.30	0.529(±0.067)	1.072(±0.102)
SOUTHERN GRENVILLE (B)	2A	SGR-B	18.06	3.30	0.471(±0.065)	1.072(±0.108)
SOUTHERN GRENVILLE (C)	3A	SGR-C	25.81	3.30	0.655(±0.074)	1.091(±0.094)
SOUTHERN GRENVILLE (A), W/. NARROW SLE	4A	SGR_N-A	16.47	3.30	0.203(±0.043)	1.141(±0.145)
SOUTHERN GRENVILLE (B), W/. NARROW SLE	5A	SGR_N-B	12.40	3.75	0.260(±0.047)	1.539(±0.156)
SOUTHERN GRENVILLE (C), W/. NARROW SLE	6A	SGR_N-C	19.64	3.30	0.289(±0.050)	1.201(±0.140)
SOUTHERN GRENVILLE (A), W/. WIDE SLE	7A	SGR_W-A	16.47	3.30	0.209(±0.044)	1.138(±0.144)
SOUTHERN GRENVILLE (B), W/. WIDE SLE	8A	SGR_W-B	13.79	3.30	0.213(±0.045)	1.165(±0.151)
SOUTHERN GRENVILLE (C), W/. WIDE SLE	9A	SGR_W-C	17.29	3.30	0.214(±0.044)	1.178(±0.150)
ST. LAWRENCE EXTENSION (A) - NARROW	4A	SLE-N-A	5.06	3.30	0.327(±0.049)	0.825(±0.093)
ST. LAWRENCE EXTENSION (B) - NARROW	5A	SLE-N-B	3.90	3.30	0.274(±0.045)	0.772(±0.096)
ST. LAWRENCE EXTENSION (C) - NARROW	6A	SLE-N-C	7.38	3.30	0.433(±0.056)	0.871(±0.086)
ST. LAWRENCE EXTENSION (A) - WIDE	7A	SLE-W-A	7.50	3.30	0.415(±0.056)	0.881(±0.090)
ST. LAWRENCE EXTENSION (B) - WIDE	8A	SLE-W-B	5.80	3.30	0.361(±0.053)	0.841(±0.093)
ST. LAWRENCE EXTENSION (C) - WIDE	9A	SLE-W-C	10.10	3.30	0.522(±0.062)	0.914(±0.083)
CLARENDON - LINDEN FALUT SYSTEM	14	CLFSS *		3.30	0.031(±0.014)	0.935(±0.044)
		CLFSW *			0.030(±0.014)	0.823(±0.170)
GEORGIAN BAY LINEAR ZONE	14	GBLZS		3.30	0.091(±0.029)	0.942(±0.044)
		GBLZW			0.091(±0.029)	0.936(±0.157)
HAMILTON - PRESOUILE FAULT	14	HPFS		3.30	0.059(±0.021)	0.942(±0.044)
		HPFW			0.059((±0.021)	0.933((±0.172)
NIAGARA - PICKERING LINEAR ZONE	14	NPLZS		3.30	0.085(±0.025)	0.942(±0.044)
		NPLZW			0.082(±0.025)	0.933(±0.158)
NIAGARA - PICKERING/AKRON MAGNETIC BNDR.	15	NPLZ-AMBS		3.30	0.217(±0.040)	0.949(±0.043)
		NPLZ-AMBW			0.220(±0.041)	0.991(±0.122)
TORONTO - HAMILTON SEISMIC ZONE	14	THSZS		3.30	0.050(±0.020)	0.943(±0.044)
		THSZW			0.050(±0.020)	0.940(±0.177)
WILSON - PORT HOPE LINEAMENT	14	WPHLS		3.90	0.006(±0.006)	0.943(±0.045)
		WPHLW			0.006(±0.006)	0.943(±0.196)

A = Area of source zone in units of 111.11^2 km^2

α = Cumulative rate (events/year) of earthquakes with magnitude $\geq m_o$

σ_α = one standard error of estimation.

b = b-value of the Gutenberg-Richter relation;

σ_b = one standard error of estimation.

* Last letters S and W refer to strong and weak priors, respectively

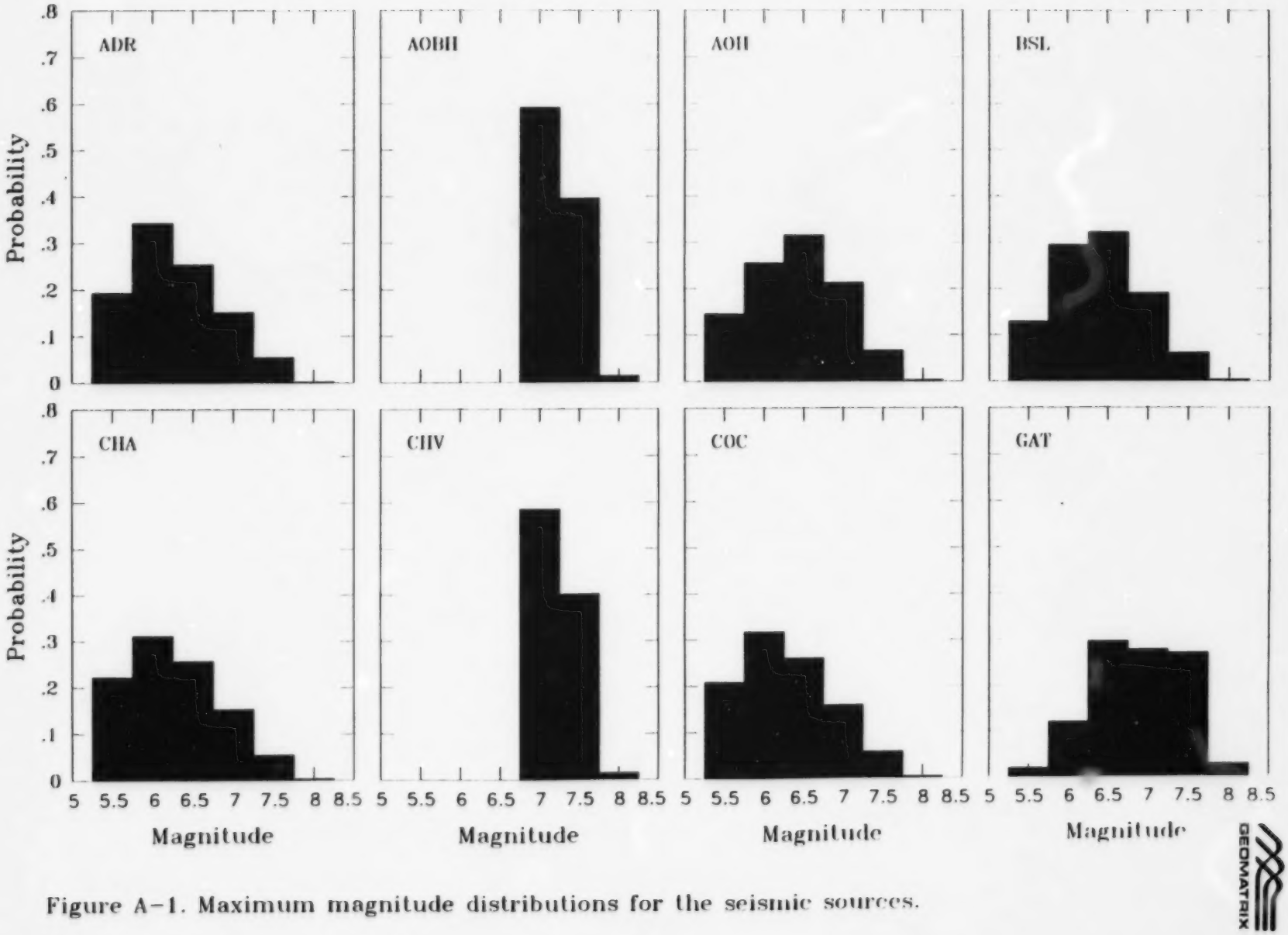

Figure A-1. Maximum magnitude distributions for the seismic sources.

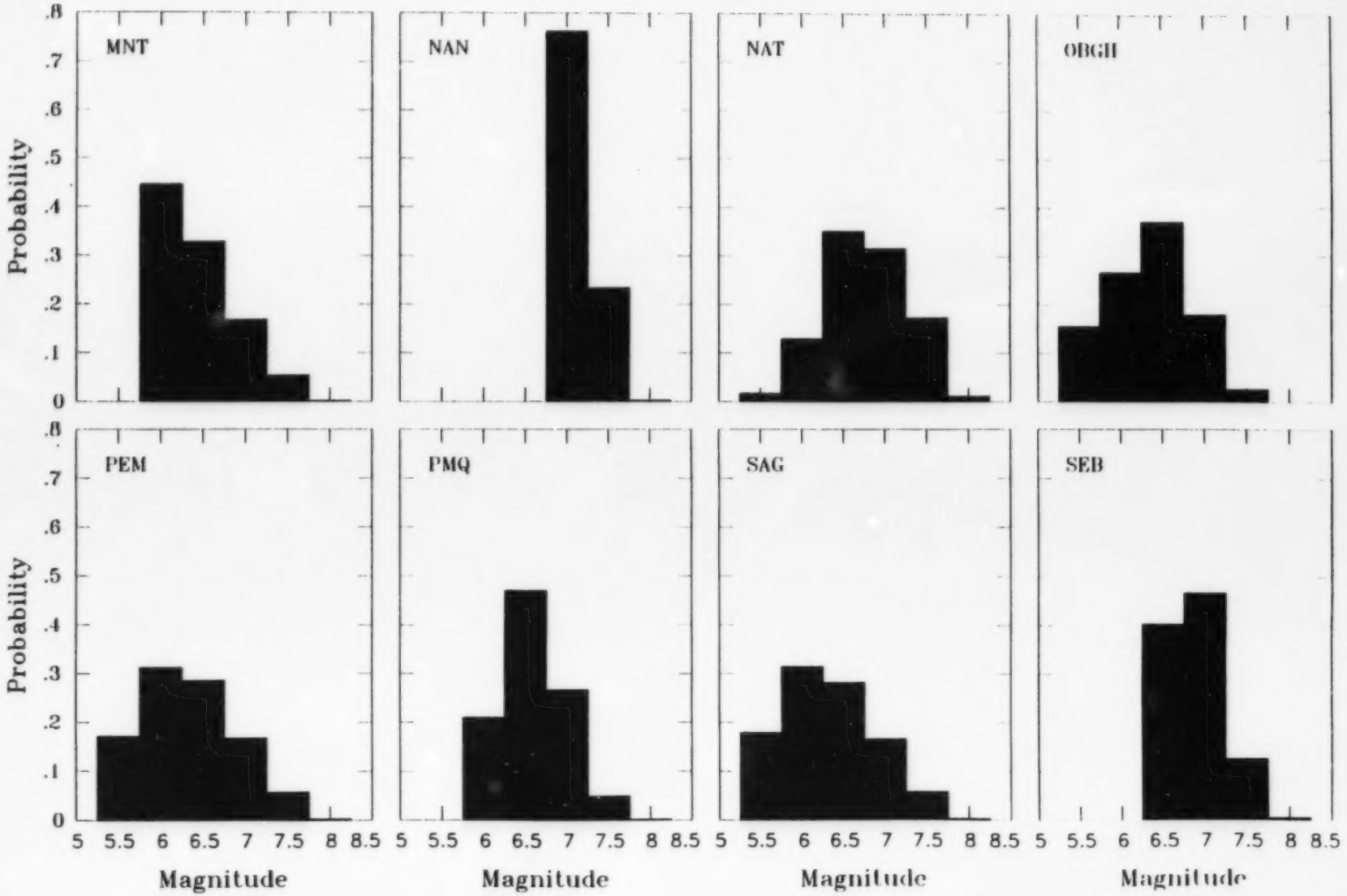

Figure A–1. (Continued).

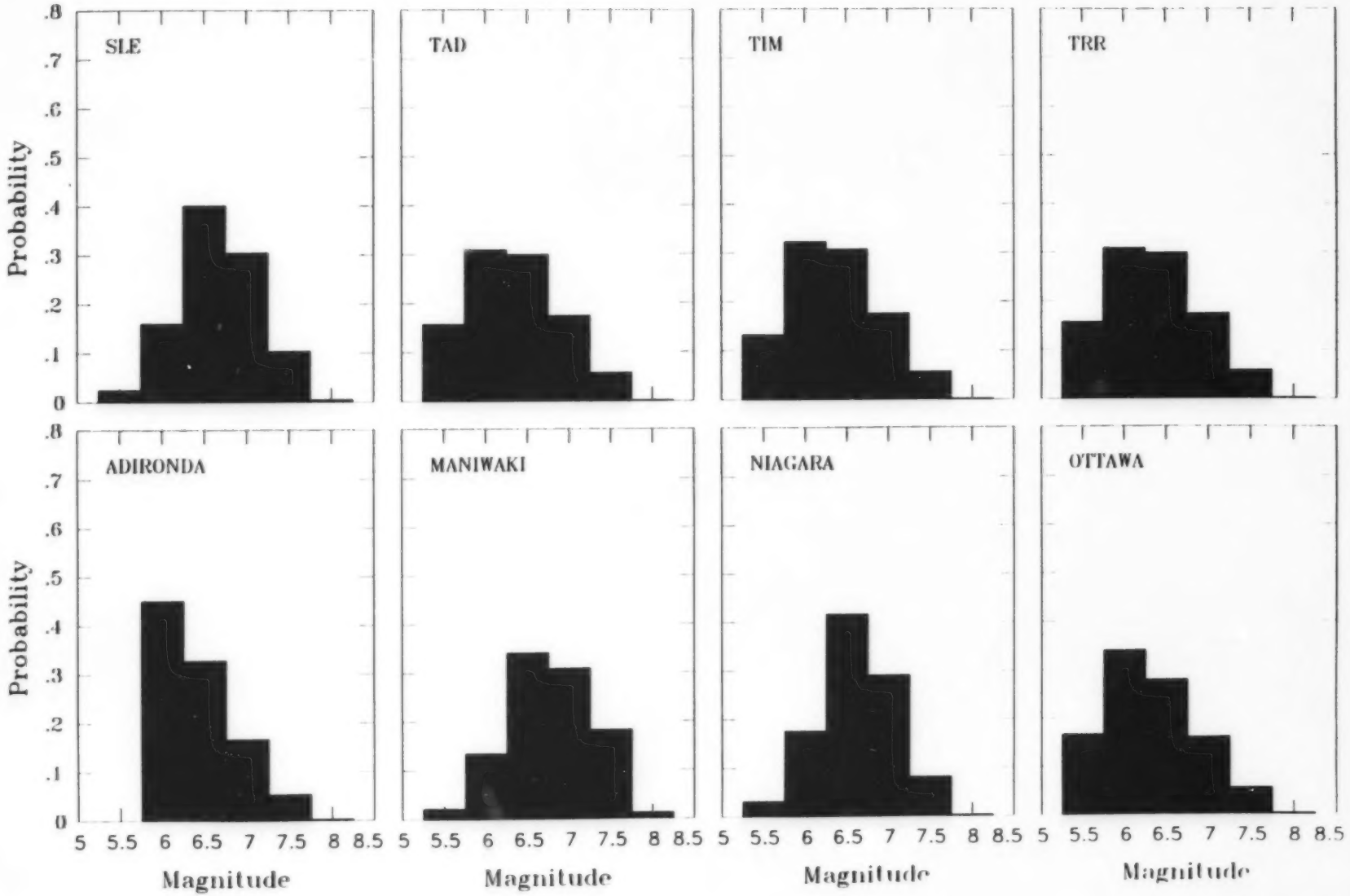

Figure A-1. (Continued).

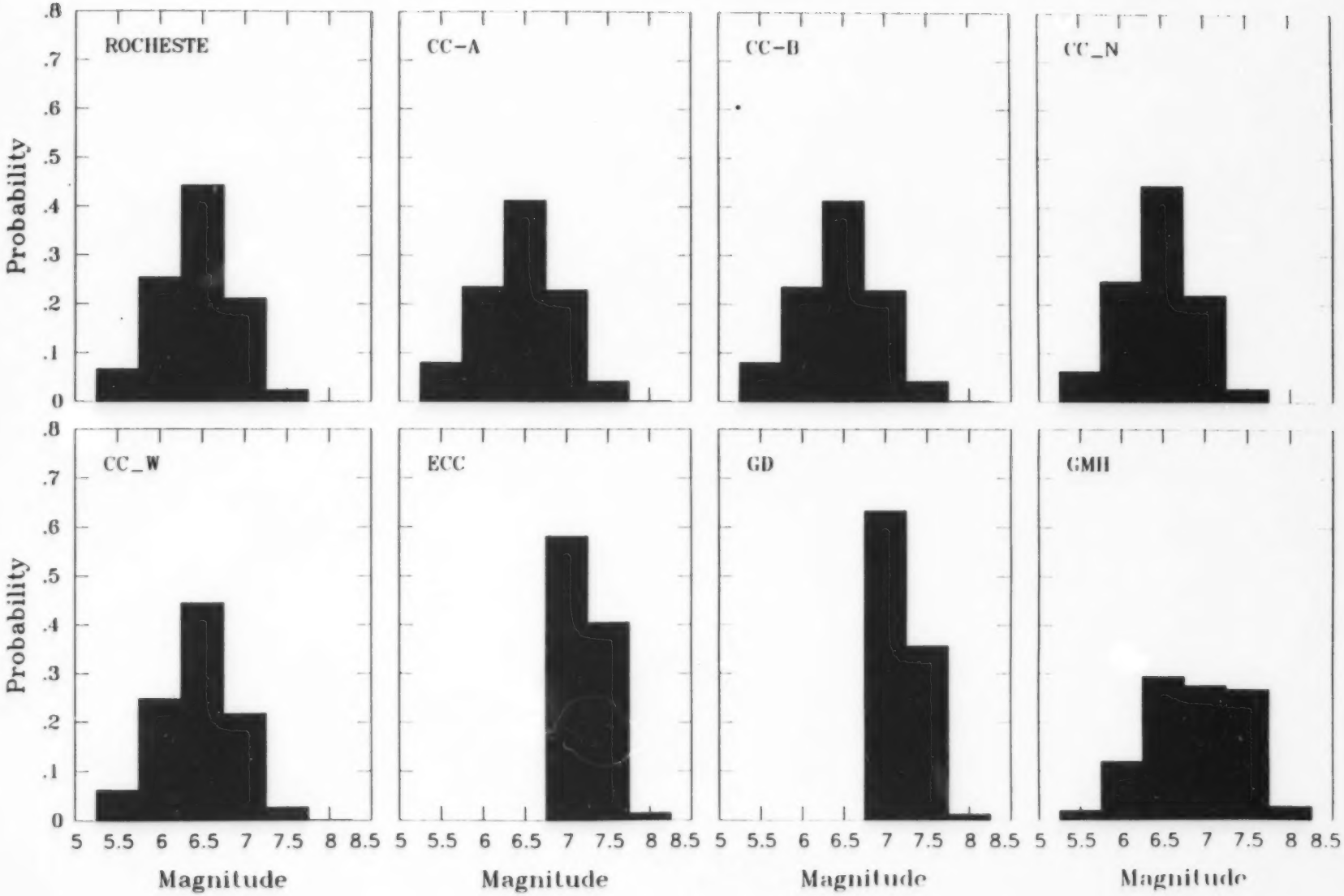

Figure A-1. (Continued).

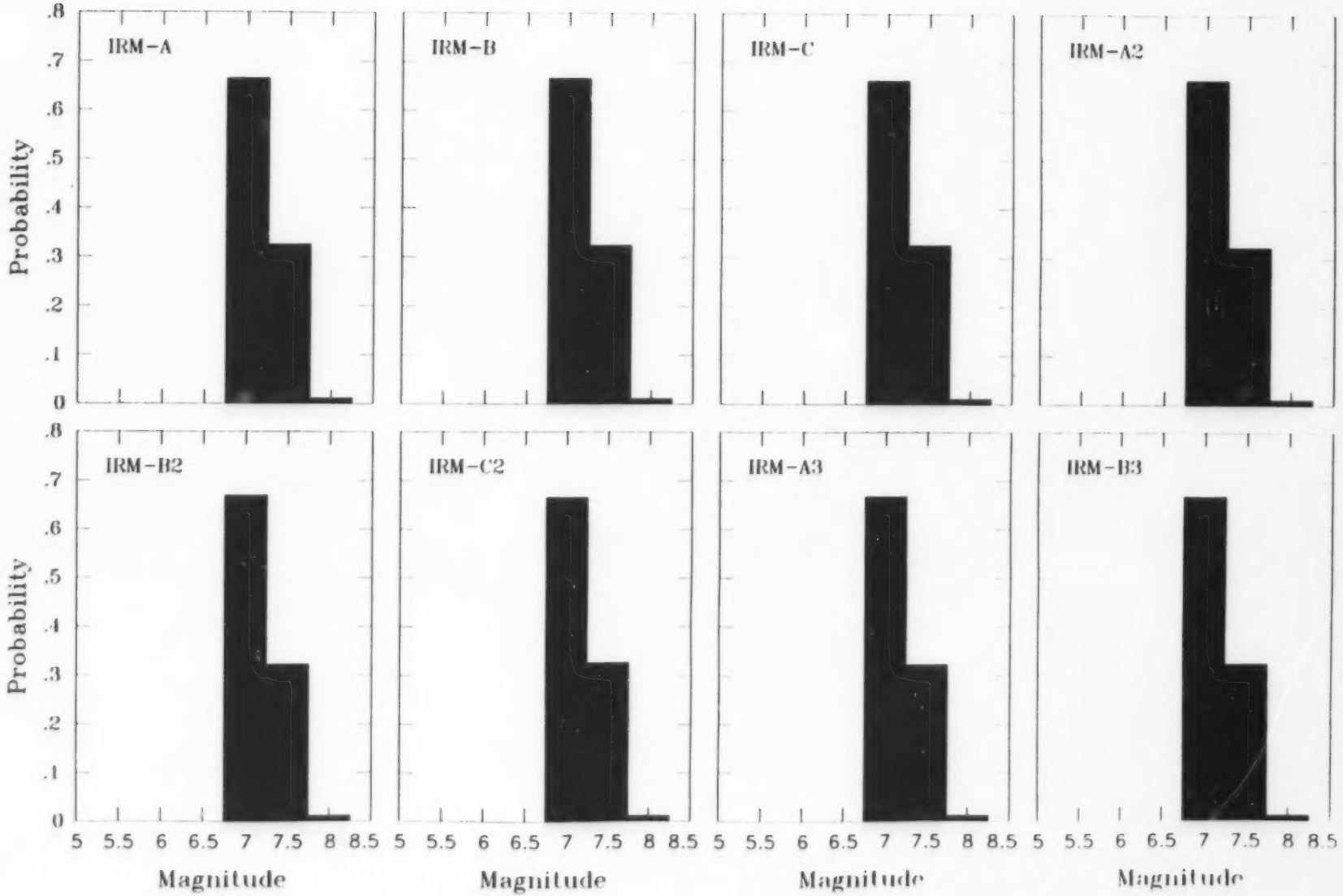

Figure A-1. (Continued).

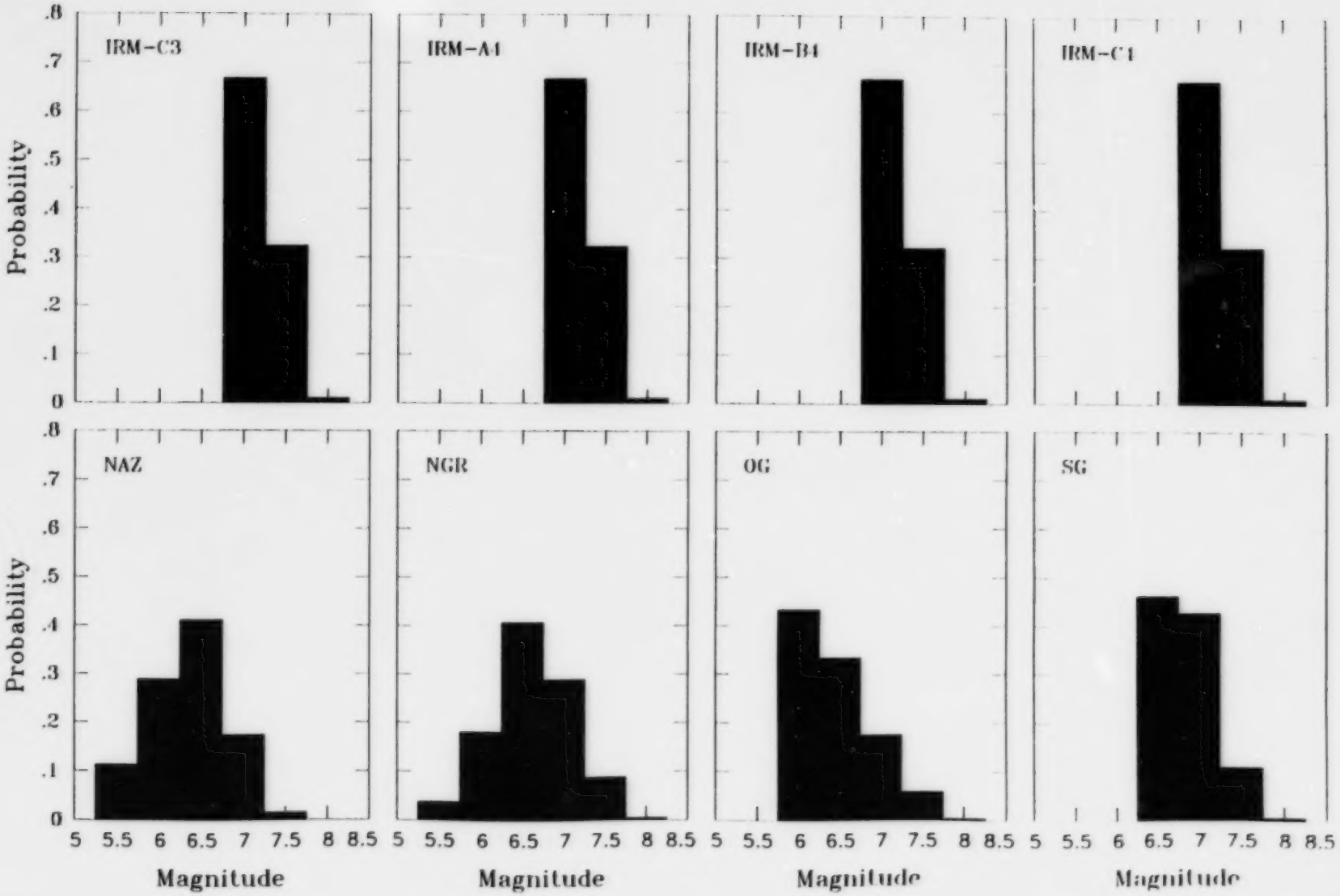

Figure A-1. (Continued).

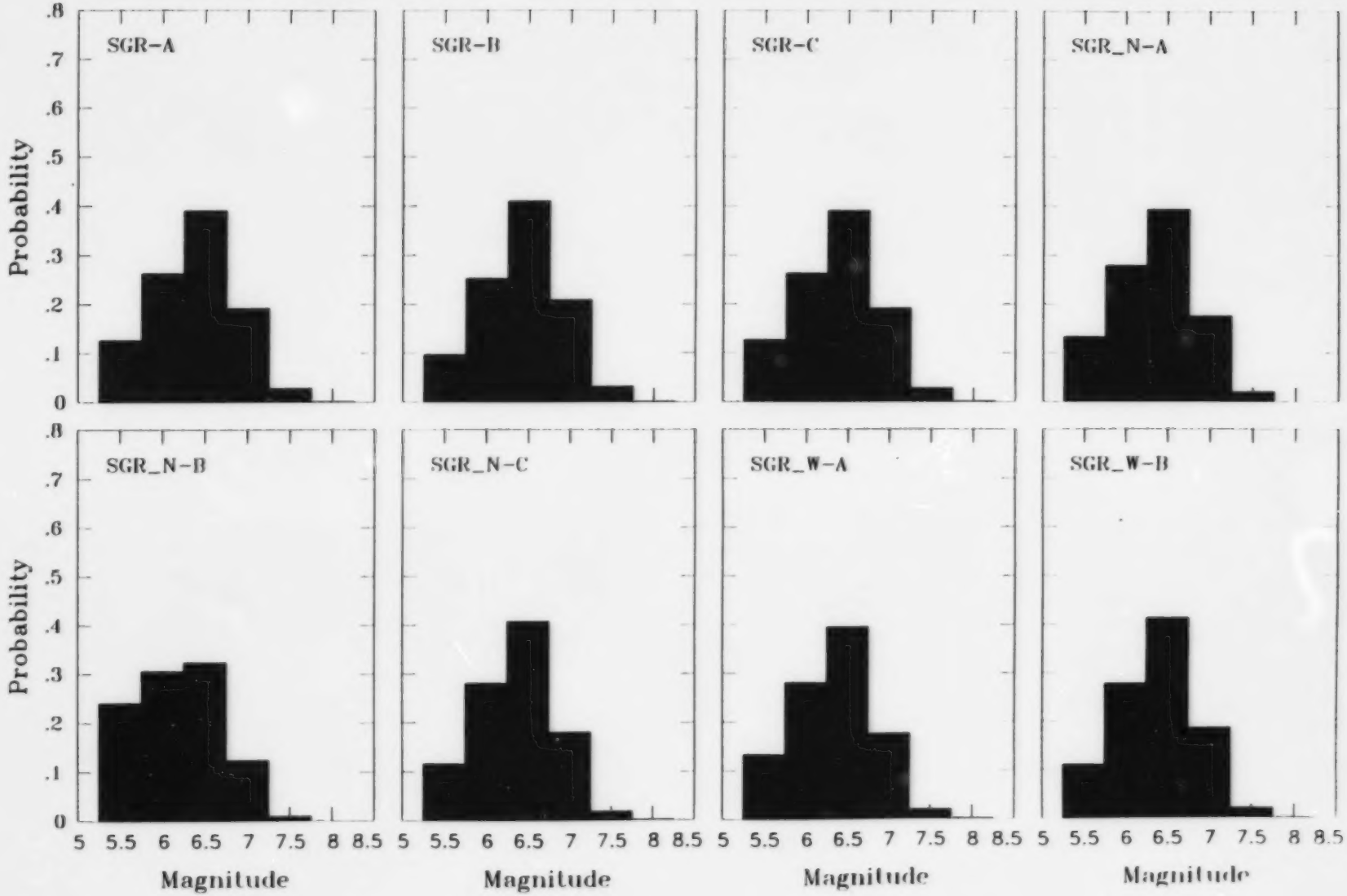

Figure A-1. (Continued).

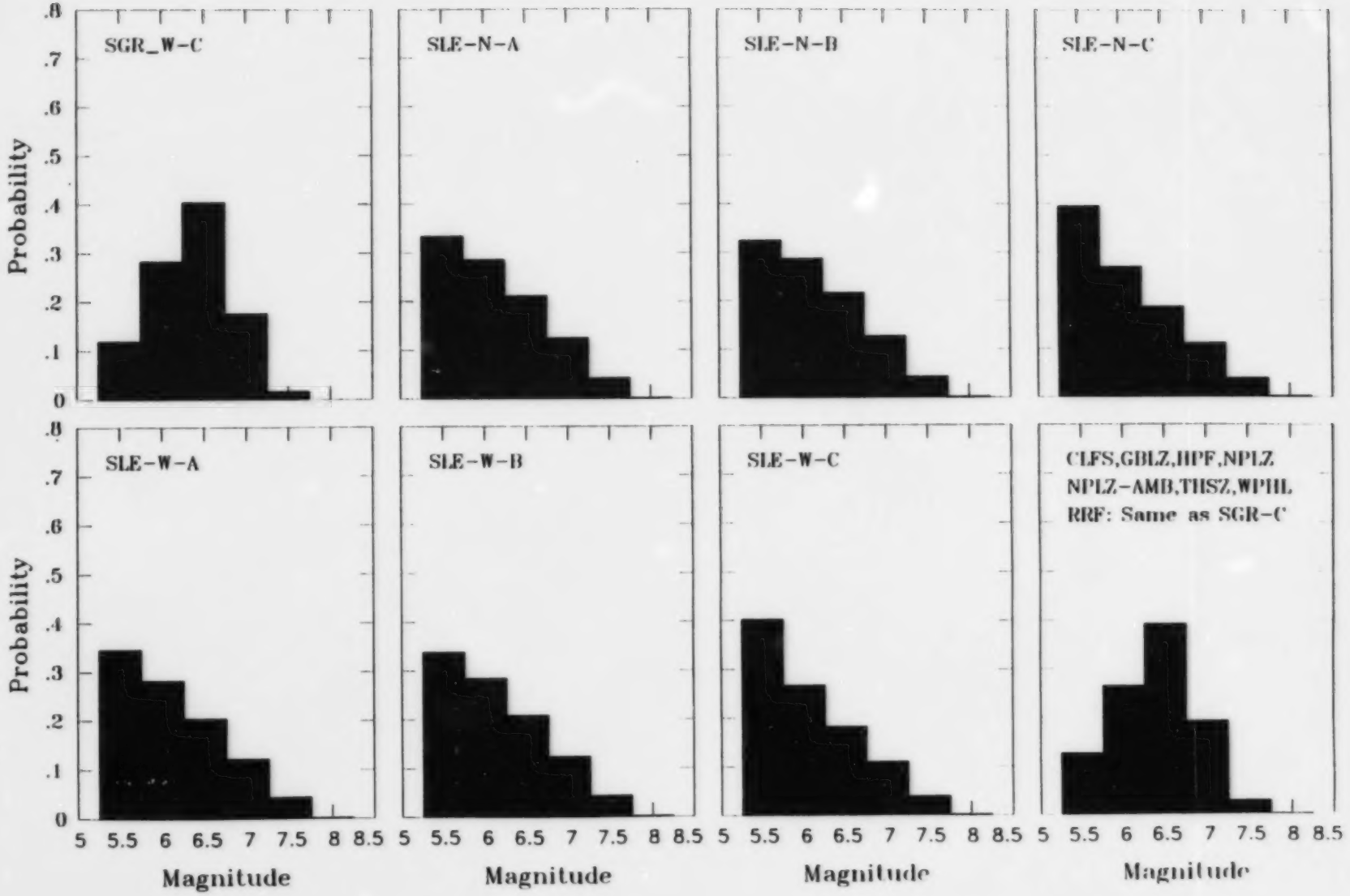

Figure A-1. (Continued).

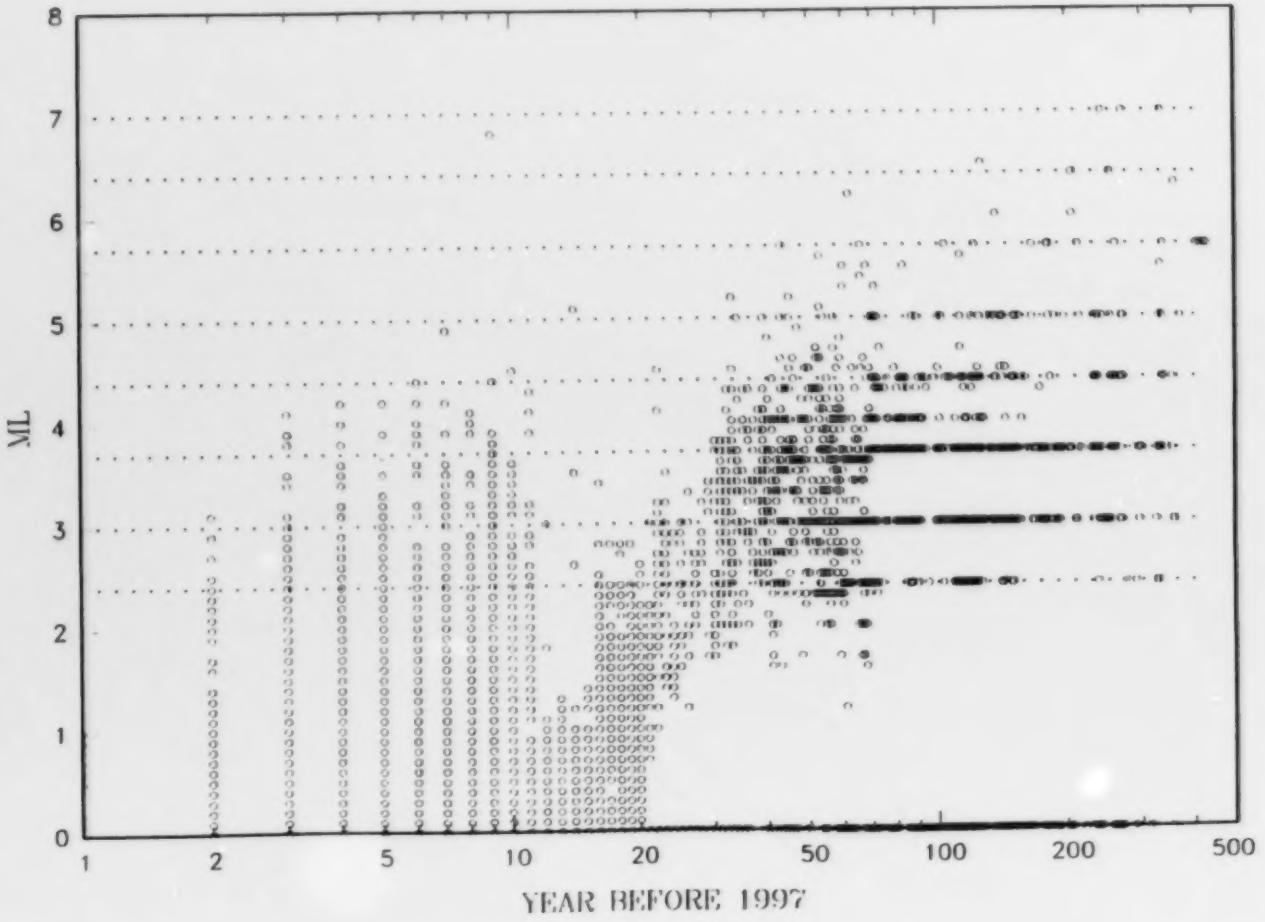

Figure A-2 Local magnitudes in catalog by year prior to 1997

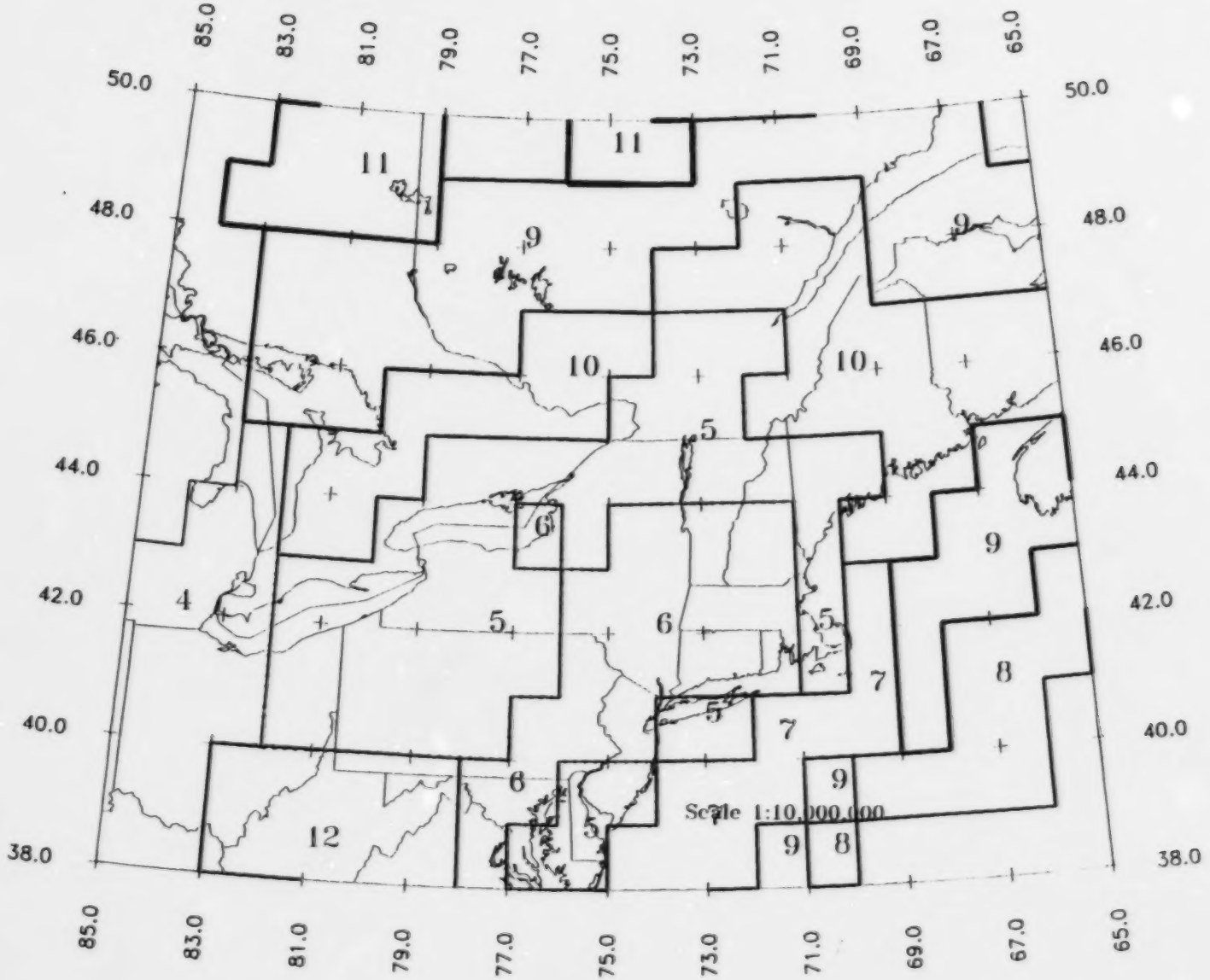

Figure A–3. Incompleteness regions in the study area.

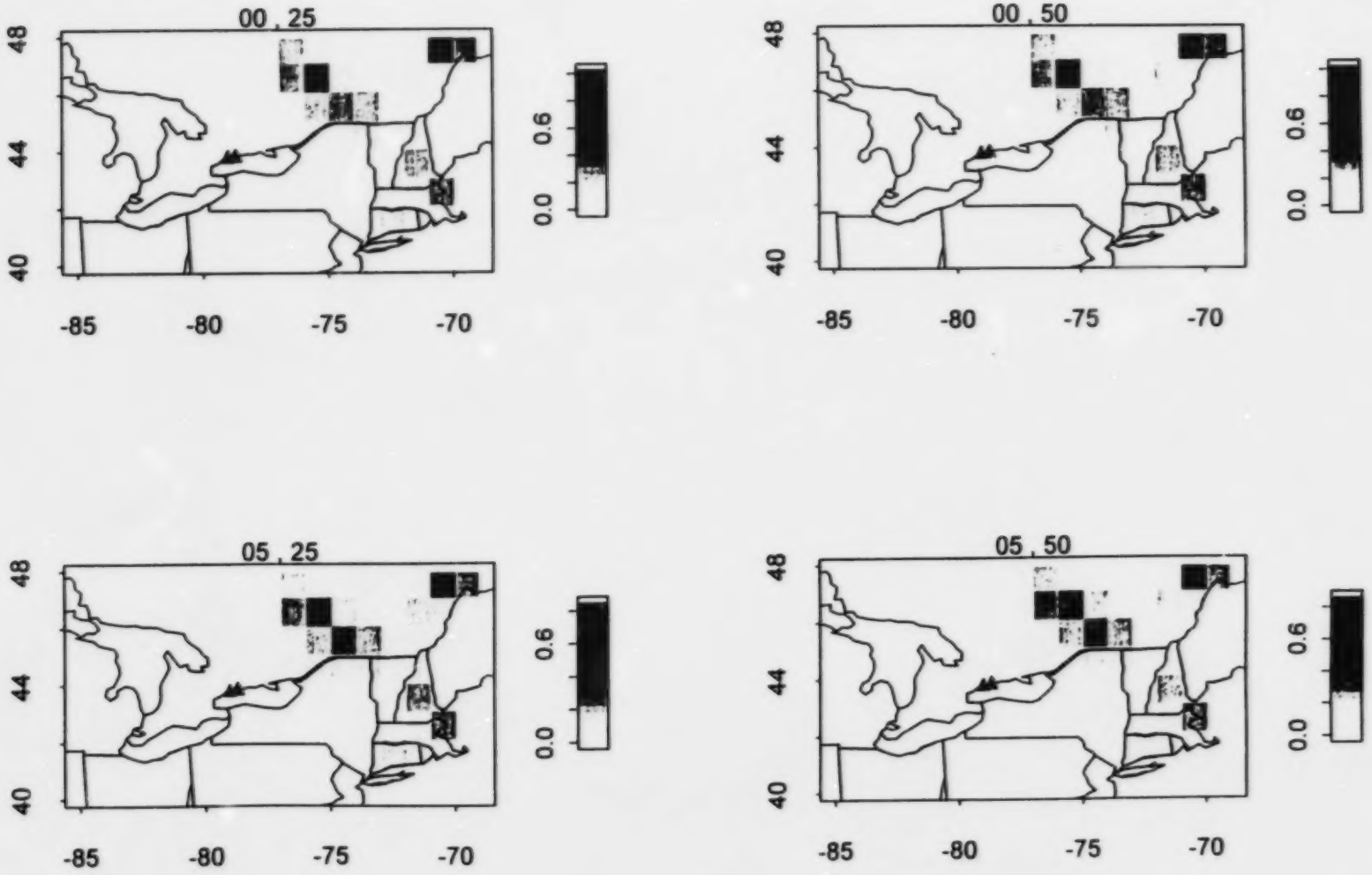

Figure A-4a. Spatial distribution of seismicity rate. The levels of smoothing are indicated at the top of each plot.

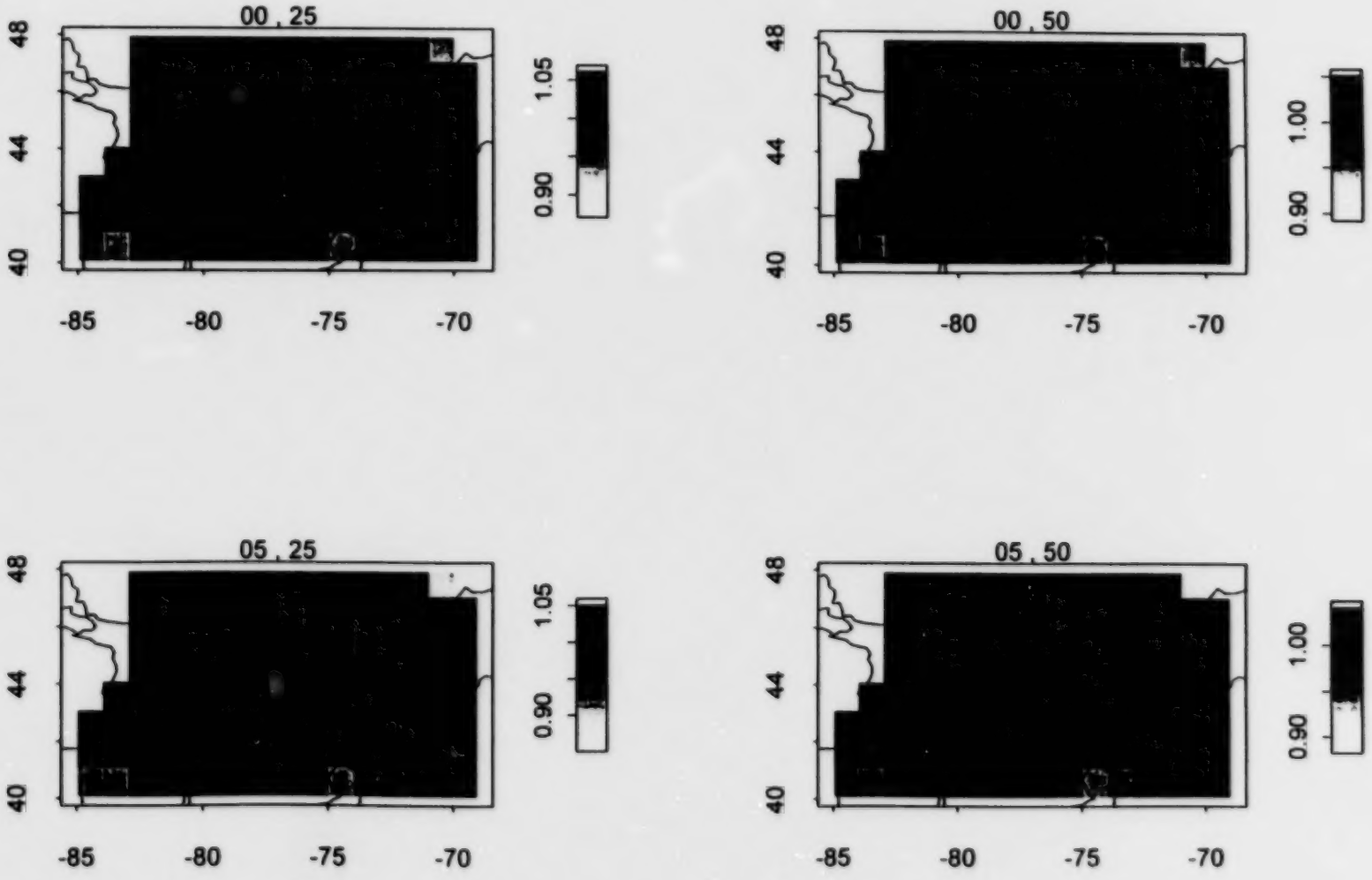

Figure A-4b. Spatial distribution of b-value. The levels of smoothing are indicated at the top of each plot.

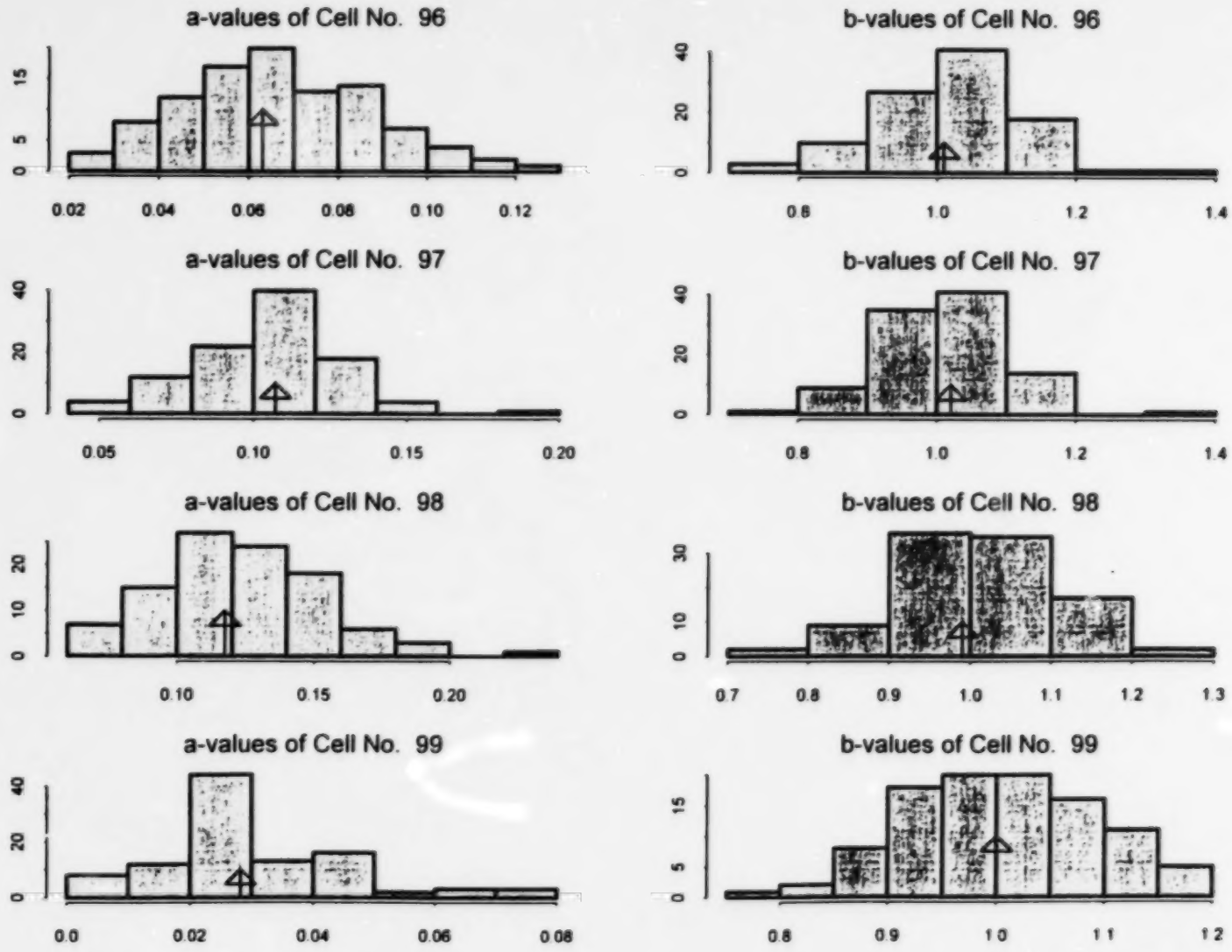

Figure A-5. Histograms showing the distribution of 100 simulations of rate and b-value for four cells of the regional source zone. Arrows indicate the maximum likelihood solution for the cell.

APPENDIX B
GROUND MOTION ATTENUATION RELATIONSHIPS

The attenuation relationships developed by EPRI (1993, also published in Toro and others, 1997) are in the form of discrete relationships for peak ground acceleration (PGA) (assumed to correspond to a spectral frequency of 100 Hz) and for 5%-damped spectral acceleration at spectral frequencies of 35, 25, 10, 5, 2.5, 1, and 0.5 Hz. The form of the relationships is

$$\ln(y) = C_1 + C_2(m-6) + C_3(m-6)^2 - C_4\ln(R_M) - (C_5-C_4)\max\left[\ln(\frac{R_M}{R_M^*}),0\right] - C_6R_M \quad \textbf{(B-1)}$$

where y is the ground motion measure, R_M is an equivalent hypocentral distance defined by the relationship

$$RM = \sqrt{R_{jb}^2 + C_7^2} \quad \textbf{(B-2)}$$

R_{jb} is the surface distance to the vertical projection of the rupture, R_M^* is set at 100 km, and C_1 through C_7 are coefficients fit to a set of numerical simulations. The attenuation relationships developed by Atkinson and Boore (1995) use the same form of simulation model as was used to develop the EPRI (1993) attenuation relationships, but they fit a simpler functional form to the simulated motions and they do not develop relationships for the same spectral frequencies. Haddon (1996) presents a model for the source spectra for eastern North America earthquakes, but he does not provide specific attenuation relationships.

For this study we developed attenuation relationships for the Atkinson and Boore (1995) ground motion model and the Haddon (1996) source spectra model by computing synthetic ground motions using the same methodology described by Atkinson and Boore (1995). The computer code TMRDRVT (Boore, 1996) was utilized to compute the simulated

motions. The model parameters specified by Atkinson and Boore (1996) were used to compute 5%-damped response spectral accelerations at the eight spectral frequencies used by EPRI (1993). Figure B-1 shows examples of the simulated results. Simulation of motions for the Haddon (1996) source spectral model required fitting an analytical form to the source spectra shown on Figure 10 of Haddon (1996). The approximating source spectra, shown on Figure B-2, were computed by cascading two one-corner source spectra, each with its own magnitude-dependent corner frequency. To complete the simulations for the Haddon (1996) model, the path and site terms used by Atkinson and Boore (1995) were used. The examples of the resulting simulated spectral accelerations are shown on Figure B-3.

Attenuation relationships for the eight spectral frequencies were then obtained by fitting Equation **(B-1)** to the simulated motions assuming that the distance term used in the simulation is equivalent to R_M. Figures B-4 and B-5 show the resulting fit to the simulations. These fits were obtained by setting R_M^* to 65 km to match the distance attenuation function specified by Atkinson and Boore (1995). The attenuation functions were then finalized by setting C_7 and the relationships for aleatory and epistemic uncertainty to the values specified by EPRI (1993) and Toro and others (1997). Figure B-6 compares the resulting attenuation relationships to those developed by EPRI (1993).

REFERENCES

Atkinson, G.M., and Boore, D.M., 1995, Ground motion relations for eastern North America: Bulletin of the Seismological Society of America, v. 85, p. 11-27.

Boore, D.M., 1996, SMSIM - Fortran programs for simulating ground motions from earthquakes: USGS Open-file Report 96-80-A.

Electric Power Research Institute (EPRI), 1993, Guidelines for determining design basis ground motions: Electric Power Research Institute Report EPRI TR-102293, v. 5.

Haddon, R.A.W., 1996, Earthquake source spectra in eastern North America: Bulletin of the Seismological Society of America, v. 86, p. 1300-1313.

Toro, G.R., N.A. Abrahamson, and J. F. Schneider, 1997, Model of strong ground motions from earthquakes in central and eastern North America: best estimates and uncertainties: Seismological Research Letters, v. 68, n. 1, p. 41-57.

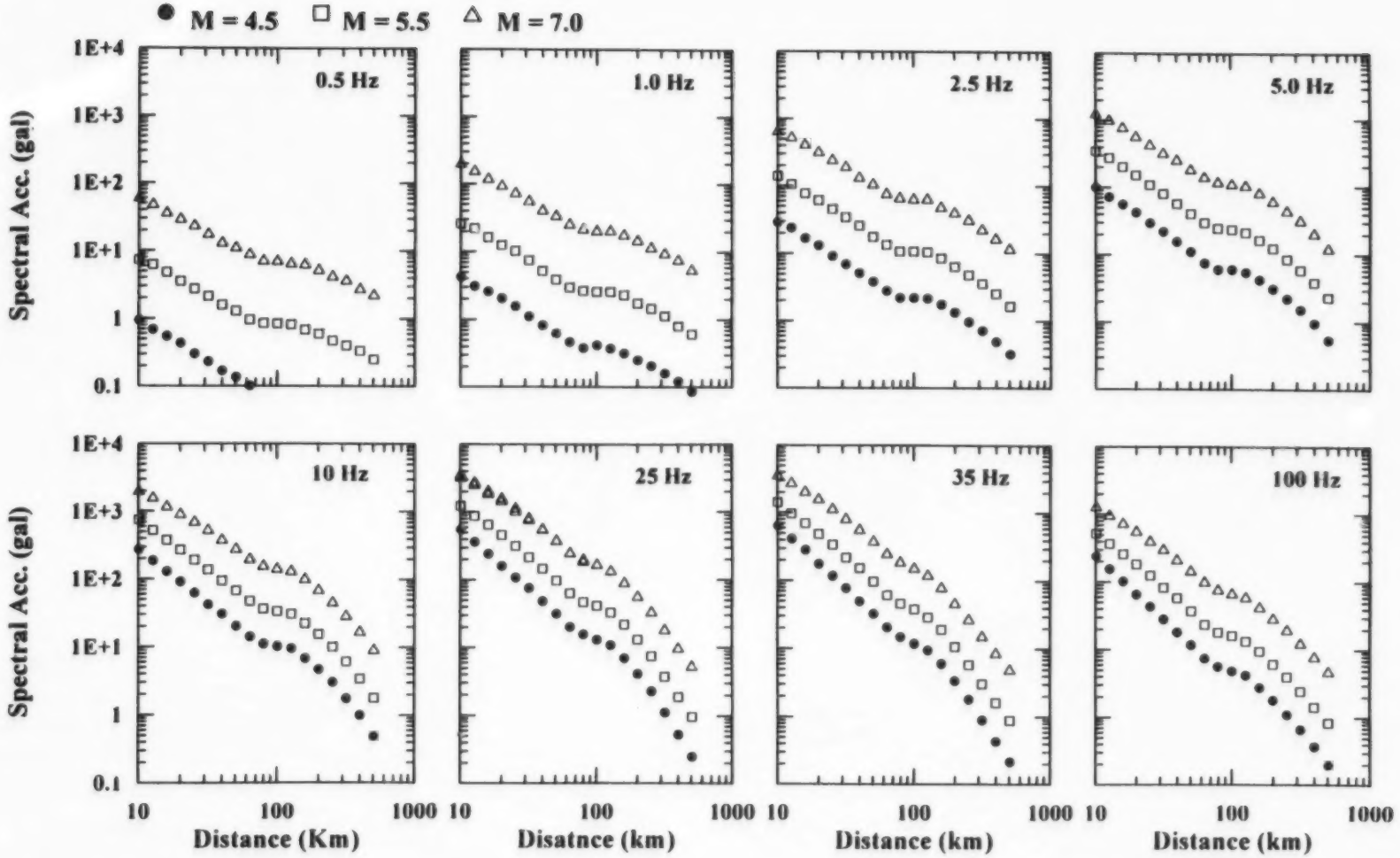

Figure B-1. Predicted response spectra values (PSA at 5% damping) for M 4.5, 5.5, and 7.0 using the same input as Atkinson and Boore (1995).

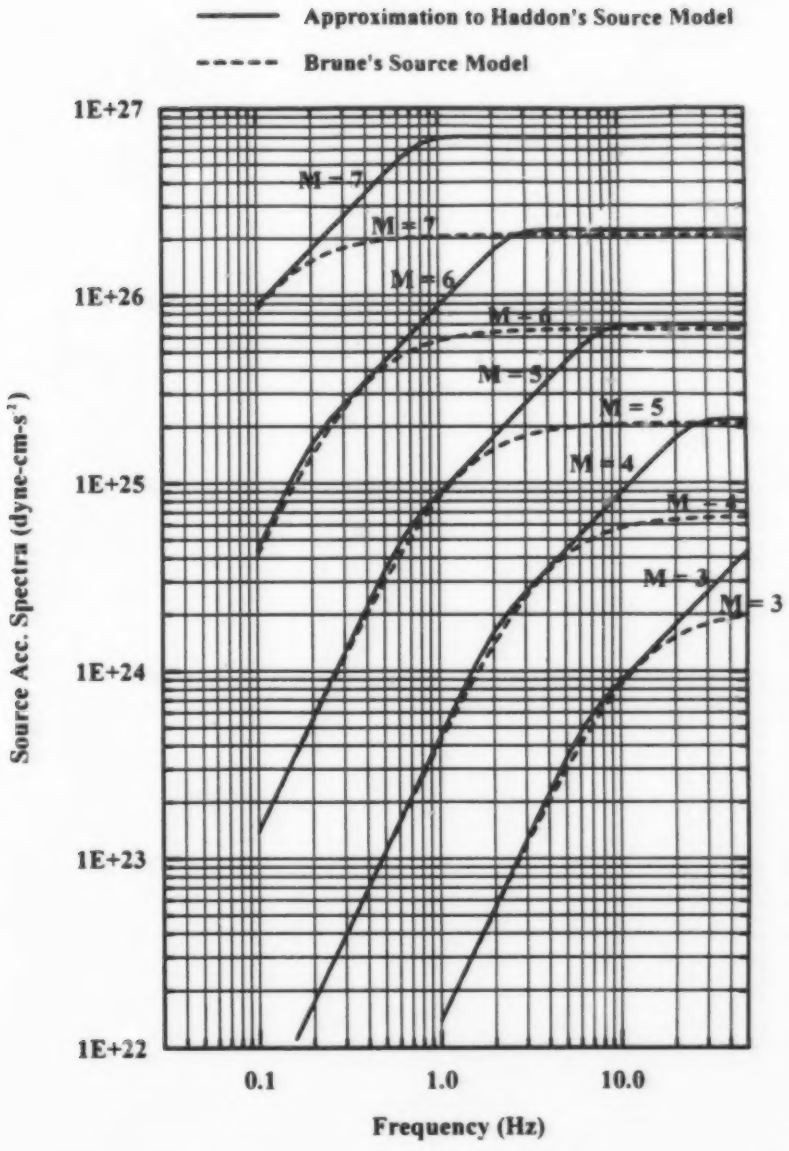

Figure B-2. Boore's approximation (1996) to the new provisional S-wave shource spectra proposed by Haddon (1996). The dashed lines are the Brune spectra for the same magnitude and effective stress.

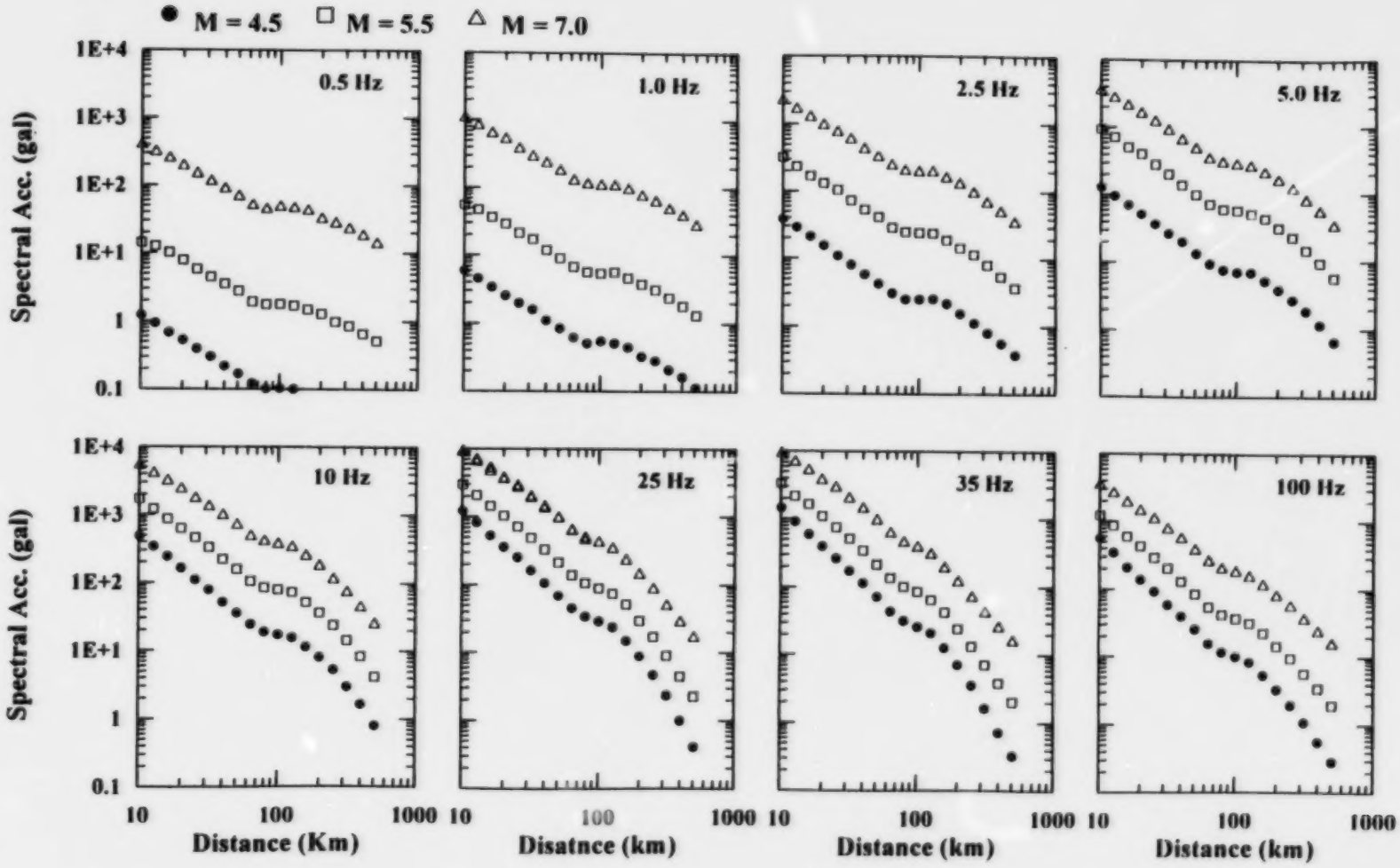

Figure B-3. Predicted repsonse spectra values (PSA for 5% damping) for M 4.5, 5.5, and 7.0 using Haddon's source model.

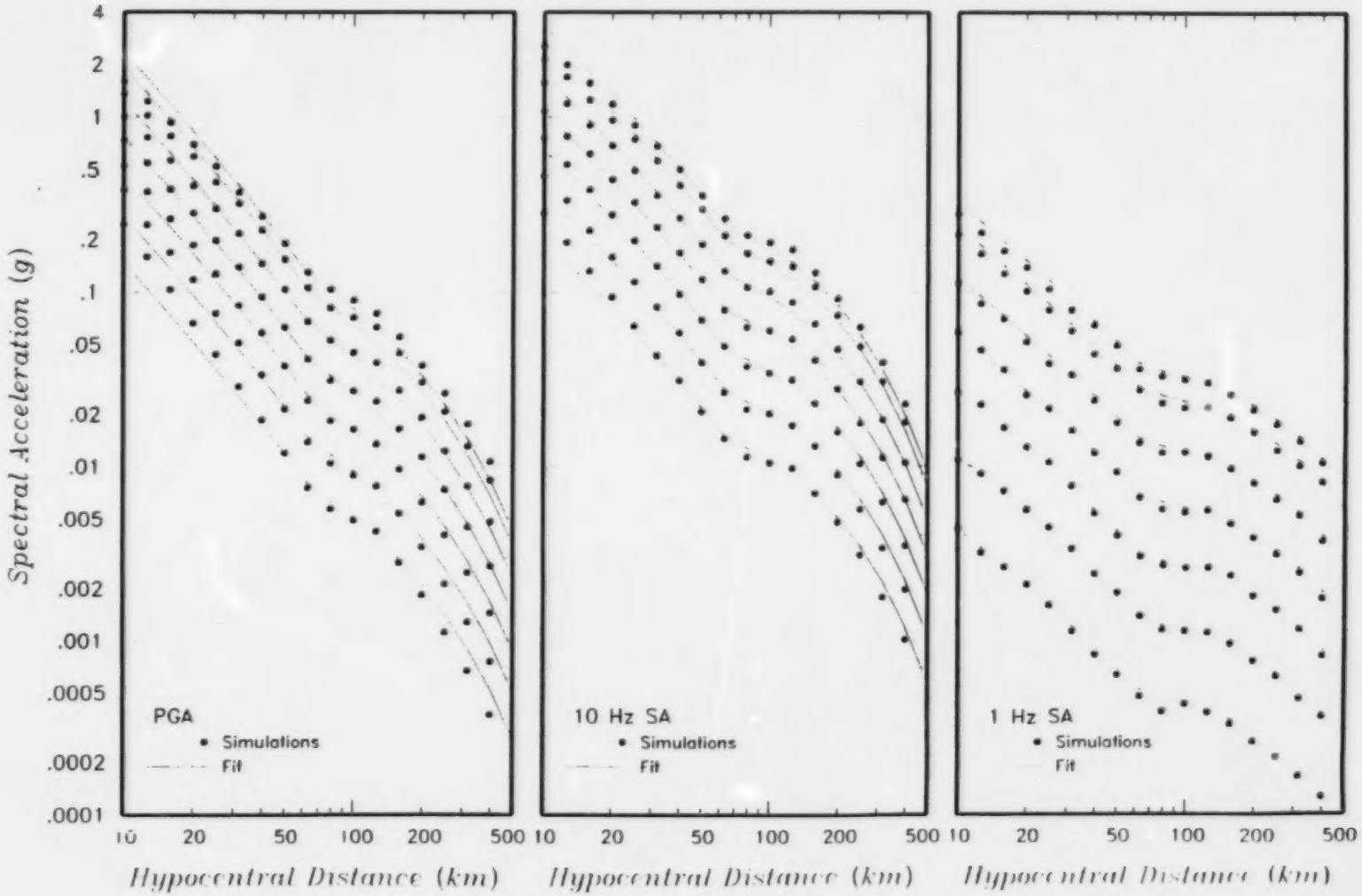

Figure B-1 Fit to simulated motions for Atkinson and Boore (1995)

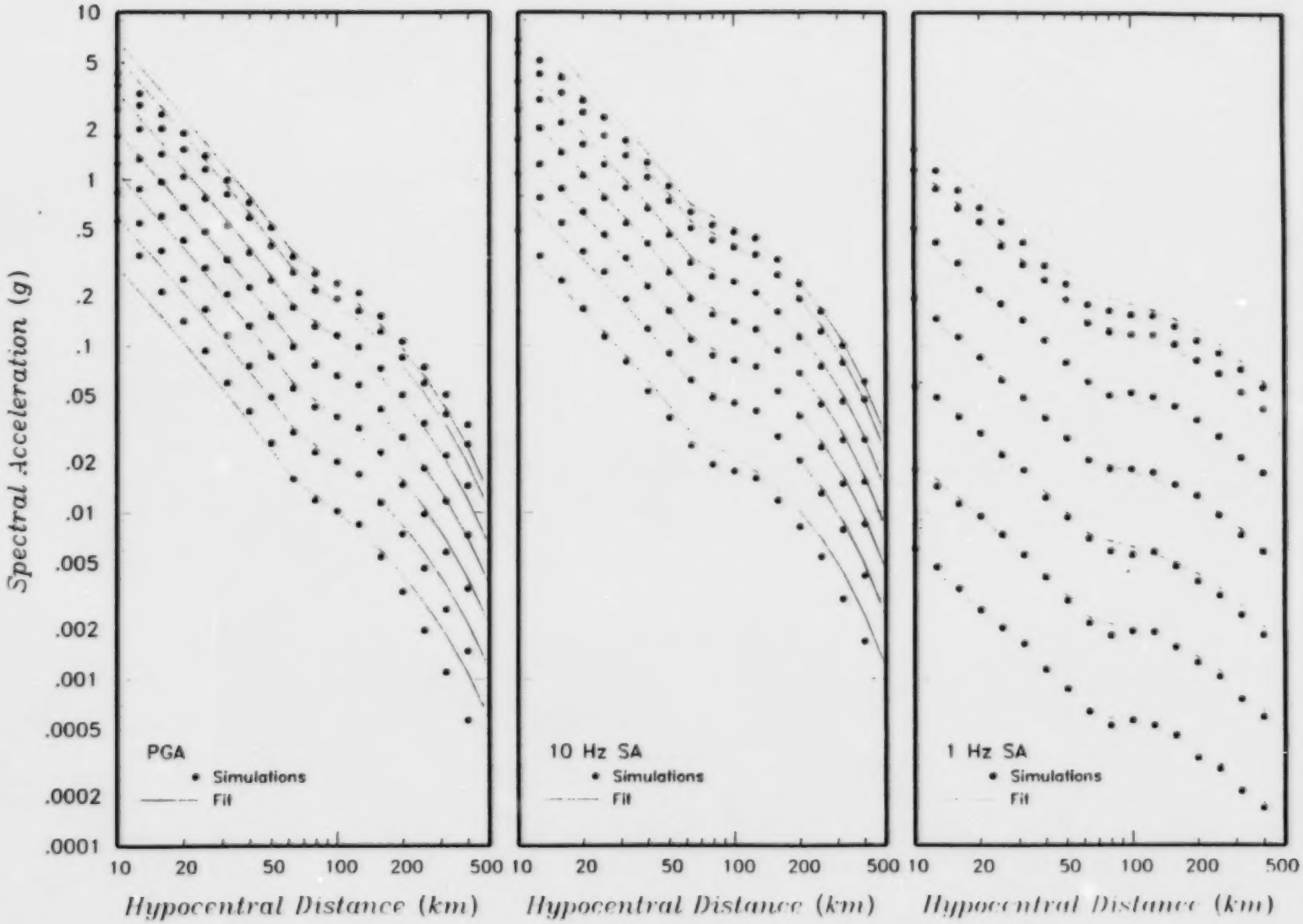

Figure B–5 Fit to simulated motions for Haddon (1996)

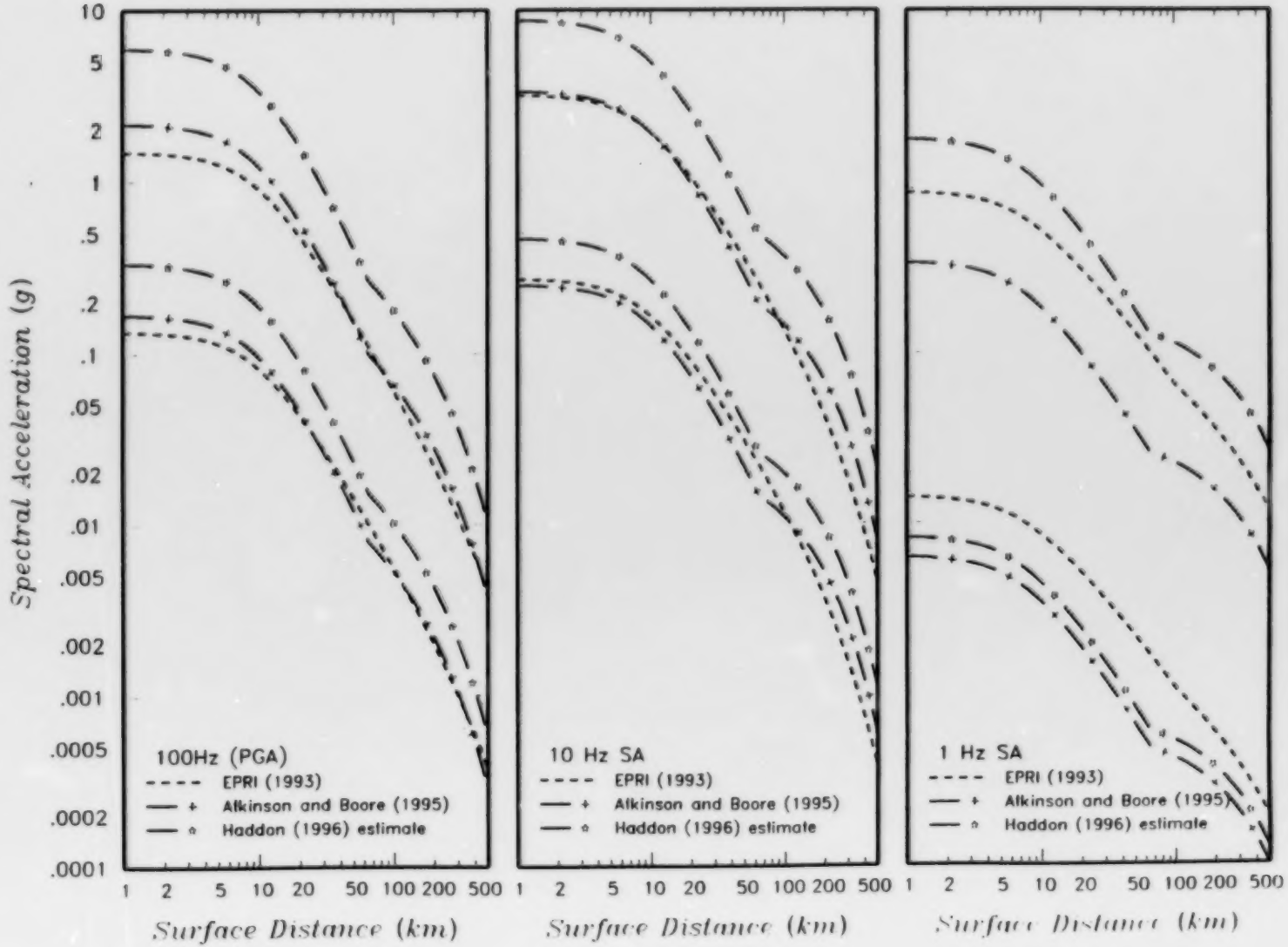

Figure B-6 Comparison of attenuation relationships for mb 5 and 7